1990

Interaction of wake form from a translating cylinder with an elliptical leading edge

Levent Takmaz
Lehigh University

INTERACTION OF WAKE FORM FROM A TRANSLATING CYLINDER WITH AN ELLIPTICAL LEADING EDGE

by

Levent Takmaz

A Thesis

Presented to the Graduate Committee

of Lehigh University

in Candidacy for the Degree of

Master of Science

in

Mechanical Engineering

1989

CERTIFICATE OF APPROVAL

This thesis is accepted and approved in partial fulfillment of the requirements for the degree of Master of Science in Mechanical Engineering.

OCTOBER 12, 1989
date

Professor in charge

Chairman of Department

To My Uncle

ACKNOWLEDGEMENTS

First, I would like to thank everybody who helped me throughout this project. I also wish to express my appreciation to Charles L. Magness, Jorge A. Kuryla, Mark Cortazzo, Frank J. Nuzzi, Ahmed Haji-Haidari, Blaine K. Taylor and Dr. Cheng-Hsiung Kuo for their valuable contributions to this project.

Finally, I would like to express my thanks to Professor Donald O. Rockwell for his advice and guidance throughout my thesis.

TABLE OF CONTENTS

LIST OF FIGURES

ABSTRACT

This investigation addresses the interaction of a concentrated vorticity field from a translating cylinder with an elliptical leading-edge of finite thickness. Two different scales of the vorticity field are generated by employing different cylinder diameters. These different scales are categorized as large- and small-scale interactions. The effect of dimensionless translation velocity and amplitude of the cylinder, as well as the gap between the cylinder and the leading-edge are considered. Detailed visualization of the flow structure and measurements of the unsteady surface pressure are addressed.

In the first part of the investigation, the unsteady flow field was visualized using the hydrogen bubble technique. For the large-scale interaction, when the largest amplitude of cylinder translation was considered, three different regimes were observed. At very low velocities of the cylinder translation (Regime I), there was a fluid injection, i.e. a jet-like flow, between the cylinder and the tip of the edge, accompanied by formation of a secondary vortex, and in some cases, a number of small-scale vortices. At the moderate cylinder velocities (Regime II), a large scale vortex formed from the translating cylinder and moved downstream, maintaining a nearly constant distance between its center and the edge surface. At the highest cylinder velocities (Regime III), there was no vortex formation along the edge surface and the flow within the large-scale vortices rapidly became turbulent.

In the second part of the investigation, pressure measurements were performed along the edge surface. The response of the pressure taps along the edge were separated into three different groups, each group showing common features of the pressure signals. In general, the pressure signal at the tip of the

edge showed identical pressure signals for the upstroke and downstroke motions of the cylinder at each value of cylinder velocity, due to symmetry. It was observed that the pressure signal was influenced by the three different effects : the flow field distortion due to the finite diameter of the cylinder; the effect of the cylinder wake involving formation of a large-scale vortex; and the effect of the mechanical noise of the system.

The correlation of the flow visualization and pressure measurement experiments showed the instantaneous relation between the pressure field, the unsteady flow structure and the cylinder motion. The onset of the pressure fluctuation at each velocity was due to the flow field distortion by the finite-size cylinder. When the cylinder velocity was increased, the initially-formed, large-scale vortex contributed significantly to the pressure signal.

CHAPTER 1

1. INTRODUCTION

It is well known that the unsteady flow in turbomachines is extremely complicated. In general, the blades of a multistage turbomachine do not operate in steady flow. They experience a row of wakes shed from the blades of the preceding stage. As a result of this phenomenon, there occur transient fluctuations of the pressure distribution on the surface of the blade. The change of pressure affects the drag, the maximum lift coefficient, and in the case of hydraulic machines, the cavitation characteristics of the affected blades. The magnitudes of the unsteady forces are difficult to determine. These forces are the cause of induced vibrations of the blades and the generation of sound. For example, it is well known that the fluctuation of the lift force on the blade during the wake passage creates a radiated pressure field associated with noise generation. This phenomenon, generally attributed to wake cutting, is one of the major sources of periodic sound produced by turbomachinery.

1.1 LOADING OF BLADES IN TURBOMACHINES

A typical airfoil in an axial flow machine is affected by the disturbance field of all the other airfoils of its own blade row and of near by blade rows. This disturbance field varies with time due to the relative motion of the rows. The time-dependent circulation of a given airfoil within the cascade is directly linked to the unsteady forces. Also, at the trailing-edge of the airfoil, there is formation of a wake of vortices, which plays a role in determining the unsteady loading.

Theoretically, Kemp and Sears (1953) obtained the unsteady lift and

moment for a stator-rotor combination. The main purpose of this work was to attack the problem of mutual interference of blades in cascades on the basis of the theory of thin airfoils in steady motion. They considered the elementary case of a single stator cascade followed by a single rotor cascade. They attempted to evaluate the magnitudes of the unsteady forces on the blades and the rate of energy transfer to the wake vortices and determined how all these were affected by the geometrical and aerodynamic parameters. In dealing with this complex problem, they made some simplifying assumptions. Incompressible flow was the first one. A blade wheel was represented by an infinite cascade of two-dimensional airfoils and the corresponding airfoil theory was based upon the inviscid flow assumption. Another assumption was that of a thin, slightly cambered (i.e. lightly loaded) airfoil. Moreover, their approximate calculation assumed that the unsteady part of the circulation about any blade was small compared with the steady part. This assumption led to the formulas for the unsteady components of lift and pitching moment of the rotor and stator blades. They also determined that the rate of energy transfer was small when it was compared with the power required to turn the rotor. This transferred energy was associated with the variable circulation and had a value about a hundred times larger for the stator (upstream) blades than for the rotor (downstream) blades.

In their subsequent work, Kemp and Sears (1955) used the theory of isolated thin airfoils in nonuniform motion. Their initial study using this approach made it possible to calculate the forces and moments that act on the affected blades of a turbomachine. Because of the complexity of this problem, they introduced some important approximations. First, they calculated the forces and moments for an elementary stage consisting of a stator and rotor. Second, they used the approximations of unsteady thin airfoil theory. Their final assumption

was that the fluctuation of blade circulation was always small compared to the mean value. Under all of the above approximations, the fluctuations of the lift, moment and circulation were determined by the potential flow field of the adjacent row of blades. These calculations included the effects of the vortex wakes of the upstream stator blades. Typical stage geometries were considered and the fluctuation of lift was found to be appreciable. In all of their work, Kemp and Sears did not account for the viscous-wake effects. When the viscous-wake effects were included in the calculations, additional approximations were needed. In the second phase of their work, including the viscous-wake effects, the flow downstream of a cascade of blades was represented by an inviscid shear flow. The velocity profile for each wake was the velocity profile of the wake behind an isolated airfoil that was determined from measurements. According to these results, the force depended on the profile drag-coefficient of the upstream blades. Previously estimated unsteady forces via the aerodynamic interference between the moving blades were same as those arising from passage through viscous wakes. This was true only for typical values of the drag coefficient of the upstream blades and for a conventional cascade geometry.

According to Lefcort (1965), unsteady forces in turbomachines are the result of four different effects: the circulation effect; the blade thickness effect; the wake effect; and the wake-distortion or cutting effect. The *circulation effect* is due to the presence of circulation about the blades of the moving adjacent blade rows. When there is no circulation about the adjacent blades, the circulation effect becomes zero. The *blade-thickness effect*, which is related to the finite thickness of the blades, is associated with the potential flow fields about the blade rows. Here, it is assumed that the boundary-layer displacement thickness is included in the blade thickness. When the adjacent blades have zero thickness, the blade thickness

effect becomes zero. The *wake effect* upon the downstream blades arises from the wake shed from the upstream blades. This effect is the result of the induced unsteady velocity fields on the downstream blade surface. The boundary layer, which is due to viscous effects, causes the fluid retardation and because of this phenomenon, a wake forms from the upstream blades. When the boundary layer is removed from the upstream blades, then the wake effect becomes zero. After the wakes are shed by the upstream blades and reach the downstream blades, the *wake distortion* effect appears due to the fact that the lines of constant vorticity forming the wake are distorted in passing over the blade. This phenomenon is known as "wake cutting". A moving jet approaching the blade is the simulation of this effect considering that the moving jet is the wake shed by the upstream blade. After reaching the leading-edge, the jet is cut in two halves which are distorted. One half of the jet contracts and the other half spreads out on the blade surface. This is a transient interaction between the blade and the nonuniform unsteady flow carrying vorticity which approaches the blade.

Lefcort (1965) proved that the wake cutting phenomenon gives rise to strong unsteady forces. He experimentally studied this problem using a moving cylinder to create a vorticity field. The purpose of this study was to simulate the wake interaction problem in a turbomachine. He measured the instantaneous pressure distribution on a compressor blade cutting into the laminar wake of a circular cylinder. Specially developed piezoelectric transducers, a cylindrical wake generator and an aluminum symmetrical NACA 65 series blade 1 ft in length with 10 percent thickness ratio were used in a two-dimensional flow for the experiments. The blade was subjected to passage of the wake shed by an upstream wake generator. Thin airfoil-wake theory was considered for the case of wakes of finite thickness. A major objective of this study was to predict the pressure change

on the blade due to the potential flow distortion about an upstream blade. The wake distortion effect was also considered. By consideration of difference between the measured and computed pressure fluctuations, it was proved that the wake distortion effect was very important in the calculation of unsteady forces.

Meyer (1958) theoretically considered an airfoil cutting through a single isolated wake of arbitrary velocity defect distribution. He obtained the instantaneous chordwise pressure distribution. Then he carried out another study to make a generalization for the limiting case where the wake was very narrow relative to the chord of the airfoil. He determined the time-dependent pressure gradient and the velocity field for the case of two-dimensional incompressible flow through lightly-loaded cascades. In that case, it was assumed that the upstream blades, from which the wakes are shed, were stationary and the downstream blades, which are the affected blades, were rotating. Meyer's prediction supported the experimental results of Lefcort.

Fujita and Kovaszay (1974) experimentally studied the transient response of an airfoil to a passing wake. Their main point was to understand the interaction between successive blade rows in turbomachines. This study was similar in concept to the investigation of Lefcort. Moving circular rods traversed periodically an open jet and created a periodic row of wakes. They measured the periodic component of the instantaneous chordwise surface pressure distribution on the airfoil and the radiated sound field from the airfoil.

1.2 DISTORTION OF VORTICITY FIELDS AT LEADING-EDGES OF BLADES

In general, the wake cutting phenomenon, which is a key point in

understanding the unsteady forces on a blade is an interaction of an unsteady vorticity field with the surface of the blade. To fully understand the wake cutting phenomenon, the interaction between the leading-edge of the blade and the vorticity field of the wake should be understood. Rockwell (1984) has reviewed the experimental results of all these types of interactions, including unsteady distributed and concentrated vorticity fields. In this overview, attention was given to understanding the relation between the unsteady pressure fields and the structure of the vorticity field-edge interaction in the region of the leading-edge. All types of interaction mechanisms create a downstream travelling pressure wave at a given phase speed. The amplitude and wavelength of this pressure wave determine the characteristics of the unsteady loading on the edge.

The incident vorticity field may be distributed or concentrated in a vortex. The consequent interactions with the leading-edge produce very different classes of unsteady flow structure. In the situation where the incident vorticity field has many concentrations of vorticity at different frequencies and wavelengths, the interaction with the leading edge generates a modulated pressure wave that has many spectral components.

All of the studies described in the foregoing show that the interaction between any kind of coherent vorticity field and the leading-edge resulted in the same common features: an unsteady separation; subsequent secondary vortex formation; a distinct relation between the instantaneous pressure field and the nature of the secondary vortex formation; and a dependence of the interaction mechanism and the pressure loading on the offset between the incident shear layer and the edge.

Considering the interaction of a concentrated vorticity field at a single

frequency with the leading-edge, Ziada and Rockwell (1982) visualized the flow structure, which was due to successive vortices impinging upon the leading-edge of a wedge. There was vortex shedding from the leading-edge and the shed vortex had a vorticity orientation opposite to that of the primary vortex. The force induced on the wedge and the visualization of the unsteady interaction mechanism showed the relation between the nature of the interaction mechanism and the relative magnitude and phase of the force exerted on the wedge. Small variations in transverse location of the leading-edge affected the interaction mechanism between the vortex and the leading-edge. When the vortex approached the edge, it had a tendency to dive to the underside of the leading edge. For the considered range of transverse offset between the vortex centre and the leading-edge, the direction of vortex shedding was from the leading-edge towards the underside of the wedge. However, the process of vortex shedding from the leading-edge was dominated by the transverse-velocity fluctuation of the incident flow. At zero offset, the induced unsteady force took on its largest amplitude. When the leading-edge was moved in either direction away from the centre of the incident vortex, the magnitude of the unsteady force dropped. The interaction at the leading edge was the main reason for the induced force. It was found that when the unsteady force on the edge took its maximum negative value, the position of the vortex center upstream of the leading edge depended on the value of offset and the degree of vorticity concentration within the incident vortex. The results of the experimental calculations did not agree with the results of the theoretical modelling. This was just due to the fact that viscous effects caused the unsteady separation at the leading edge and a consequent shedding of the opposite vortex. The dominance of vortex shedding on the lower side of the wedge at the negative offset values gave rise to the inaccuracy between the experiments and theory.

In Kaykayoglu and Rockwell's work (1985), vortices were generated using a mixing layer flow that was formed by high- and low-speed streams. Looking at the results of the flow visualization and pressure measurement experiments, they related the distortion of each primary vortex, the secondary vortex shedding and the "sweeping" of flow about the tip of the edge to the instantaneous pressure fields, which were interpreted as travelling waves along the upper and lower surfaces of the edge. Rapid flow distortion occurred near the tip of the edge. In the same region, the pressure fields were non-wavelike. On the lower surface, because of the secondary vortex shedding, there was negligible phase variation. On the upper surface, there was a phase jump. Downstream of the near-tip region, wavelike pressure fields appeared as shorter and longer wavelengths on both surfaces. An important observation was the difference between these wavelengths and those of the primary-vortex instability. The maximum pressure amplitude always occurred at the tip of the edge and took its maximum value when the scale of the secondary vortex shedding from the tip of the edge was pronounced. Perhaps the most important observation was the crucial role of the local flow distortion on the net force. One of the most significant results of this investigation was the suggestion that the inviscid modelling of the interaction should not incorporate a leading-edge Kutta condition. The Kutta condition requires that the pressure slowly goes to zero as the tip of the edge is approached.

Sohn and Rockwell (1985) studied the case of a concentrated vorticity field at a single frequency interacting with a finite-thickness leading-edge. Instead of using thin leading-edges as in previous works, they used a finite-thickness, elliptically-shaped edge. From the previous studies, it was determined that the offset between the incident shear layer and the body affected the unsteady pressure fluctuation. The secondary vortex formation was an important factor in

determining the pressure field. For the interaction with the edge of finite thickness, primary and secondary vortices did not leave the surface. Flow was not swept about the tip of the edge, as in the case of thin-leading edge. When the edge had a large thickness relative to the scale of the incident vortex, most of the primary vortex moved along the lower surface of the edge. When the edge thickness was decreased, the incident vortex was divided into two different parts, one travelling along the upper surface with a larger phase speed, and the other moving along the lower surface. The thickness of the edge did not affect the secondary vortex formation. For all of the offset cases, the primary vortex passed along the upper or lower surface of the edge but was not severed. When a distorted vortex and/or secondary vortex moved along the upper or lower surface of the edge, the unsteady pressure field had a propagation speed and its phase had an increasing slope with streamwise direction. When there was no vortex on the surface, the phase of pressure was constant. At different offsets, the wavelength of the propagating pressure wave was different. At negative offset, the wavelength of the pressure field was two times larger than for the positive offset case.

Gursul and Rockwell (1988) investigated the interaction of a Karman vortex-street with a finite thickness, elliptical leading-edge. They measured the unsteady pressure fields induced by this interaction and compared the results with the visualized flow patterns. There resulted three basic interaction mechanisms. First, the vortex street did not lose its identity. Second, the vortex street was separated into two halves, each half being a single row of vortices. Third, one of these two rows was split and lost its coherence. The first two of these mechanisms were possible only for the small-scale vortex streets; the last one was observed only for large-scale vortex streets.

1.3 PROPOSED RESEARCH

The interaction of a concentrated vorticity field at a single frequency with a finite-thickness elliptical leading-edge will be the focus of this investigation. The distinguishing feature is that the vorticity field will be formed from a translating cylinder past the edge. Although the concept of this study seems similar to the Lefcort's work, the approaches are quite different. In this study, the cylinder is very close to the leading-edge, and instead of an airfoil, a finite-thickness leading-edge is used. High resolution flow visualization experiments will be done to see the unsteady vortex-leading edge interaction. Then, pressure measurement experiments will be performed to understand the instantaneous pressure field on the surface of the edge. The correlation of the flow visualization and pressure measurement experiments will show instantaneously the relation between the pressure field, the unsteady flow structure, and the cylinder motion.

CHAPTER 2

2. EXPERIMENTAL SYSTEM AND TECHNIQUE

2.1 OVERVIEW OF THE EXPERIMENTAL SYSTEM

A free surface closed loop water channel was used for the experiments (Figures 1 and 2). The test section of the channel, 12 in (30.5 cm) wide and 18 in (45.7 cm) high, was made of Plexiglass to allow flow visualization experiments. The water level in the test section was maintained at 13 in (33 cm). At this level, the mean velocity of the channel was typically 2.85 in/sec (Figures 1 and 2).

As shown in Figures 3, 4 and 5, the vertical elliptical leading-edge was positioned in the middle of the channel. The ratio of the major to the minor axis of the elliptical edge was 5:1. The test cylinder was mounted vertically from the head of the forcing system, which involved a moving table and a computerized stepping motor. The bottom end of the cylinder was free with a distance of 0.3 cm from the floor of the channel, its top end was screwed to the driving mechanism. A stationary probe was attached to a rail above the main test section for the flow visualization experiments. During the experiments, the mean velocity and water level were kept constant but the velocity of the cylinder, its diameter, its amplitude and the distance between the edge and the cylinder were changed.

Two different computer programs were employed: one for the flow visualization experiments; and the other for the pressure measurements. These programs allowed simultaneous translation of the cylinder and acquisition of the data. The pressure data were analyzed using a Fast Fourier Transform (FFT) technique. Another program was written to carry out the ensemble averaging of the pressure data. All the programs of the pressure measurement experiments

were written by Charles Magness in C programming language. To make sure that the velocity values of the two different programs were the same, the motion of the cylinder was recorded by using the video system and the frame numbers were checked for each different velocity on the screen. The difference in velocities was the order of two percent, which was considered negligible.

Once the unsteady flow field was illuminated by the hydrogen bubble lines, the video system was positioned to record the images as shown in Figure 16. Both far and close-up views of the edge-cylinder combination were obtained. These views were obtained by transmitting the image through the bottom surface of the channel, then reflecting it from a mirror to the camera. The angle between the mirror and the channel bottom surface was 45 degrees.

2.2 ELLIPTICAL LEADING EDGE

The elliptical leading-edge of finite-thickness included four different parts: the leading-edge; the valve body; the manifold plenum; and the transducer mounting plate (Figure 5). The leading-edge part was manufactured from one piece of plexiglass block that was cut into three pieces to allow placement of the brass tubes that connected the pressure taps on the elliptical contour to the pressure transducer via a valve arrangement. The edge contained 12 pressure taps on each surface and one pressure tap at the tip (Figure 6). Experiments were run only for 9 pressure taps, 8 pressure taps on one of the surfaces and one pressure tap at the tip. Along the leading edge, the transverse offset from one tap to the next one was 1/8 inch, in order to prevent wake effects on the pressure measurements. More pressure taps were located in the tip region in view of the large pressure gradient there. Each pressure tap on the elliptical leading-edge had a diameter of 0.79 mm (1/32 in) to prevent the significant error in the pressure

measurement. All of them were connected to the transducer by the brass tubing (Figure 7). The diameter of the tubes was 1.59 mm. The lengths of the tubes were between 5.5 and 12.1 cm. The differences of the lengths of the tubes could potentially introduce undesirable amplitude attenuation and phase distortion. Sohn (1985) did a calibration to determine this effect. In that calibration method, a fixed volume container containing water was sinusoidally displaced in water to produce static pressure variations. This was done using an eccentric motor drive. The frequency of the input signal was from 0 to 5 Hz. The leading edge was located at the bottom of the tank. Another transducer was mounted next to the active pressure tap. Then, the pressure signals from the active pressure tap and the reference pressure transducer were compared to each other to determine the effect of the pressure tube connection on the pressure signal. Using the recorded pressure signals, a cross-spectral analysis was done. Only two taps representing the extreme cases were checked, tap No. 1 which had the longest tube and the tap No. 13 which had the shortest tube in the edge (Figure 8). According to the results, tap No. 1 showed minimal amplitude attenuation but tap No. 13 did not have any amplitude distortion. As shown in Figure 11, there were phase distortions of 0.18π and 0.05π for taps No.1 and 13 respectively for 5Hz sinosoidal input signal. These results proved that errors induced in transmitting the pressure signals from the taps to the pressure transducer were so small. The valve body part together with manifold plenum connected the individual pressure taps to the transducer, which was placed in the transducer mounting plate. The valve body part and the manifold plenum are shown in Figures 9 and 10.

2.3 FORCING SYSTEM

2.3.1 Motor-Controller

In research and test labs, Compumotors are used frequently because of their precise control of speed and position. A Compumotor system has three different parts: an indexer; a driver; and a motor (Figure 13). High level commands are sent to a Compumotor indexer from a computer or an operator through a front control panel. Then, the on-board microprocessor generates the necessary step pulses by interpreting the high level commands. Sending these pulses to the driver, the Compumotor indexer controls the velocity, acceleration, position and direction of the Compumotor. After the Compumotor driver recieves the digital step and direction inputs from the indexer, the internal drive logic and power amplifiers of the driver set the output current levels to drive the Compumotor that is a form of stepping motor. It has a magnetic armature with electric coils wound around it in a circular array. An output shaft, which moves the sliding mechanism in the experiments, is connected to this armature. When the coils are activated with on or off pulses, the resulting motion comes out in discrete steps and the armature is rotated together with the shaft. In the present experiments for example, as the stepper motor runs in a 25,000 step per revolution mode, the cylinder travels a distance of one-half inch. The motor and thereby the cylinder are driven by a Zenith Z-241 microcomputer.

2.3.2 Positioning Table

In general, linear motion is produced by a linear sliding mechanism that consists of a stationary part and a moveable part. The motion between these two different parts is made possible by one of these three different slides: the dovetail slide; the ball bearing slide; or a roller bearing slide (Figure 12). A linear positioning table driven by the Compumotor provides linear motion and accurate positioning between two different points. This table is driven by a lead screw

assembly that consists of a leadscrew and a lead screw nut. The moveable part of the table (upper part) is forced by the leadscrew nut which is moved along the lead screw and unable to turn. A flexible shaft coupling connects the motor to the end of the lead screw which is fixed to the stationary part of the table (base). When the motor rotates the shaft, the leadscrew nut that is fixed to the moveable part follows the lead screw threads and moves the table along the table base. This linear motion is controlled by the preloaded linear bearing system. As a result, the rotation of the leadscrew is turned to a linear motion of the table using a stepper motor and a low friction leadscrew nut (Figure 13). The leadscrew is connected to the table base with two radial and angular contact bearings. The housing of the table is made of anodized aluminum.

The positioning table that was used in the experiments had a ball bearing slide mechanism. There were two rows of hardened steel balls which rolled on either side of the base. Four hardened and precision ground steel rods held the balls to permit the upper part to slide on the base. Two of these four rods moved with the upper part and the other two were stationary on the table base. The balls were preloaded to prevent their random movement. This ball bearing mechanism compares with the dovetail slide, which has an angular design to hold the lower stationary and upper moveable parts. A low friction bearing material is used on the sliding surfaces to reduce the friction. In this type of linear slide, there is rapid wear due to the loading and it is very difficult to produce a short move for accurate positioning. Because the force must be sufficiently large enough to initiate the movement, this might result in jumping or skipping. Wear causes an error which requires frequent adjustment. In the cross roller slide mechanism, two rows of rollers are located on the moveable upper and stationary lower parts of the table. Each roller is placed in "V" grooves. For the larger loads, this

mechanism is better than the ball bearing slide due to the fact that the rollers provide a larger contact surface than the balls. The angle between the centerline of the rollers is 90 deg. The disadvantages of this slide are the shock loads and low accuracy. The ball slide has the same disadvantage; it can't withstand the shock loads like the roller slide but it gives high accuracy and it is cheap. Therefore, for the present experiments, the positioning table was chosen with the ball slide. The table was manufactured by Daedal, Inc. The specifications are as follows: Total travel distance=10 in; Weight=33 lbs. ; Pitch of lead screw=0.5 in.

2.4 CYLINDER SYSTEMS

Figure 14 defines the amplitude A of the cylinder motion and the diameter D of the cylinder, the thickness T of the edge, the velocity U of the mean flow, and the velocity V of the cylinder. The Reynolds number was approximately 920 for the 1/2 in diameter cylinder and 230 for the 1/8 in diameter cylinder. In general, for the flow visualization experiments, two different cylinder diameters, D=1/2 in (for the large scale interaction), and D=1/8 in (for the small scale interaction), were used. For each diameter, three different amplitudes were employed: A=1/2 in, 1 in and 2.5 in. For each diameter D and each amplitude A, eight (for 1/2 in diameter cylinder) or five (for 1/8 in diameter cylinder) different velocities V of the cylinder were investigated. The distance L between the cylinder and the edge had one value. In the pressure measurement experiments, only one cylinder diameter, D=1/2 in, and one amplitude, A=2.5 in, were examined. The cylinder was oscillated at six different velocities. The distance L between the cylinder and edge was kept constant at 1/4 in. Eight different L/D values were considered at the dimensionless cylinder velocity V/U=0.38. The six values of the velocity were same as the velocities in the flow visualization

experiments, in order to make a correlation between two different experiments. For all the experiments, the free-stream velocity U was constant at 2.85 in/sec, the thickness of the edge was 1 in, the range of V/U was between 0.043 and 1.43, and D/T had only two different values of 1/2 and 1/8. Nondimensional values of amplitude A/T were 0.5, 1 and 2.5.

2.5 FLOW VISUALIZATION TECHNIQUE

2.5.1 Overview of Visualization Method

For the visualization of the unsteady flow field, the hydrogen bubble technique was used. As a cathode, a platinum wire of diameter 0.001 in was stretched between the ends of the probe that was designed using four brass tubes (Figure 15). This probe was insulated with heat shrink plastic tubing and the insulated area was protected by coating the soldered joints at the ends of the stretched platinum wire. Therefore, there was no water leakage that could cause bubble generation from the support probe. A potential difference between the platinum wire and the carbon rod (anode) in water electrolized the medium, giving hydrogen bubbles. Since twice as many hydrogen bubbles were generated as oxygen bubbles during the reaction, they were used in the flow visualization experiments. The condition of the water was one of the most important factors for the high quality visualization. Before the experiments, the channel pump was turned on overnight to create circulation between the tanks to clean the test water. After the tanks were filled, no experiment was done for a sufficiently long time to allow release of dissolved air and to age the test water. Chlorine prevented the algae growth and Sodium Sulfate kept a good Ph balance. The amounts of Chlorine and Sodium Sulfate were arranged by using an Equality brand swimming pool test kit, which showed the chlorine level 1 to 3 and Ph level 7.6 to 7.8 for a

good bubble generation. The test water was checked before every experiment to measure the Chlorine and Ph level. After all of the above water treatment procedures, the hydrogen bubbles were very small and the bubble lines were sharp. A bubble generator with a voltage range between 0 and 90 volts powered the platinum wire with the square wave voltage pulses. Adjusting the voltage to an appropriate level 30 volts for high quality bubble generation was the key point of this experiment. The next step was to obtain the frequency of bubble generation, which was in the range between 0 and 340 Hz.

In order to satisfy the visualization requirements, it was necessary to paint the cylinder and the elliptical leading-edge black. The visualized unsteady flow was recorded using a high speed video recording system (Figure 16) that involved two high speed video cameras equipped with variable shutter speed capability and a monitor. It also had a split screen capability which allowed two cameras to display two different views on the video screen simultaneously. The speed of the system was 120 frames per second. Although +2 and +3 lenses were tried , only +1 lense worked best for the camera. Two Instar 90 strobes illuminated the interested flow region. The strobes were arranged at different angles to get the best contrast in recording. By examining the recorded movies, important frame numbers were defined. Then, the pictures were taken from the video screen in a darkened laboratory using a NIKON F3 camera and 35 mm black and white or color film.

2.5.2 Assessment of Hydrogen Bubble Technique

Although the hydrogen bubble technique is a very well known way to visualize the region of interest of an unsteady flow, there are uncertanties that must be considered. These uncertanties are the frequency response of the bubbles

to flow velocity perturbations, bubble rise due to buoyancy, bubble slip arising from pressure gradients in the flow, and retardation of the bubble velocity in the wake of the generating wires.

When the velocity changes via the unsteadiness of the flow, each bubble can not response instantaneously because of its inertia. This finite frequency response of the bubbles is a source of uncertainty. Schraub et al. (1965) showed that bubbles with 0.001 in diameter should respond very well to velocity fluctuations less than 500 Hz (Figure 17). In this study, the maximum frequency of the driven cylinder is less than 90 Hz, which is much smaller than 500 Hz. Therefore, the major concern about the severe amplitude or phase distortion is not considered here.

Another problem is the generation of large bubbles. They have a higher bubble rise velocity via the buoyancy effect. Actually, only the small bubles are considered for the visualization and the large ones are ignored. The diameter of these small bubbles is approximately 0.001 in. According to Lusseyran and Rockwell's (1988) study, a dimensionless terminal rise velocity V_t/ U is almost 0.04 for a value of 1 cm/sec (Figure 18). In the present experiments, the mean velocity of the channel was 7.23 cm/sec. For this value, V_t/ U is approximately 0.01. It means that V_t= 0.0723 cm/sec. Over a distance of 20 cm, the bubble drift due to buoyancy is small compared to the length scales of the flow. Therefore, this effect is considered to be negligible.

The uncertainty of the bubble slip is considered when there is a pressure gradient $\frac{\partial P}{\partial s}$; it is driven by a density difference between the bubbles and the surrounding water . The bubble slip velocity can be determined as follows. The force balance between the radial pressure gradient and the drag on the bubble is

$$\frac{\partial P}{\partial s}\left(\frac{4\pi R^3}{3}\right) = \frac{1}{2}\rho\ U_S^2\ \pi R^2\ C_D \qquad (2.1)$$

After the simplification, this equation becomes

$$\frac{\partial P}{\partial s} = \frac{3}{8}\rho\ U_S^2\ \frac{C_D}{R} \qquad (2.2)$$

The pressure gradient for an isolated vortex is

$$\frac{\partial P}{\partial s} = \rho\ \frac{\Gamma}{4\pi^2 r^3} \qquad (2.3)$$

Defining the circulation as

$$\Gamma \approx \pi\ d\ V_\theta \qquad (2.4)$$

the bubble slip velocity can be calculated from the following equation,

$$U_S^2 = \frac{8}{3}\ \frac{R}{C_D}\ \frac{\Gamma}{4\pi^2 r^3} \qquad (2.5)$$

Here, R is the radius of the hydrogen bubble (D=0.001 in), Γ is the circulation, r is the radius of the vortex measured from its center and C_D is the drag coefficient of the bubble.

Assuming that r=0.04 ft, d=0.08 ft, V_θ=0.3 ft/sec, C_D=0.2, U_S can be calculated as

$$\frac{U_S}{V_\theta} \approx 0.085 \qquad (2.6)$$

It is clear that the bubble slip effect must be accounted for in quantitative measurements.

The other major concern is the bubbles that are in the wake of the wires. Schraub et al. (1965) showed that the defect velocity reaches the free stream velocity within 70 wire diameters. For the flow visualization experiments of the present study, the wire diameter was always 0.001 in, which means that the streamwise effect of the wake effect was approximately 0.07 in (1.78 mm). Concerning this effect, the wire was always located at least 5 mm in front of the cylinder and the ends of the probe were made as large as possible to prevent the side effects from the probe.

2.6 PRESSURE MEASUREMENT TECHNIQUE

A PCB transducer was used in the pressure measurement experiments because of its high sensitivity. This kind of transducer transforms dynamic pressures into high-level, low-impedance analog voltage signals. It consists of a microelectronic amplifier, an accelerometer and ceramic crystal elements. If it is desired, for very low pressure measurements a recessed invar diaphragm and a bender mode crystal element are added into this structure. The diaphragm is strained or deflected by the applied net force, which is resulted by the applied pressure. Then, the diaphragm bends the crystal and creates an output voltage proportional to the applied pressure. The output impedance of this voltage is reduced to less than 100 Ohms for the transmission of the signal along the long cables. Usually, a second diaphragm is attached to another bimorph bender crystal behind the pressure diaphragm to provide compensation working in the opposite manner.

The PCB transducers should be calibrated to determine the pressure values in psi. The specifications for the transducer employed in this study are as follows: Calibration range=0-3 psi; Average sensitivity=1203 mv/psi; Natural frequency=13 khz.; Rise time=25 μsec.

In the present experiments, a mounting was designed for the placement of the transducer into the edge. When the pressure was measured using one pressure tap, all the other taps were locked. It was necessary to amplify the pressure signal using an amplifier and then to filter it (Figure 19). For this reason a Tektronix, model TM502 differential amplifier and a Krohn-Hite, model 3700 bandpass filter were used. After the filter, the pressure signal was monitored using a Tektronix 5223 Digitizing Oscilloscope. The high and low cutoff frequencies of the filter were 0.2 and 10 Hz. Many different high cutoff frequencies were tried in order to verify that there was no distortion due to the filter. For each experiment, five different data samples were taken and stored to carry out an ensemble averaging of 8192 data points.

For the pressure experiments, the amplitude of the cylinder oscillation was 2.5 inches. The total distance covered by the cylinder during each run was 10 in. A computer program in C language was used to force the cylinder and to acquire pressure data from the channel simultaneously. During the experiments, there were no chemicals in the test water in order to prevent damage to the PCB transducer. Experiments were run during the late evening, in order not to encounter any noise problems from the building. In the pressure measurement experiments, vibration was a major problem. The forcing system vibrated the channel and the water in the test section. This vibration of the pressure transducer triggered the overrange light of the amplifier, which means that the acquired data was meaningless. The vibration was damped using sponge between

the forcing system and the channel frame. The overrange light was monitored for each experiment. By decreasing the amplification factor of the detected pressure signal, the overrange light was triggered at a higher value of oscillation amplitude of the cylinder.

CHAPTER 3

3. EXPERIMENTAL RESULTS

The central goals of this investigation were to determine the types of vortical structures that are generated due to translation of the cylinder past the elliptical leading-edge, the unsteady pressure distribution along the surface of the edge, and the phasing between the induced vortical structures and the surface pressure field. In this chapter, we focus on the basic mechanisms of vortex generation as a function of the translation speed V of the cylinder relative to the freestream velocity U, i.e. V/U. Two different scales of the translating cylinder of diameter D, and thereby scales of the generated vortical structures are considered. The scale of the cylinder D is normalized by the thickness T of the elliptical leading-edge, i.e. D/T (See Figure 14 for definitions of symbols). Although several values of normalized scale D/T were investigated during the preliminary stages of the experiment, it was found that the two extreme values of D/T described herein show the basic features of so-called large-scale (large D/T) and small-scale (small D/T) interactions. Moreover, all visualization experiments were carried out at a constant value of normalized gap distance L/D between the downstream surface of the cylinder and the tip of the elliptical leading-edge. As will be addressed subsequently, in the description of the unsteady pressure distributions, the induced loading on the edge is relatively insensitive to the value of the normalized gap L/D. Finally, the half-amplitude of the cylinder motion (measured from the centerline of the leading-edge to the maximum distance travelled from the centerline) was varied from a relatively large normalized value of A/D, which approximates essentially infinite excursions in the transverse direction, to a relatively small value of A/D that represents relatively small

amplitude perturbations about the equilibrium position of the cylinder.

3.1 FLOW VISUALIZATION

3.1.1 *Large-Scale Interaction* (D/T =0.5 ; A/T =2.5)

The evolution with time of the flow structure resulting from the translating cylinder-edge interaction is illustrated in Figures 20 through 31 for normalized values of cylinder velocity V relative to the freestream velocity of V/U = 0.043 to 1.43. In these series of photos, the dimensionless amplitude A/D of the cylinder oscillation is maintained at a constant value of A/D=5, and the normalized diameter of the cylinder D/T = 0.5 for all cases.

For the lowest values of the cylinder velocities V/U=0.043 and 0.087, after the cylinder crossed the tip of the edge, many small vortices were produced due to the low velocity of the cylinder (Figure 20 and 21). There was no large-scale vortex formation. For the value of cylinder velocity, V/U =0.19 (Figure 22), the striking feature was the injection of fluid between the (slowly) translating cylinder and the tip of the edge. This so-called injection process is illustrated most clearly in the fourth photo. The distance between the timeline markers from the gap between the cylinder and the tip is of the same order as the distance between the markers in the freestream shown along the upper edge of the photo; consequently, the injection velocity is of the same order as the freestream velocity. As a consequence of this injection process, the formation of a large-scale vortex street from the cylinder is inhibited. However, the injection process does seem to promote the growth and stabilization of the vortex initially formed when the cylinder initially travels upward across the tip of the leading-edge. This process is evident in the second through fourth photos of Figure 22. At a later stage of development, as shown in the fourth photo, there emerges a secondary vortex

adjacent to the primary vortex along the wall of the elliptical edge.

For larger values of V/U, illustrated in Figures 23 through 26, there is also evidence of an injection region between the translating cylinder and the leading-edge. The formation of the large-scale vortex is very pronounced. Moreover, in all of these cases, the vortex formed from this interaction (during the upstroke motion) is quite coherent and, in all cases, it moves along the surface of the edge in the downstream direction, maintaining a relatively constant distance between the center of the vortex and the surface of the edge (during the upstroke motion).

Further considering the upstroke motion of the cylinder, at the highest values of V/U shown in Figures 27 and 28, the interaction process takes on a markedly different form. Due to the high translation velocity of the cylinder, there is no formation of a large-scale vortex along the surface of the edge, followed by its movement downstream along the edge as for the lower values of V/U. Rather, there appears to be formation of smaller scale vortices in the wake of the translating cylinder. Except for the short-lived small-scale vortex along the surface of the edge apparent in the fourth and fifth photos of Figure 27 (V/U=1.11), there is no vortex formation at all along the surface of the edge.

The far views of the three different cases at the lowest values of velocity are shown in Figures 29 through 31. These views clearly show the flow distortion as the cylinder crosses the leading-edge.

An overview of the interaction mechanisms during the upstroke motion of the cylinder is illustrated in Figure 32. Comparisons are made of the flow structure at constant values of location Y of the center of the cylinder above the centerline of the edge normalized by the cylinder diameter D, i.e. at constant

values Y/D=1, 2, and 3. The first column of photos shows that as the normalized velocity V/U of the cylinder is increased, the degree of development of the initially-formed vortex decreases substantially. A similar trend is evident in the second and third columns of photos of Figure 32. At lower values of V/U, the initially-formed vortex is located much further downstream. From this overview of Figure 32, it is possible to define three basic regimes of interaction mechanisms. In regime I, which occurs for V/U less than or equal to 0.19, there is no formation of a large-scale vortex that moves along the surface of the leading-edge. In regime II, there is pronounced formation of a large-scale vortex, which moves downstream along the surface of the edge, maintaining its approximately constant distance from the surface of the edge. In regime III, there is no large-scale vortex along the surface of the edge.

During the downstroke motion of the cylinder, as illustrated in Figures 20 through 31, the existence of a quasi-organized vortex street prior to the encounter of the cylinder with the leading-edge is clearly evident. Depending upon the value of V/U, the degree of coherence of the vortex street, as well as the angle of the vortex street with respect to the centerline of the leading-edge, can vary significantly. For the final stages of the downstroke motion, there exists a row of alternating vortices along the surface of the edge, which are rapidly swept downstream as the cylinder passed beneath the centerline of the edge.

3.1.2 *Large-Scale Interaction* (D/T =0.5 ; A/T = 1)

When the amplitude of the oscillation was decreased to A/D=2, while all other parameters were retained constant, there resulted complex patterns of vortex generation and interaction along, and adjacent to, the surface of the leading-edge.

At the lowest value of V/U=0.19, illustrated in Figure 33, a single vortex is generated in conjunction with the injection process during the upstroke motion of the cylinder, much in the same manner as that occurring for the high amplitude case A/D=5 described in the preceding section. During the downstroke motion, existence of a vortex street above the surface is evident in the ninth photo. It rapidly changes character as the cylinder translates downward past the tip of the edge, giving rise to a series of vortices immediately adjacent to the surface in photos 12 and 13, before this pattern is swept downstream.

At the cylinder velocity V/U=0.38 shown in Figure 34, the formation of the large-scale vortex along the surface of the edge is, once again, similar to the upstroke motion illustrated at the higher amplitude in the previous section. During the downstroke motion, the vortex pattern passes through a succession of states, characterized by the appearance of a vortex pair, which rapidly disintegrates to a pocket of a large-scale turbulent propagating downstream along the surface of the edge.

At values of V/U=0.56 through V/U=1.23 shown in Figures 34 through 37, the vortex patterns generated during the initial stages of the upstroke are, as for previous situations, similar to the higher amplitude cases A/D=5 shown in the previous section. However, during the downstroke motion, a variety of patterns can be generated, including rows of vortices along the surface of the edge (e.g., seventh photo in Figure 34, V/U=0.56), a very large scale vortex near the end of the downstroke motion (eighth photo in Figure 34, V/U=0.56), a counterrotating vortex pair along the surface of the edge (last photos in Figure 35), and a large-scale vortex pair that eventually transforms into what apparently is a single large-scale vortex (last photos in Figures 36 and 37).

3.1.3 *Large-Scale Interaction* (D/T=0.5 ; A/T =0.5)

The vortical structures arising from small amplitude A/D=1 translation of the cylinder are given in Figures 38 through 41. A wide variety of vortex patterns again arise from these types of interactions, though, in general, they are not quite as coherent and persistent as their large-scale counterparts at higher values of amplitude A/D illustrated in the previous sections. There appear to be two "resonant" values of V/U that give rise to relatively coherent and persistent vortex patterns. The first occurs at V/U=0.54 in Figure 39 where the interaction is in the form of a single, moderate-scale vortex that moved along the surface of the edge. The second is for V/U=0.92 in Figure 40, corresponding to formation of a large-scale vortex pair that translates intact downstream along the surface of the edge.

Certain of the basic features of the vortex patterns are summarized in the overviews of Figures 45 through 47, which directly compare the vortical flow structure at constant values of distance Y/D from the centerline of the leading-edge. The far views of the three different velocity cases are shown in Figures 42 through 44.

3.1.4 *Small-Scale Interaction*

For the case of the translating cylinder having a relatively small diameter compared to the thickness of elliptical edge, i.e. A/T=2.5 through A/T=0.5, it is possible to obtain relatively large values of dimensionless amplitude of the cylinder translation, ranging from A/D=20 down to A/D=4. For the large amplitude oscillation A/D=20 illustrated in Figure 48, a well-defined vortex street is inclined at an angle of γ. This angle represents the tangent of the dimensionless cylinder

velocity V/U and equals 29.6 degrees for the case of V/U=0.57 as it is shown in Figure 48. The effect of the velocity ratio V/U on this angle of inclination of the vortex street and the various stages of the interaction mechanism at constant values of Y/D are illustrated in Figure 48.

For a smaller value of the oscillation amplitude A/D=8 of the cylinder, illustrated in Figures 49 and 50, the vortex pattern is considerably more complex. Figure 49 shows that the centerline of the vortex street becomes severely curved due to the change in direction of the cylinder motion after it reaches its upstroke maximum and proceeds in the downstroke direction. Accompanying this curved trajectory, at a later instant of time, are the interactions of adjacent vortices and vortex pairs to form complex arrangements of the vortical structures. Comparison of the interaction patterns at constant values of Y/D is given in Figure 50.

The case of the vortex interactions at the smallest value of amplitude A/D=4 is given in Figure 51. In this case, there appear a succession of vortex pairs generated along the surface of the edge. In Figure 51, an overview of the direction patterns at one value of Y/D is given for this amplitude of oscillation. At the highest value of V/U, a train of vortices along the surface of elliptical edge is evident, but for the lowest values of V/U, the distance between the vortices along the surface is very large.

3.2 PRESSURE MEASUREMENTS

For the pressure measurement experiments, the cylinder having a dimensionless diameter D/T=0.5 was used. The dimensionless amplitude A/D=5 was kept constant. The cylinder velocity V/U was $0.043 \leq V/U \leq 0.70$. The six

values of velocity were the same as those used in the flow visualization experiments, in order to allow a direct correlation between the visualized flow structure and the instantaneous pressure fluctuation. Nine out of the twelve available pressure taps along the surface of the edge were successively opened and locked in a manner such that when one of them was activated, all the others were closed. The pressure tap at the tip of edge was considered first. After the pressure data were acquired, it was stored on floppy disks. Then it was transfered to the mainframe computer at Lehigh University to be plotted using the Quick Plot subroutine. In all of the pressure plots, 1 Volt value on the Y axis corresponds to 0.83 psi.

The pressure taps located downstream of the tip of the edge were classified into two different groups in regard to their similarity of response of the pressure fluctuations: The first group included the pressure Taps No. 14, 15, 16, 17 and 18; the second group included the pressure taps No. 20, 22 and 24. It is important to note that the pressure tap No. 13 responded differently from all the other pressure taps. This pressure tap showed nearly identical fluctuations for the upstroke and downstroke motions of the cylinder due to symmetry. For all the pressure taps, there were three different effects contributing to the unsteady pressure signal: the effect of the potential flow of the moving cylinder; the wake effect of the cylinder related to the initially formed vortex; and the effect of the mechanical noise. Particularly for the upstream pressure taps, the pressure began to fluctuate before the cylinder crossed the tip of the edge due to the potential flow distortion.

3.2.1 *Pressure tap at tip of edge*

For pressure tap No. 13 located at the tip of the edge, multiple peaks were generated at the lowest cylinder velocity V/U=0.043, as illustrated in Figure 52.

The pressure tap was in the wake of the cylinder for a relatively long time at the lower values of velocity. The high frequency fluctuations of the mechanical noise due to system vibration, are postulated to contribute to the multiple peaks at V/U=0.043. However, the vortex formation at the low values of cylinder velocity, which produced many small vortices on the edge surface, also contributed to the appearance of the multiple pressure peaks. The multiple positive and negative peaks appeared midway during the upstroke or downstroke due to the arrival of the cylinder in front of the tip of the edge. When the dimensionless cylinder velocity V/U was increased to higher values, one positive and one negative peak were formed when the cylinder passed the edge, evident at V/U=0.38, 0.57, and 0.70. At the values of V/U=0.087 and V/U=0.19, there was a transition in the form of the pressure signal from multiple peaks to single positive and negative peaks.

In all cases, a negative peak formed first. Above the velocity of V/U=0.043, the velocities of V/U=0.087 and V/U=0.19 showed a positive peak between two negative peaks. The velocity values of V/U=0.38, V/U=0.57 and V/U=0.70 produced first a negative, then a positive peak. In all cases, the first negative peak of the pressure fluctuation occurred before the cylinder crossed the tip of the edge, due to the potential flow distortion of the cylinder-edge system. The apparent effect of the mechanical noise due to the vibration of the cylinder motion on the form of the pressure peaks, evident at the lower velocities of V/U=0.043 and V/U=0.087, did not appear at the higher cylinder velocities.

As shown in Figures 53 and 54, when the distance between the backface of the cylinder and the tip of edge (See Figure 14) was increased, the form of the pressure signal did not change significantly. However, the unsteady flow structure changed its character. For example, there was no concentrated, single vortex

formation on the edge surface for the larger values of L/D at the cylinder velocity V/U=0.38 . This reaffirms the view that the motion of the cylinder is the primary source of the pressure fluctuation at the tip of the edge.

3.2.2 *Pressure Taps Located Immediately Downstream of Tip of Edge*

As illustrated in Figures 55 through 59, the group of pressure taps located immediately downstream of the tip of the edge i.e. taps 14 through 18, showed similar forms of the pressure signal at the lowest cylinder velocity of V/U=0.043. Multiple positive and negative peaks appeared in the pressure signal. This type of pressure fluctuation was due to the contributions from two possible sources: the mechanical noise; and the flow structure. Both could produce high frequency fluctuations. It was observed from the flow visualization experiments that, at this velocity, there were many small vortices formed on the edge surface after the fluid injection process (See Figure 20). At the velocity V/U=0.043, after the formation of a secondary vortex, many small vorticies were formed. The formed vortices could not retain their individual concentrations as they moved downstream (See Figure 20). The mechanical noise effect appearently became stronger than the effect of the unsteady flow structure. It is hypothesized that this is the main reason for the multiple peaks in the pressure fluctuation, especially evident at tap No.18 .

At the velocity value of V/U=0.087, there was a transition in the pressure signal for the first group of pressure taps. A pronounced, single peak formed at the pressure taps No 14 and 15. At taps located further downstream, additional peaks appeared. Many small vortices formed from the translating cylinder at this value of V/U (See Figure 21). The small vortices are felt to be related to the peak at taps No. 14 and 15. These vortices eventually lost their identity and the

pressure signal took a similar form at the pressure taps No. 16, 17 and 18, showing multiple positive and negative peaks. The mechanical noise may play a role in these pressure signals.

At the velocity of V/U=0.19, the pressure signal showed first a negative peak and then two small positive peaks for the upstroke motion. This was true for all of the pressure taps from pressure tap No. 14 through 18. The negative peak occurred before the wake of the cylinder reached the pressure tap. There were neither small vortices nor a concentrated single vortex formed from the translating cylinder. A bubble occurred on the edge surface and moved downstream (See Figure 22). The pressure fluctuation is hypothesized to be the result of this bubble together with the potential flow distortion induced by the translating cylinder. The beginning of the disturbance was due to the potential flow distortion. After the pressure began to fluctuate, the effect of the moving bubble became important in forming the pressure signal. The downstroke motion showed a negative peak between two positive peaks due to the small concentrated vortices hitting the edge surface at a small angle.

For the velocity V/U=0.38, a negative pressure peak occurred between two small positive peaks, except at the pressure tap No. 14 . Only one positive peak was obtained after the negative peak at the tap No. 14 . From the flow visualization experiments, it was clear that a concentrated vortex formed on the surface of the edge (Figure 23). This vortex appeared upstream of a given pressure tap showing a negative peak. This suggests that the pressure fluctuation was the result of both the vortex formation and the potential flow distortion induced by the translating cylinder. The beginning of the pressure fluctuation was due to the potential flow distortion of the moving cylinder. Then this effect and the effect of the initially-formed vortex worked together to form the pressure

signal. For the downstroke motion, the pressure first took a positive value and then a negative pressure peak formed.

The velocity V/U=0.57 showed relatively small amplitude peaks of the pressure fluctuation at each tap during the upstroke motion. Pressure taps No. 14 and 15 showed similar pressure signals. First a negative pressure peak and then a positive value were obtained for the first two pressure taps. Taps located further downstream showed a negative pressure value between two positive ones. At this cylinder velocity, a highly concentrated initial vortex formed from the translating cylinder and the center of this vortex appeared nearly above the tap when a negative peak occurred at a given tap. This observation suggests that the effect of the initially-formed vortex was more predominant in determining the pressure fluctuation. For the downstroke motion, all the pressure taps showed the same result, which was a positive peak, except at tap No. 14 . Pressure tap No. 14 gave first a negative and then a positive peak. This effect may be related to the high angle of the wake when it hit the taps during downstroke. The pressure tap No. 14 is the first tap to experience the oncoming wake. That is the reason it shows a pressure signal different from the other taps. It is important to note that its pressure signal is identical to the pressure signal of tap No. 13 .

For the highest velocity of V/U=0.70, the pressure signal took the same form at each pressure tap during the upstroke. It had first a negative and then a positive value. Although the flow visualization photos showed the same flow structure as in the case of the previous velocity (See Figure 25), the highly concentrated, initially-formed vortex was not the predominant contributor to the negative pressure peaks in this case. When the negative peaks occurred, there was no vortex on the pressure tap. This was the important difference between this case and the previous one. Both of these high velocities, V/U=0.57 and

V/U=0.70, showed the same pressure peaks for the downstroke motion.

3.2.3 *Pressure Taps Well Downstream of Tip of Edge*

As shown in Figures 60 through 62, at the lowest velocity value of V/U=0.043, the second group of pressure taps responded in a manner similar to that of the first group of pressure taps discussed in the foregoing. They did not show a pronounced peak of the pressure signal.

Multiple positive and negative peaks were also obtained at the velocity V/U=0.087. For both of the cases V/U=0.043 and 0.087, the high frequency pressure signal is apparently dominated by the mechanical noise of the system at locations well downstream.

At the velocity V/U=0.19, there occurred first a negative peak and then multiple positive and negative peaks during the upstroke motion due to the high velocity flow structure. There was no significant change in the general form of the pressure signal for the downstroke motion of the cylinder at different pressure taps. As explained before, at this velocity there was vortex formation, but more than a vortex it was a kind of bubble (See Figure 22), which contributed to the pressure fluctuation after the initial pressure disturbance due to the potential flow distortion. For the downstroke motion, the angle of the vortex street, made up of small vortices, was small relative to the freestream. There was no single, well-defined peak of the pressure fluctuation during this downstroke motion.

When the velocity was increased to a higher value of V/U=0.38, a concentrated vortex was initially observed from the flow visualization experiments. When a negative peak occurred in the pressure signal, the center of the vortex was upstream of each pressure tap. The downstroke motion showed

only a negative, broad distribution of total fluctuating pressure value. The same pressure signal persisted for each tap during the downstroke motion.

For the higher value of the velocity V/U=0.57, a negative peak occurred between two positive peaks during the upstroke motion. The highly concentrated, initially-formed vortex was the reason for this kind of signal. When the negative peak occurred at each pressure tap, the center of the vortex was at that location. The downstroke motion showed a negative peak due to the small vortices impinging upon the edge surface (See Figure 24). The same pressure signal was obtained for each tap. It is clear that for the downstroke motion, the detailed flow structure did not depend on the different cylinder velocity values of V/U; however the angle of the wake formed from the translating cylinder did depend upon V/U. High velocities V/U produced a large angle and one negative peak. This was true irrespective of the value of velocity and the pressure tap under consideration.

At the highest velocity of V/U=0.70, the nature of the pressure signal did not change significantly. The first group of pressure taps from No. 14 through 18 showed, in general, only a single negative peak and there was no initial vortex when the negative peak occurred. For the second group of pressure taps from No. 20 through 24, the second negative peak occurred when the center of the vortex was at the location of the pressure tap. This observation reveals the strong effect of the initially formed vortex on the pressure fluctuation for the second group of pressure taps.

3.3 CORRELATION BETWEEN PRESSURE MEASUREMENTS AND FLOW VISUALIZATION

The main objective of this investigation was to understand the causes of

the unsteady pressure distribution on the edge surface by determining the correlation between the pressure measurements and the flow visualization. The case of the large-scale interaction D/T=0.5 was considered for the largest amplitude A/D=5. The unsteady pressure fluctuations during the upstroke motion of the cylinder were caused by : the flow distortion due to the finite thickness of the cylinder; the wake effect of the moving cylinder; and the effect of the mechanical noise. These three effects contributed, to varying degrees, to the pressure signal. Flow visualization photos and the pressure plots were correlated with each other in order to provide insight into the relative contributions of these sources. Six different cylinder velocities were considered: V/U=0.043; 0.087; 0.19; 0.38; 0.57; and 0.70 .

If a vortex translates along a flat surface, according to the potential flow solution, a negative peak of the surface pressure occurs beneath the center of the vortex. In this investigation, the elliptical leading-edge had a curved surface along which the pressure taps were located. The tangent to the surface of the edge varied with streamwise distance. It took on its maximum value of 90 degrees at the pressure tap No. 13, and decreased continously to approximately 5 degrees at the pressure tap No. 24. A large-scale vortex formed, and rolled up along this curved surface, at cylinder velocities of V/U=0.38, 0.57 and 0.70 . At the value of velocity V/U=0.19, instead of vortex formation, a bubble formation was observed.

To determine the origin of the pressure wave, it was necessary to carry out experiments with pressure taps clearly marked on the video. By knowing the location of the pressure taps, it was possible to determine if the vortex initially formed from the translating cylinder was above the pressure tap or not when there occurred a negative pressure peak. The procedure was to follow the initially-formed vortex along the edge in relation to the occurrence of the negative pressure

peaks. After the cylinder started its upstroke motion, the instant of occurrence of the first negative peak was defined from the pressure signal plot. Then, still pictures of the flow visualization video were taken using the same time sequence to determine the location of the initially-formed vortex. Using this approach it was straightforward to correlate the flow visualization and the pressure measurement experiments for the same time sequence. In general, it was observed that the center of the initially-formed vortex could be located upstream of, or at downstream of the pressure tap at which there occurred a negative peak.

To determine this correlation, only three different velocities were chosen: V/U=0.043 (the lowest velocity); and V/U=0.57 and V/U=0.70 (the highest velocity). At these values of velocity, three pressure taps were considered: pressure tap No. 13 (the pressure tap at the tip of the edge), tap No. 17 (the pressure tap downstream of the tip) and tap No. 24 (the pressure tap furthest downstream of the tip).

3.3.1 *Pressure fluctuations at tip of edge*

At the first pressure tap No. 13, for the lowest cylinder velocity of V/U=0.043, the pressure signal took the form of multiple peaks. The flow structure is correlated with this pressure signal in the following. As illustrated in Figure 63, before the cylinder crossed the tip of the edge, the pressure disturbance was evident due to flow distortion by the finite-thickness cylinder (first photo). During the downstroke motion, the same kind of pressure signal was obtained. At this value of V/U=0.043, there was no initial vortex formation from the translating cylinder immediately after it passed the leading-edge. The unsteady flow structure consisted of many small vortices (sixth and seventh photos), which may contribute to the pressure peaks, perhaps downstream of the tip. Also,

small vortices impinging upon the edge surface during the downstroke motion (ninth photo) may have affected the pressure signal. When the cylinder velocity was increased to the value of V/U=0.57, there was an initially-formed vortex due to the high cylinder velocity and this vortex contributed to the pressure fluctuation, at least in regions downstream of the tip. The pressure signal was identical during the upstroke and downstroke motions because of symmetry. At the highest velocity of V/U=0.70, the same kind of pressure signal was obtained as in the previous velocity case. For both V/U=0.57 and 0.70, the pressure fluctuation began before the cylinder crossed the tip of the edge, as illustrated in the first photos of Figures 64 and 65. Again, this was because of the flow distortion by the finite-thickness cylinder. Also the third photos of these figures show the relation between the location of the initial vortex and the pressure signal at the tip. The mechanical noise effect was not apparent at these high velocities.

3.3.2 *Pressure fluctuations immediately downstream of tip of edge*

For the pressure tap No. 17, at the lowest velocity of V/U=0.043, the multiple peaks were again obtained during the upstroke and downstroke motions. The first photos of Figures 66, 67 and 68 show the effect of the flow distortion by the finite-thickness cylinder on the formation of the pressure signal at the velocity values V/U=0.043, 057 and 0.70 . These photos show that the pressure fluctuation began before the cylinder crossed the edge. Although, many small vortices were produced at the velocity value of V/U=0.043, they lost their coherence as they moved downstream. Therefore, it is likely that the mechanical noise effect contributed to the formation of the pressure peaks more than the effect of the unsteady flow structure. This is shown on the region of the pressure trace lying between the third and fourth photos of Figure 66. During the

downstroke motion, the pressure signal also exhibited very high frequency fluctuations.

For the higher velocity V/U=0.57, the third photo of Figure 67 shows the location of the pressure tap and the initial vortex. When negative peak occurred, the initial vortex was nearly above the pressure tap. This meant that the effect of the initially-formed vortex on the pressure signal was more predominant than the other sources. During the downstroke motion, as shown between the sixth and seventh photos of Figure 67, when the oncoming wake impinges upon the leading-edge, the unsteady pressure shows a positive peak. Also the bubble formed from the translating cylinder causes a negative peak after the cylinder crosses the tip of the edge, as illustrated between the seventh and eighth photos of the same figure.

At the velocity of V/U=0.70, the same kind of pressure signal was obtained as in the previous case with only one difference. There was no vortex on the edge surface when the negative peak occurred at the pressure tap No. 17. During the downstroke motion, the oncoming wake impinged upon the leading-edge causing a positive peak as shown in the fourth and fifth photos of Figure 68. The reason for the unsteady pressure going to a negative value was again the moving bubble on the edge surface shown between the fifth and sixth photos of the same figure.

For the downstroke motion, the pressure signal changed its form at the pressure taps located further downstream because of the angle of oncoming wake. This angle was large for the higher velocities. The fourth photo of Figure 66, sixth photo of Figure 67 and fourth photo of Figure 68 show the angle of wake very well. The fourth photo of Figure 68 shows a large angle of about 35 degrees with respect to the free stream.

3.3.3 *Pressure fluctuations immediately downstream of tip of edge*

For the last pressure tap No. 24, at the lowest velocity of V/U=0.043, the pressure signal (See Figure 69) was same as that at the upstream tap (No. 17). Many small vortices were formed and then lost their concentration as they moved downstream. The mechanical noise effect shows large amplitude fluctuations in the pressure signal.

When the velocity was increased to V/U=0.57, the highly concentrated vortex contributed to the appearence of the negative pressure peak, as illustrated in the third photo of Figure 70. The center of the vortex was nearly above the pressure tap when the negative peak occurred. During the downstroke motion, the wake of the cylinder impinged upon the edge and then a moving bubble caused a negative peak as shown in the sixth photo of Figure 70.

The velocity V/U=0.70 showed two negative peaks in the pressure trace for the upstroke motion. The highly concentrated vortex was above the pressure tap when the second negative peak occurred, as illustrated in the third photo of Figure 71. The pressure disturbance for the downstroke motion began when the wake of the cylinder impinged upon the edge surface as shown in the fifth and sixth photos of Figure 71. After the impingement process, a bubble-type flow structure remained on the edge surface and moved downstream. The sixth and seventh photos of Figure 71 show the reason for the negative pressure peak due to this flow structure.

Several basic mechanisms occur in the foregoing. First, the effect of the flow distortion of the finite cylinder creates a pressure wave on the edge; then, the effect of the unsteady flow structure, or the effect of the mechanical noise of cylinder-edge system, becomes the predominant contributor to the pressure signal.

At low velocities, the contribution of the mechanical noise effect may be of the same order as the effect of the flow structure. Small vortices can not retain their concentration as they move downstream and this weakens the effect of the flow structure. At high velocities, the effect of the highly concentrated, initial vortex contributes to the formation of the pressure fluctuation more than the effect of the mechanical noise showing single positive and negative peaks. During the downstroke motion, at low velocities, the wake of the cylinder takes the form of a street of small vortices impinging upon the edge surface. At high velocities, large-scale vortices appear in the cylinder wake and the angle of the wake becomes large. For the downstroke, the upstream pressure taps are more sensitive than the downstream pressure taps due to the fact that they experience the wake before the downstream taps. Consequently, the pressure taps located further downstream respond to the pressure fluctuation after the taps in the tip region during the impingement process, because of the impingement angle of the oncoming wake.

The relation between the vortex motion and the first negative peak motion is given in Figure 72 for the translating cylinder when V/U=0.57. It is important to note the similarity between the curves of the vortex and peak motions. This similarity means that when the negative peak occurred, the vortex was nearly above the pressure tap.

CHAPTER 4

4. CONCLUSIONS

The interaction of a wake formed from a translating cylinder with a finite-thickness leading-edge showed many interesting features. The most important ones are described in the following .

Large-Scale Interaction at Large Amplitude of Cylinder Motion

When the large-scale vortex-edge interaction was considered for the largest amplitude case A/D=5, three different flow regimes were observed from the flow visualization experiments. These regimes are detailed in terms of the dimensionless velocity V/U of the cylinder translation.

The first regime involved generation of a number of small vortices at the lowest values of cylinder velocity $V/U \leq 0.19$. These small-scale vortices moved downstream along the edge surface after they formed from the translating cylinder. In this regime, there was no formation of a large-scale vortex along the edge and the most important feature of the unsteady flow structure was the fluid injection process between the backface of the translating cylinder and the tip of the edge. Examination of the timeline markers of the bubble visualization revealed that the injection velocity was of the same order as the free stream velocity. Moreover, secondary vortex formation was observed in this low velocity regime.

The second regime, corresponding to values of $0.38 \leq V/U \leq 0.94$, showed a large-scale, initially-formed vortex moving downstream while keeping a nearly constant distance between its center and the edge surface. At the higher values of cylinder velocity in this regime, the initial vortex did not travel along the edge for

a significant streamwise distance.

In the third regime, corresponding to high velocities, $V/U \geq 1.11$, the vortex formation occurred much later during the cylinder motion, and was not as coherent as in the foregoing cases; the vortical structures rapidly became turbulent.

Large-Scale Interaction at Small Amplitude of Cylinder Motion

When the smallest amplitude case, $A/D=1$, was considered, two "resonant" values of V/U were apparent at the velocities $V/U=0.54$ and 0.92 . At $V/U=0.54$, the flow structure showed a single vortex moving along the edge surface. The second "resonant" value $V/U=0.92$ introduced a large-scale vortex pair moving downstream along the edge.

Small-Scale Interaction at Large Amplitude of Cylinder Motion.

For the small-scale interaction, at the largest amplitude $A/D=20$, the translating cylinder showed a well-defined vortex street with an inclination at an angle of γ. The value of γ was equal to the tangent of dimensionless V/U. Moreover, for the amplitude $A/D=8$, the vortex street had a curved shape in the middle of its centerline. This curvature was due to the influence of the end of the upstroke motion of the cylinder. When it stopped, then started its downstroke motion, the vortex-vortex interactions took on a different form.

For all cases, the flow structure of the downstroke motion involved two different phases. During the first phase, the oncoming wake impinged upon the edge surface at an inclination angle γ. During the second phase, the distorted wake moved downstream along the edge surface.

Large-Scale Interaction: Pressure Measurements

When the pressure measurements were carried out for the largest amplitude A/D=5 value at six different cylinder velocities in the range $0.043 \leq V/U \leq 0.70$, it was observed that the response of the pressure taps along the edge could be classified into three different groups according to the similarity of their response to the pressure fluctuation : the pressure tap at the tip of the edge; the pressure taps located immediately downstream of the tip; and the pressure taps located well downstream of the tip of the edge.

Three different effects contributed to the pressure signal. These effects were deduced from correlation of the flow visualization photos and the pressure measurement plots for the upstroke motion. The effects were: the flow distortion due to the finite size of the cylinder; the wake effect of the moving cylinder related to the initially-formed vortex; and the effect of the mechanical noise. In all cases, the beginning of the pressure fluctuation was due to the effect of the flow distortion by the finite-size cylinder. The mechanical noise effect contributed significantly to the pressure fluctuation at the lowest values of cylinder velocity where the unsteady flow structure was in the form of many small-scale vortices along the edge. These small vortices lost their concentrations as they moved downstream. At the high velocities, the contribution of the unsteady flow structure to the formation of the pressure signal was due to the highly concentrated, initially-formed vortex.

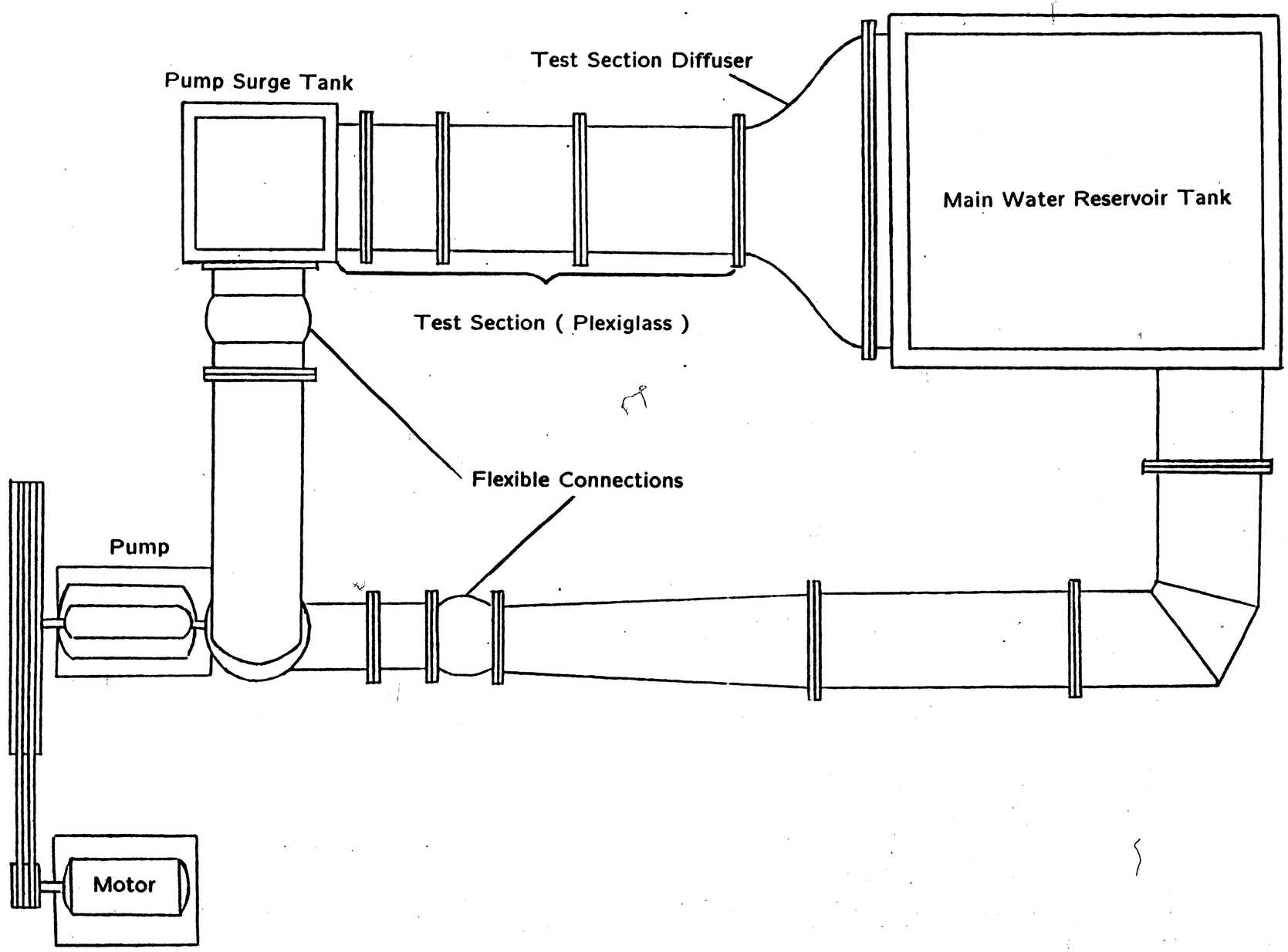

Figure 1 : Plan view of the closed loop water channel.

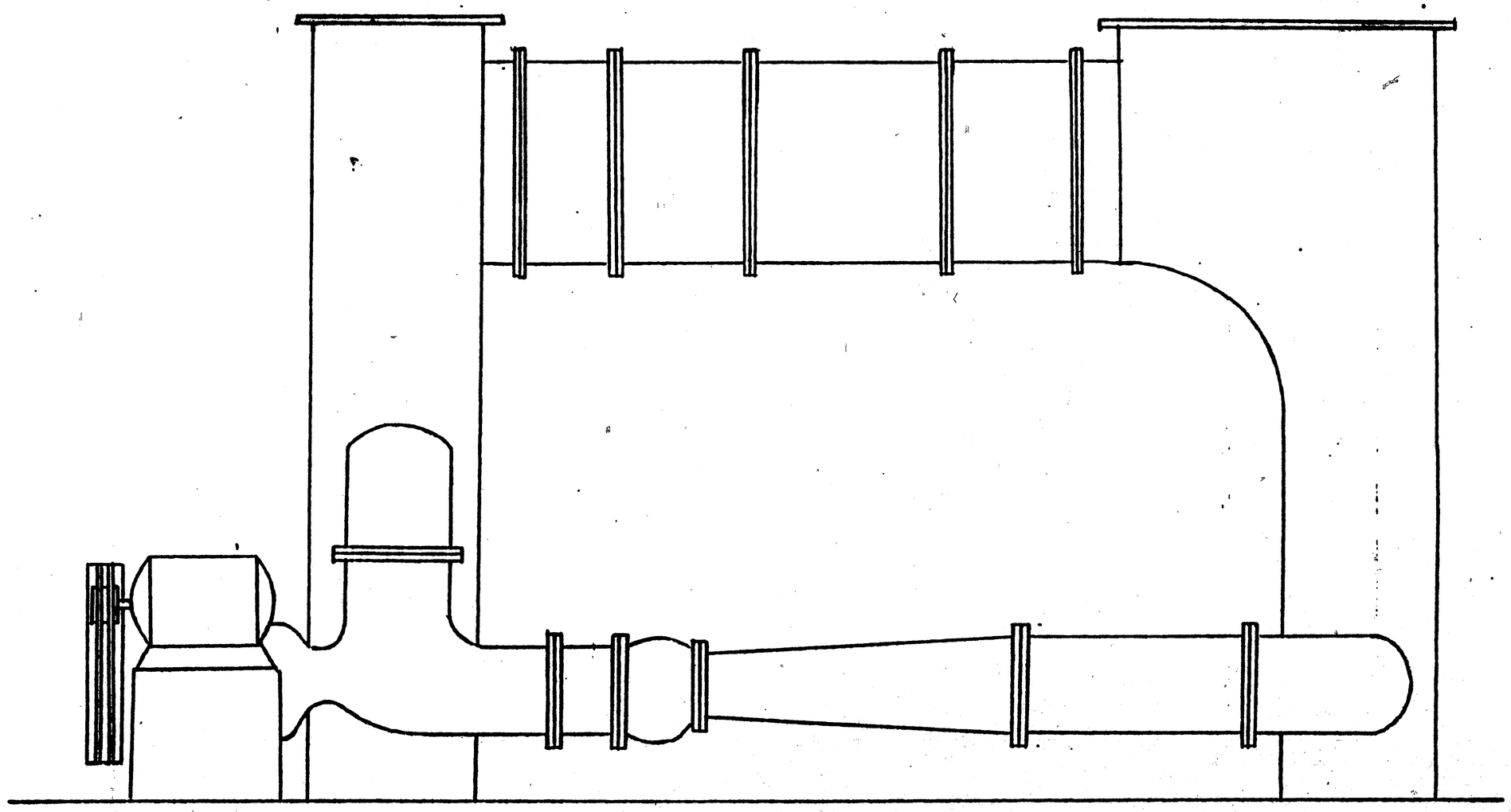

Figure 2 : Front view of the closed loop water channel.

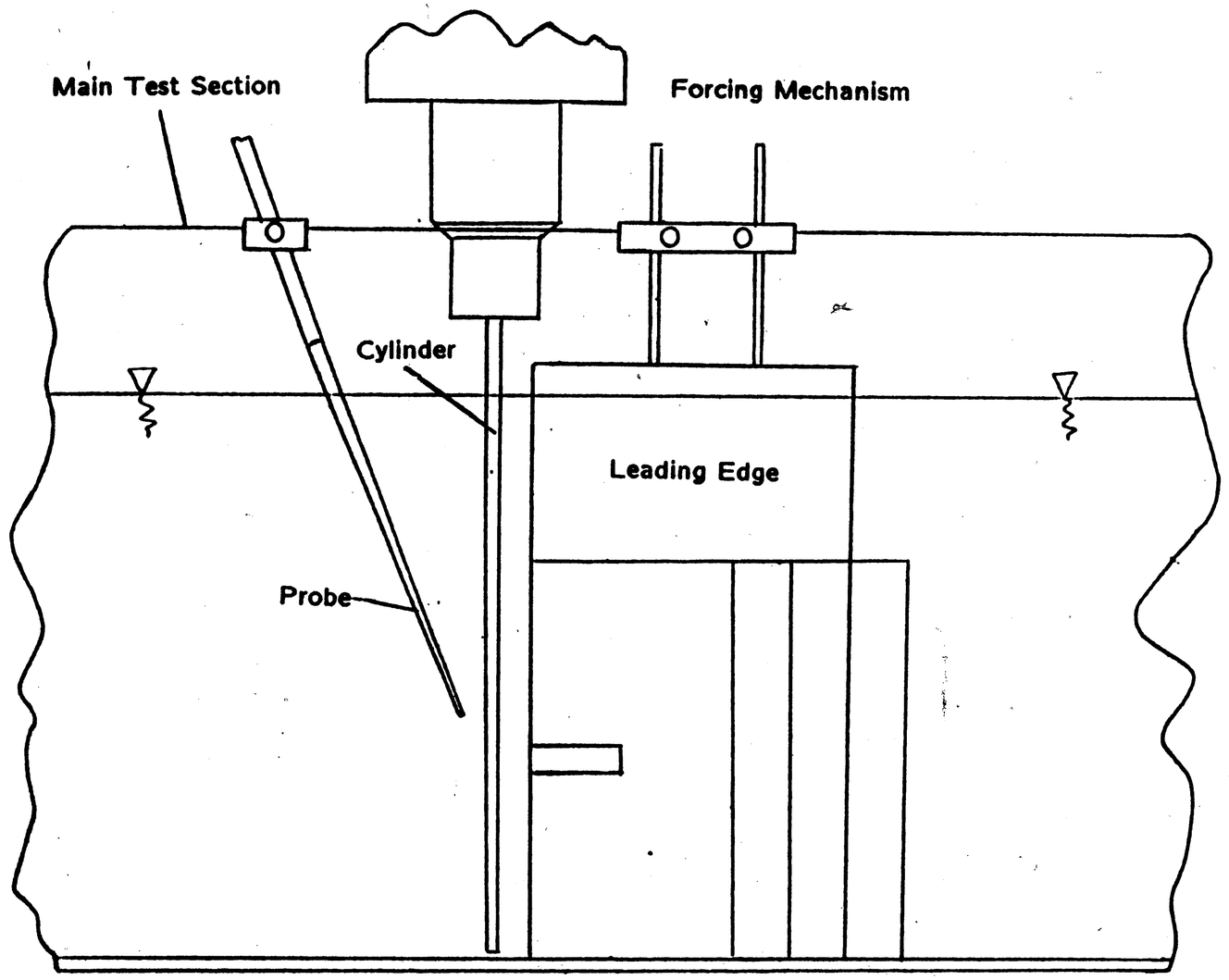

Figure 3 : Front view of the experimental set-up.

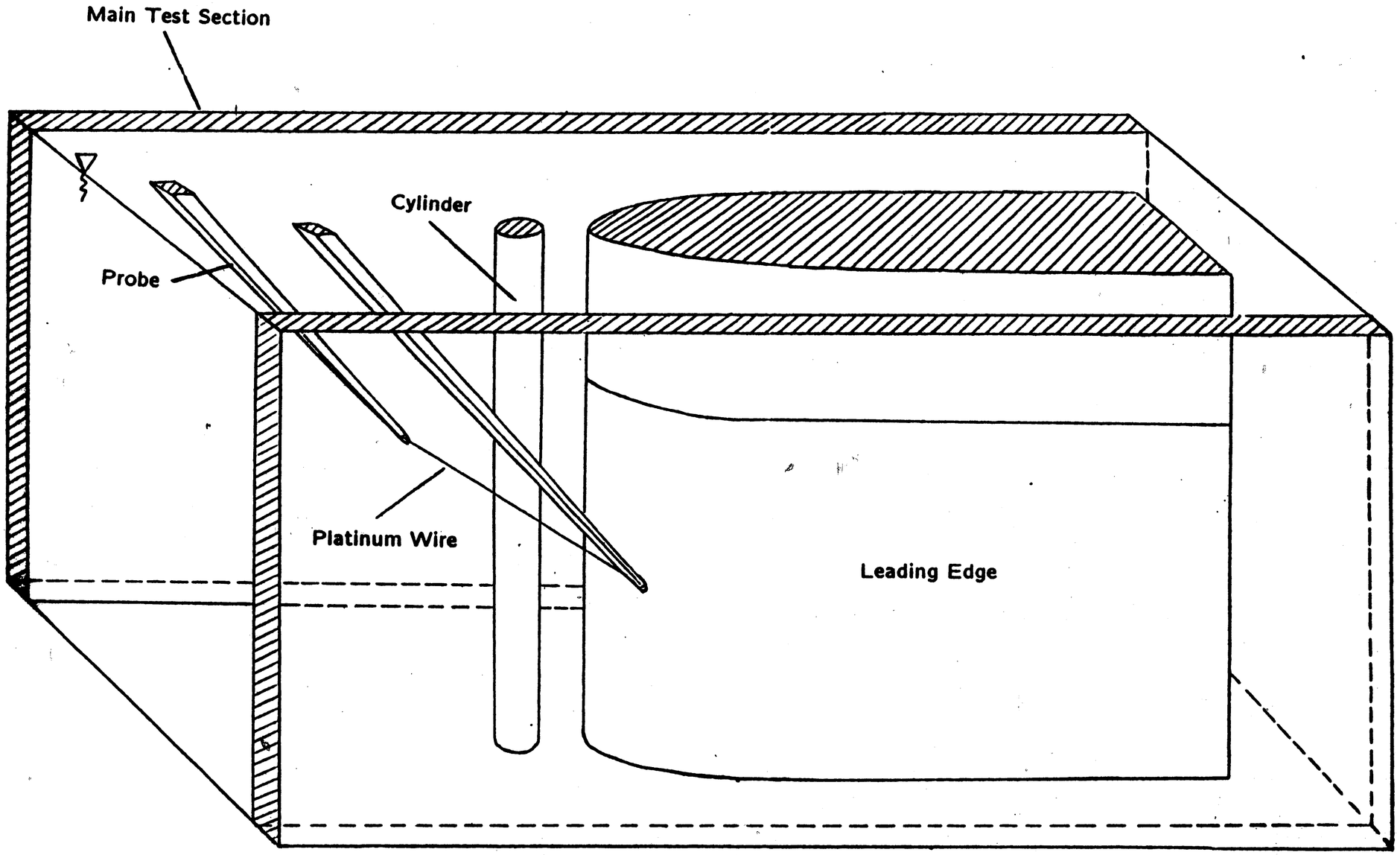

Figure 4 : Close-up view of the experimental set-up.

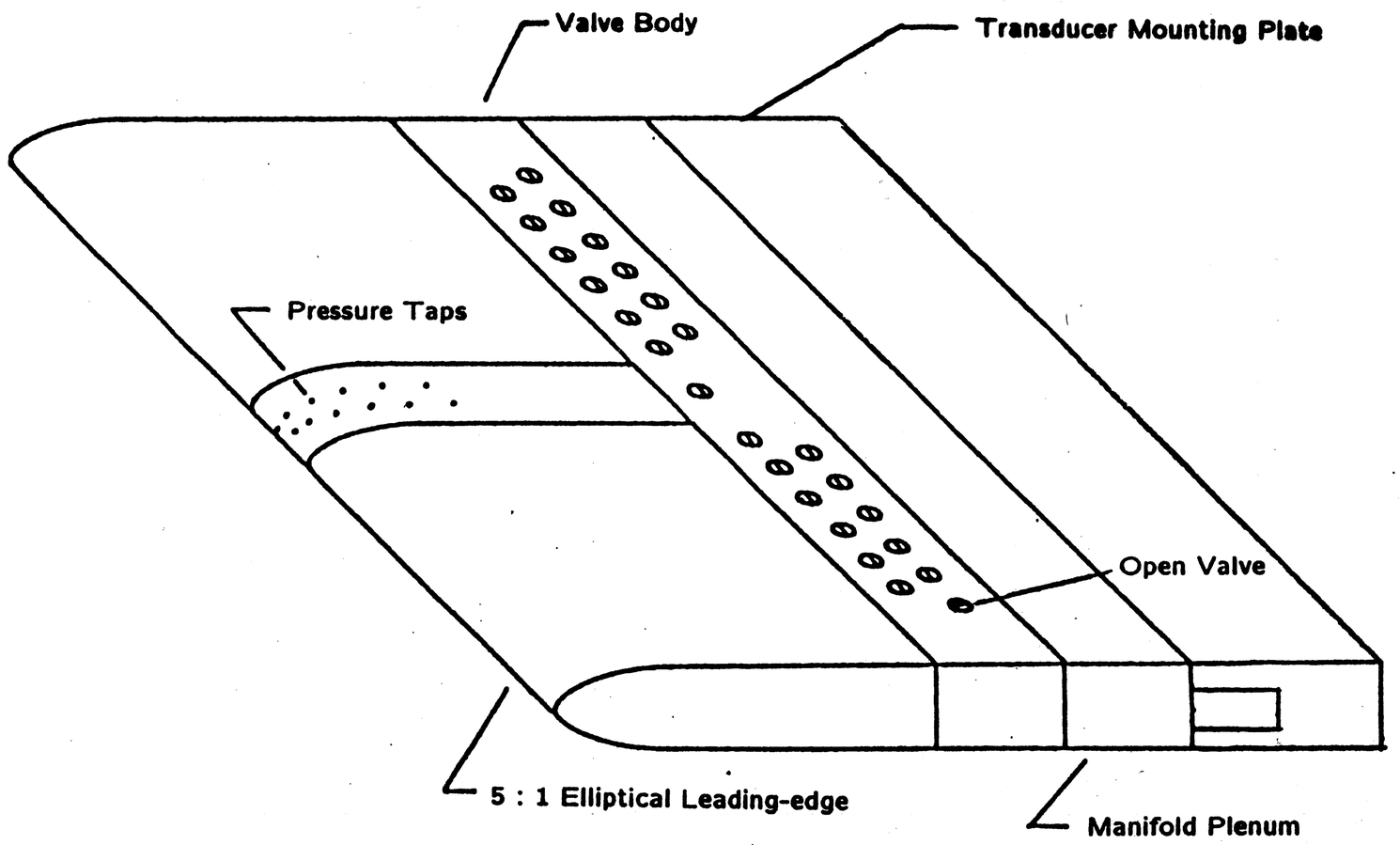

Figure 5 : Elliptical finite thickness leading-edge. (Scale 2.5 : 1)

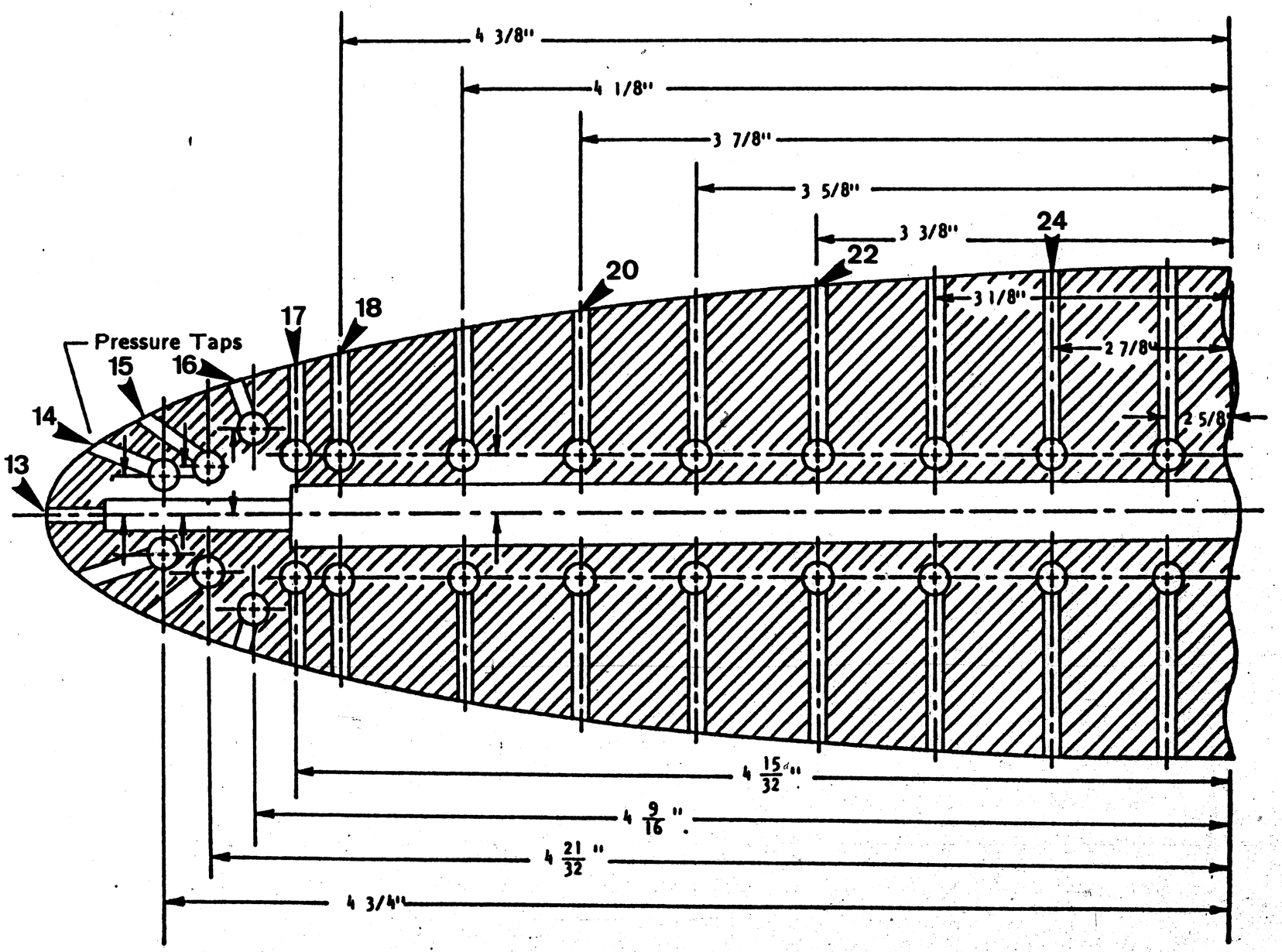

Figure 6 : Details of tap and brass tubing locations on the elliptical leading-edge. Reproduced from Sohn (1985).

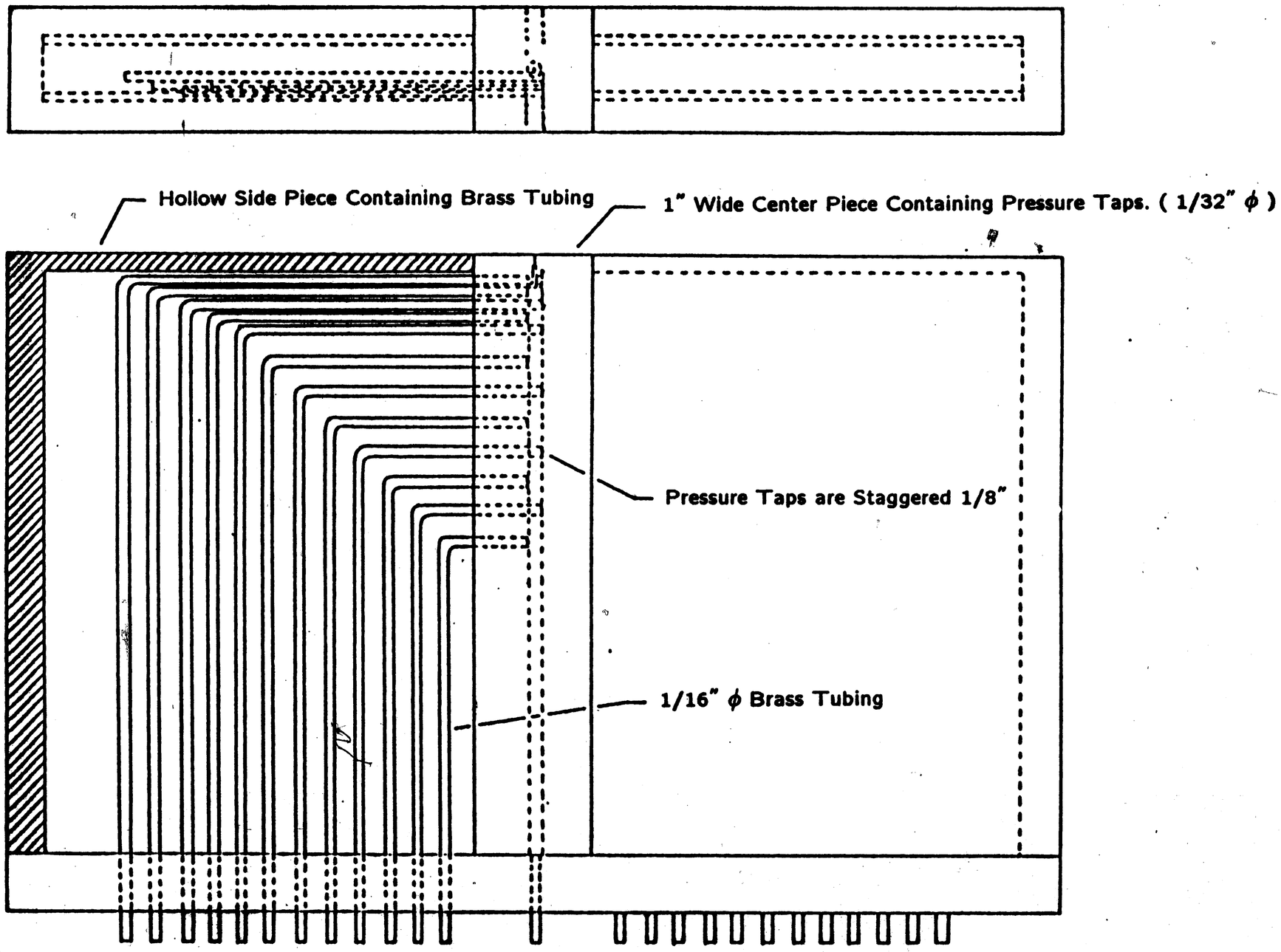

Figure 7 : Brass tubing layout for 5 : 1 elliptical leading-edge. (Scale 1.42 :1) Reproduced from Sohn (1985).

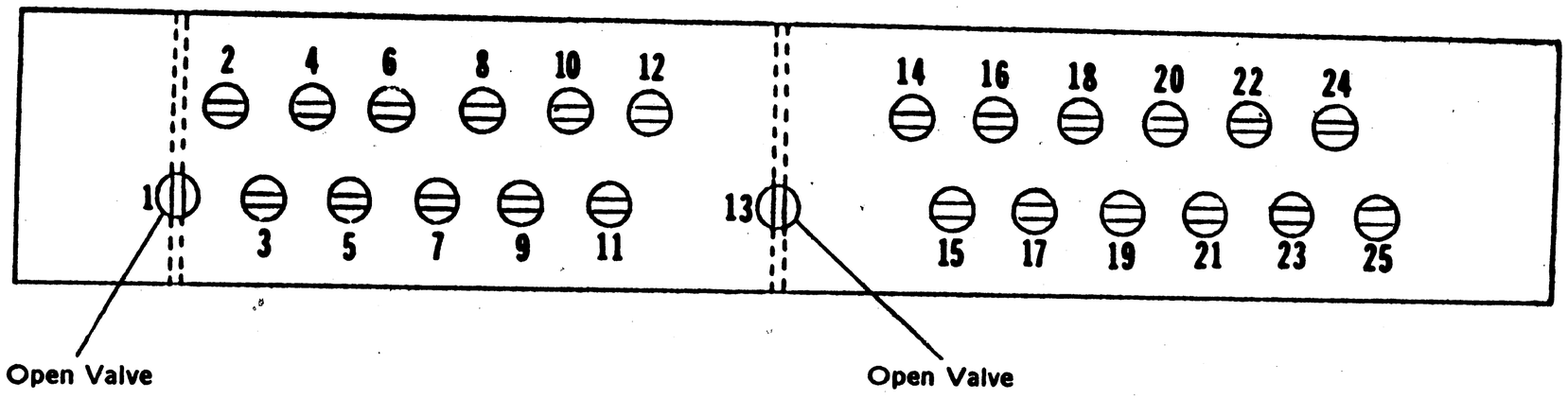

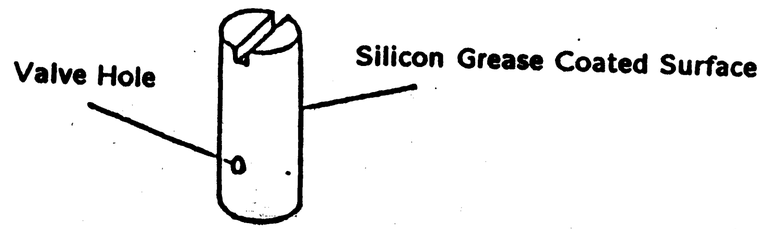

Figure 8 : Tap No.1 and Tap No.13 are opened, all the others are closed. Reproduced from Sohn (1985).

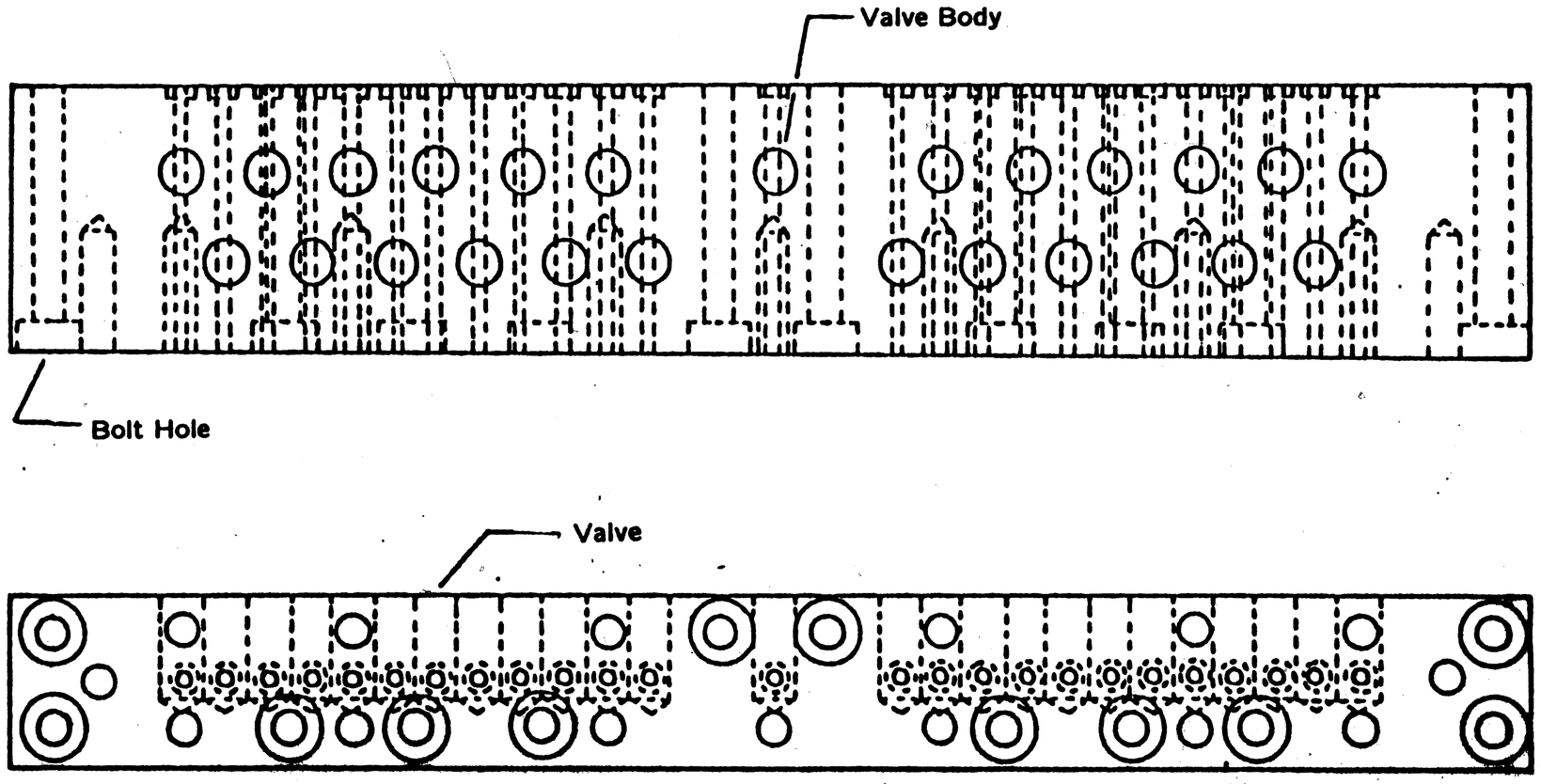

Figure 9 : Valve body section containing 25 valves for the individual pressure taps. Reproduced from Sohn (1985). (Scale 1.25 : 1)

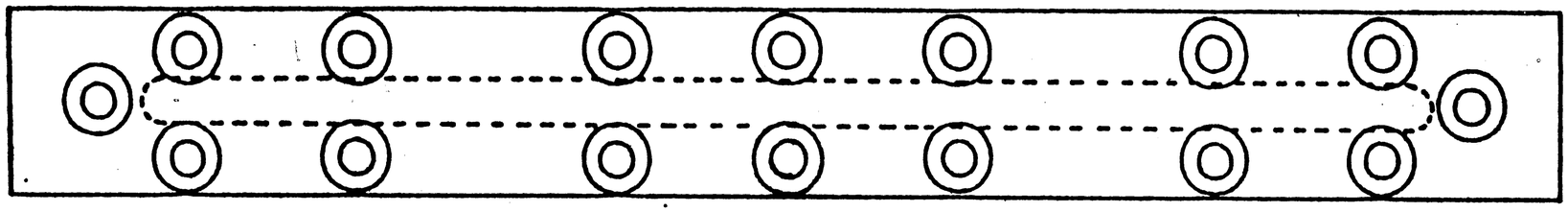

Figure 10 : Manifold plenum containing the pressure hole for the transducer. Reproduced from Sohn (1985). (Scale 1.25 : 1)

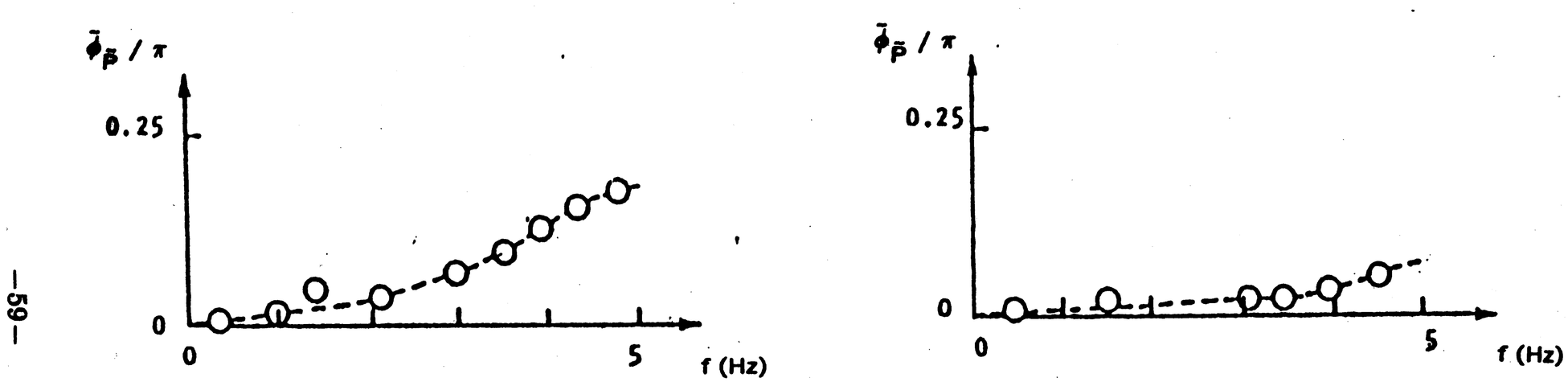

Figure 11 : Phase shift for tap No. 1 and tap No. 13. Reproduced from Sohn (1985).

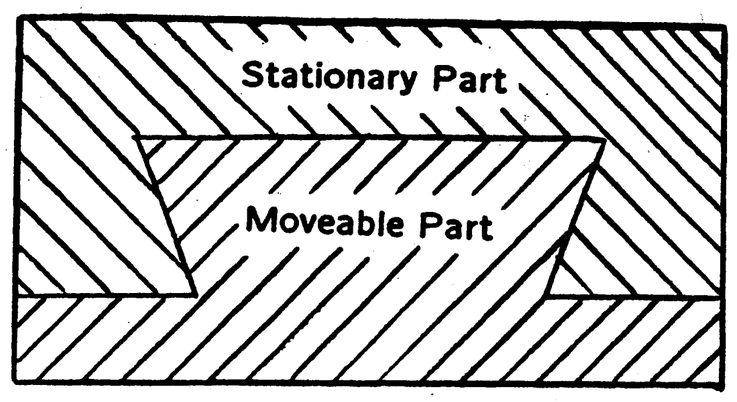

Dovetail Slide

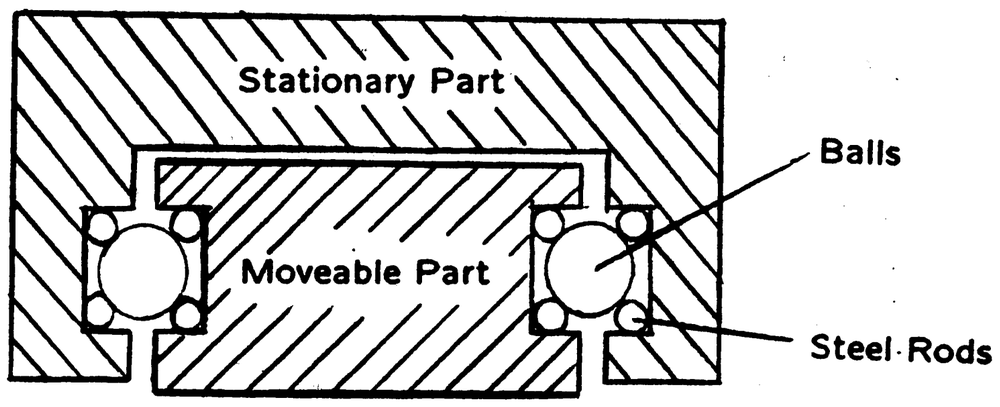

Ball Slide

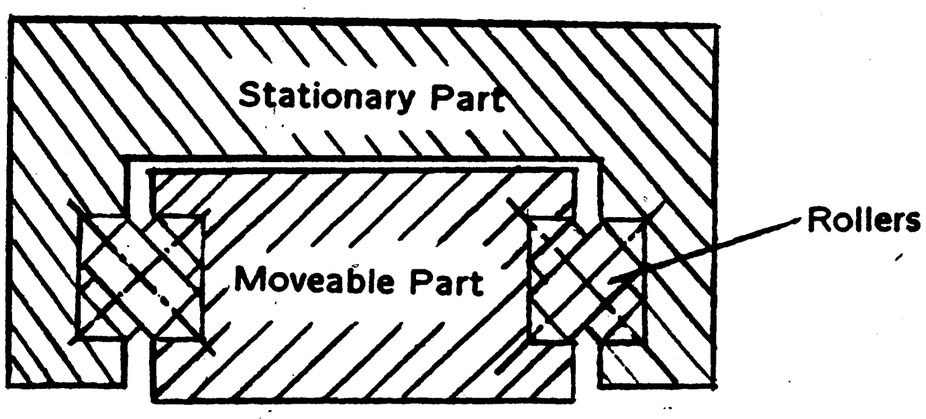

Crossroller Slide

Figure 12 : Different slide mechanisms to produce the linear motion.

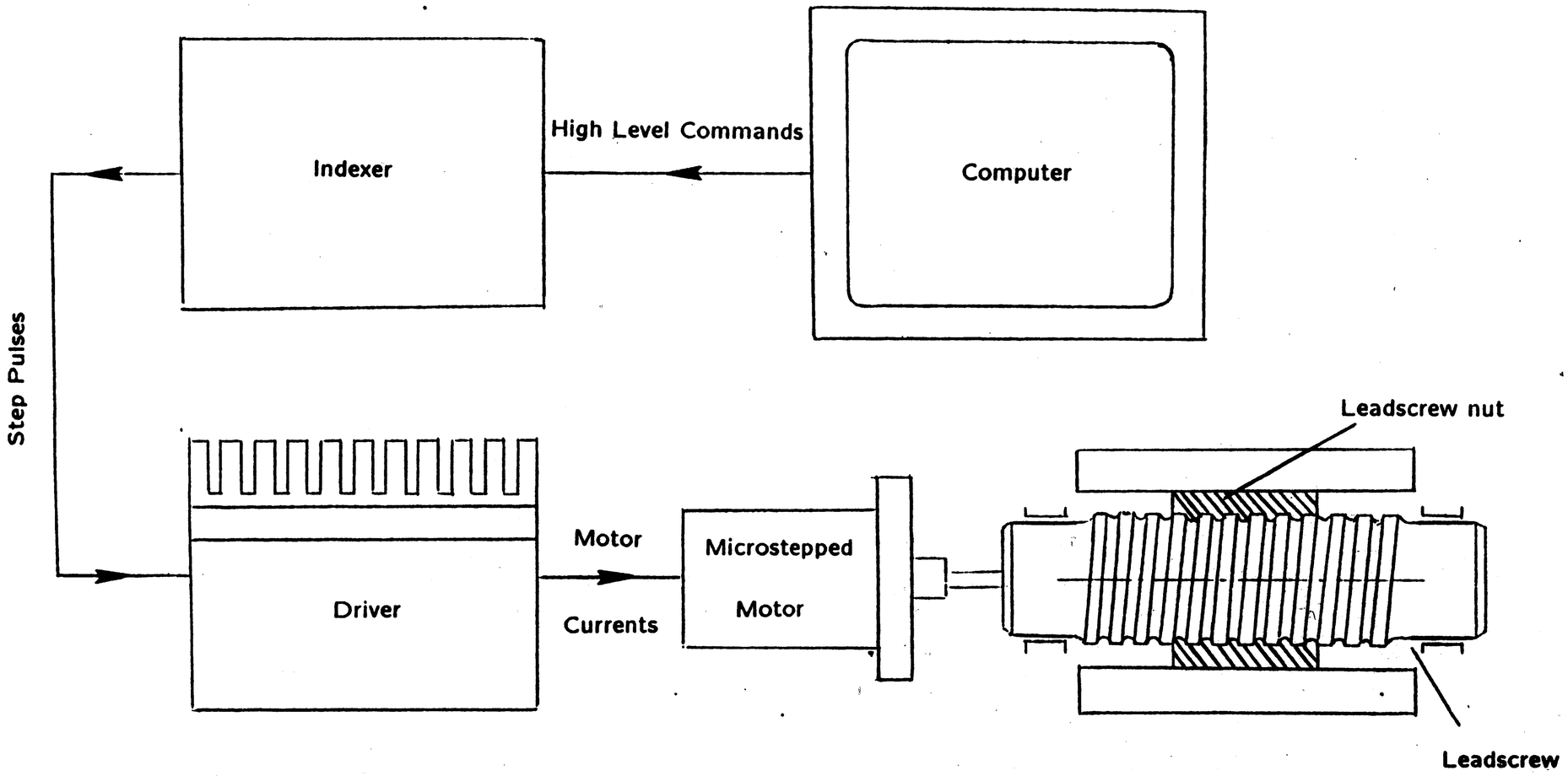

Figure 13 : The Compumotor control system.

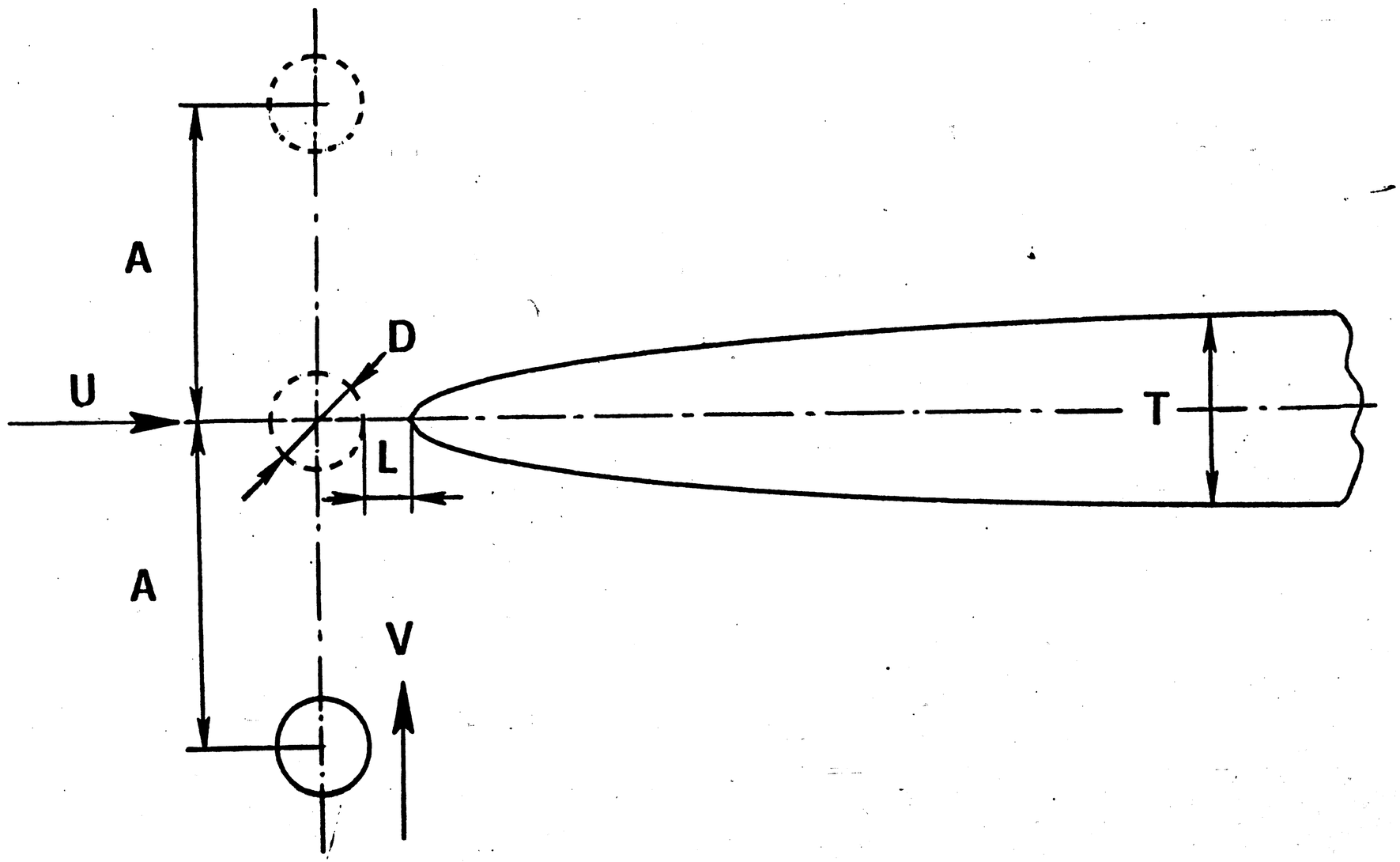

Figure 14 : Variables for the experiments.

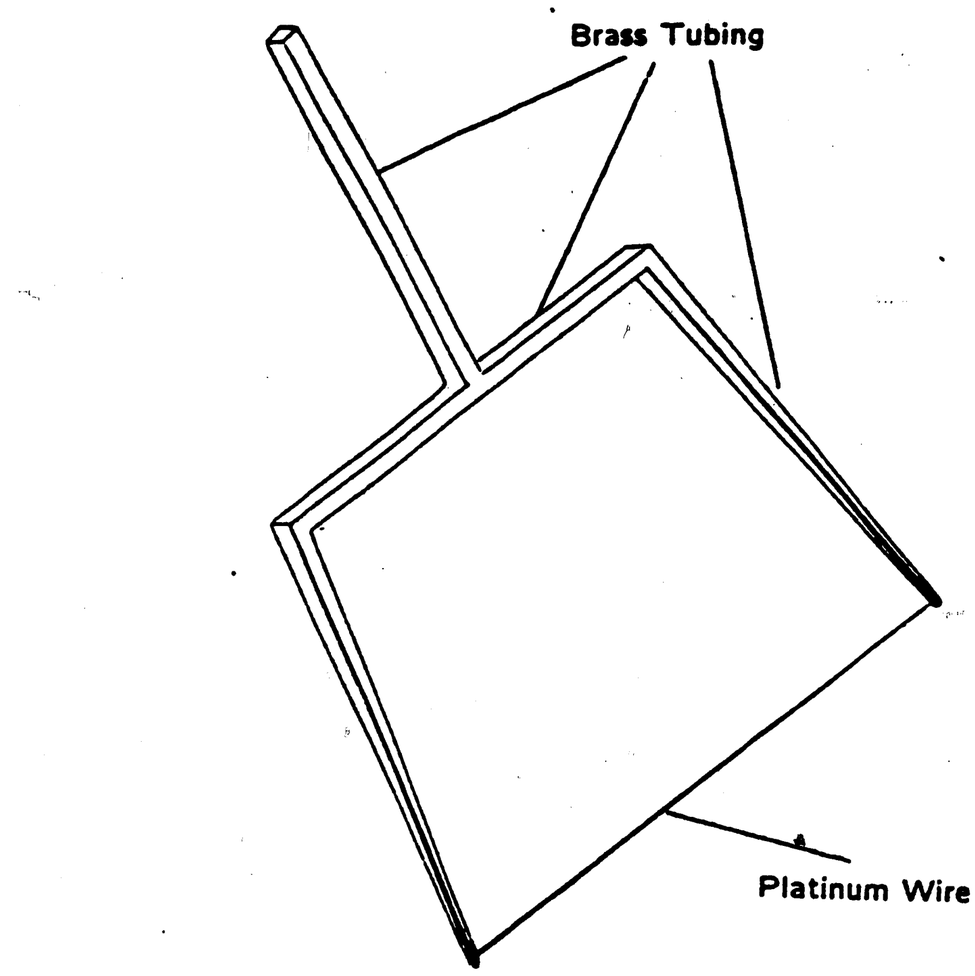

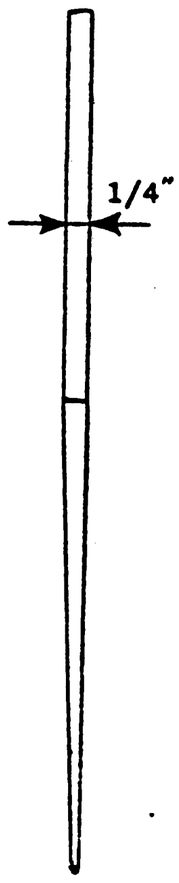

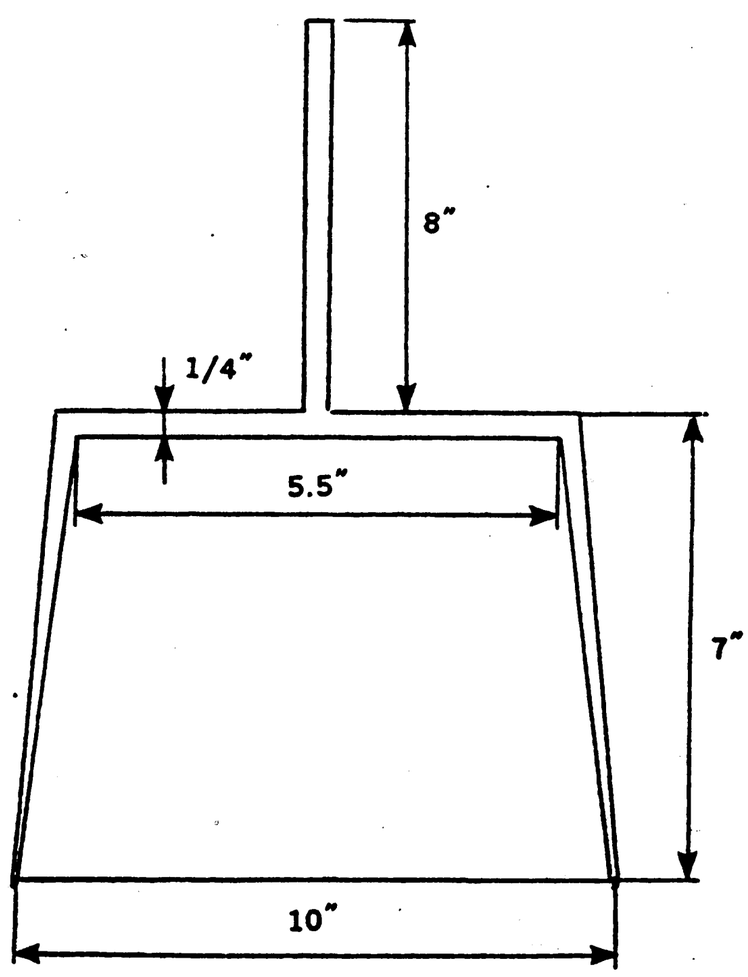

Figure 15.: Hydrogen bubble probe.

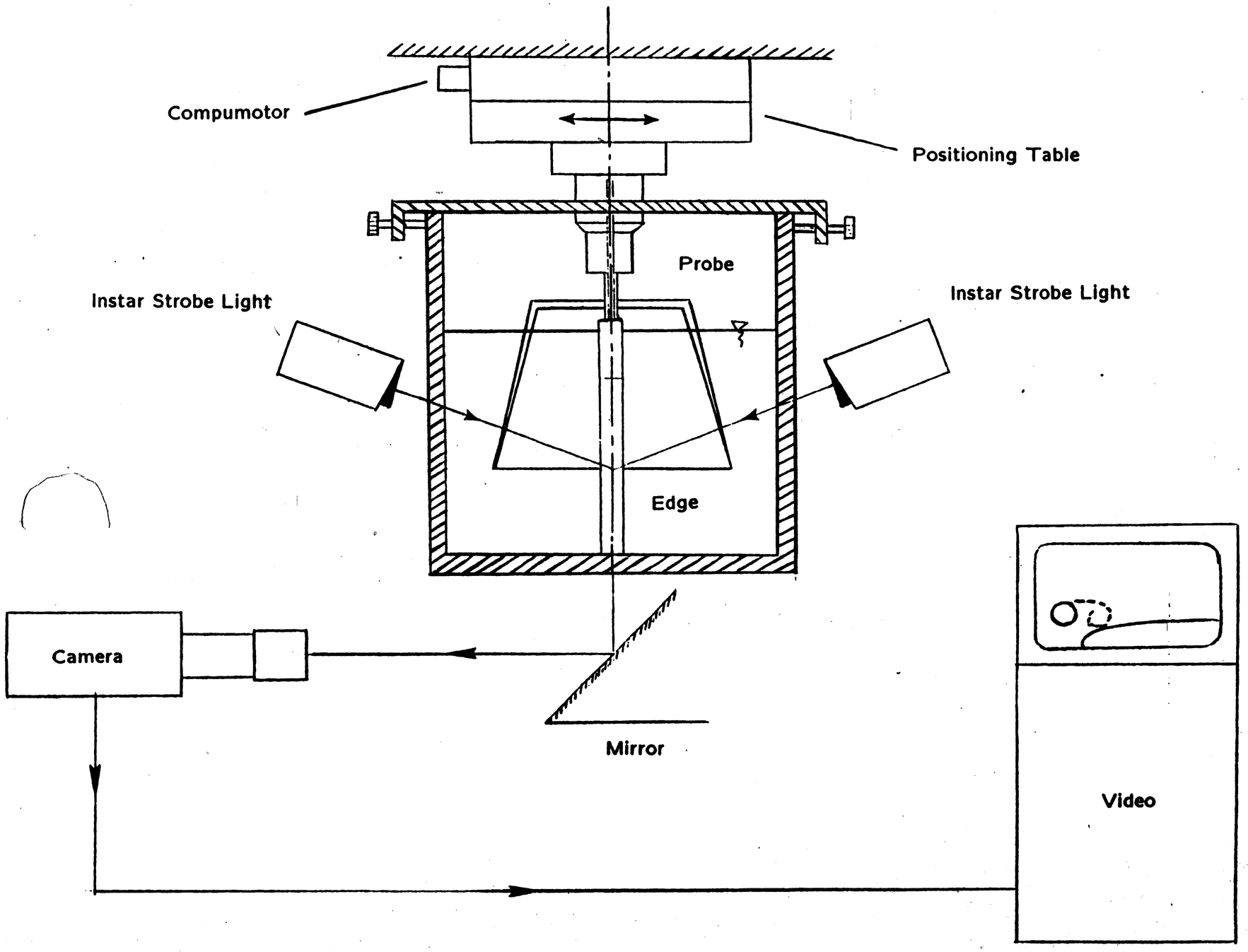

Figure 16 : Overview of flow visualization experiments.

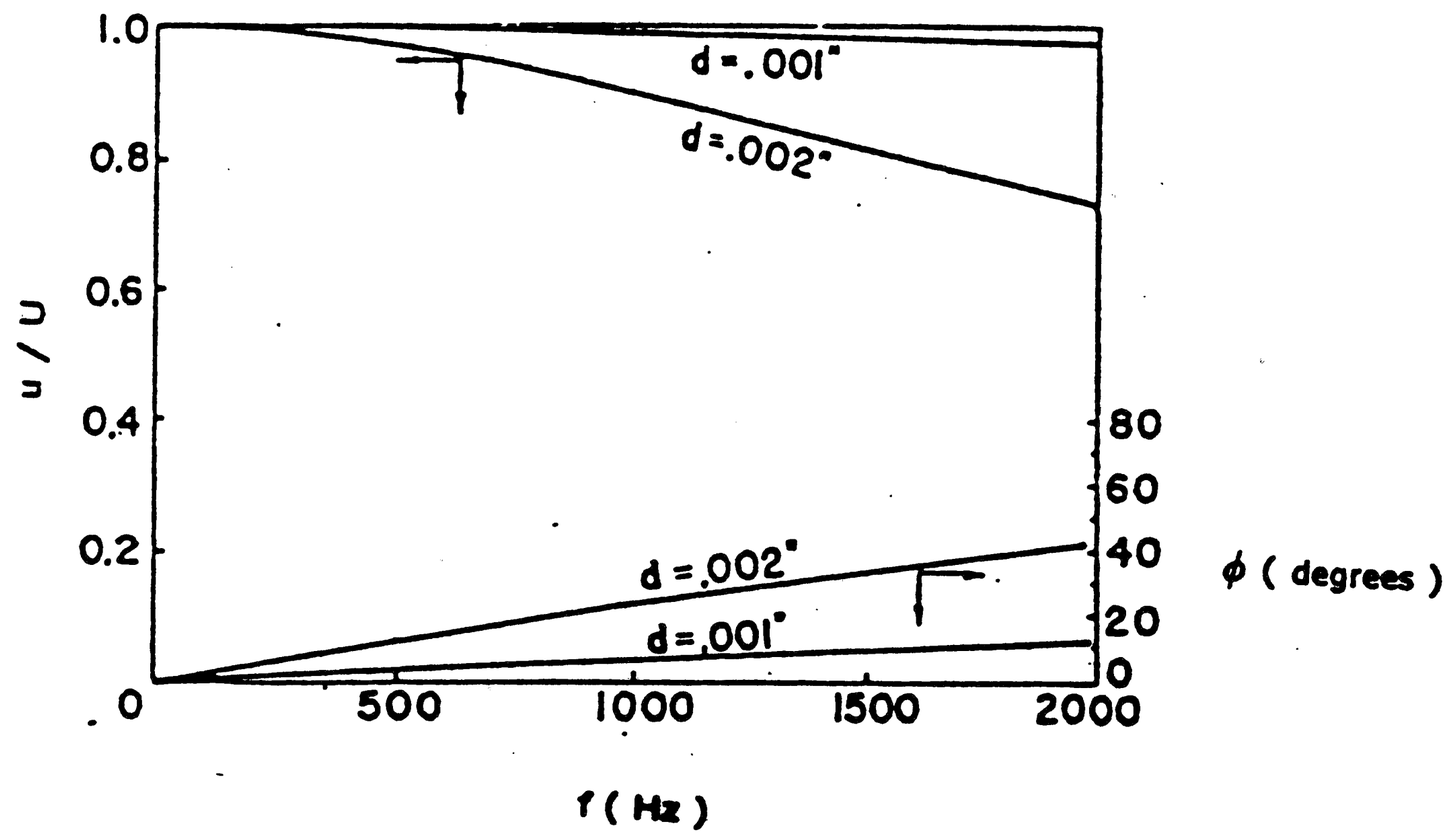

Figure 17 : Frequency response of Hydrogen bubbles. Reproduced from Schraub et al. (1965).

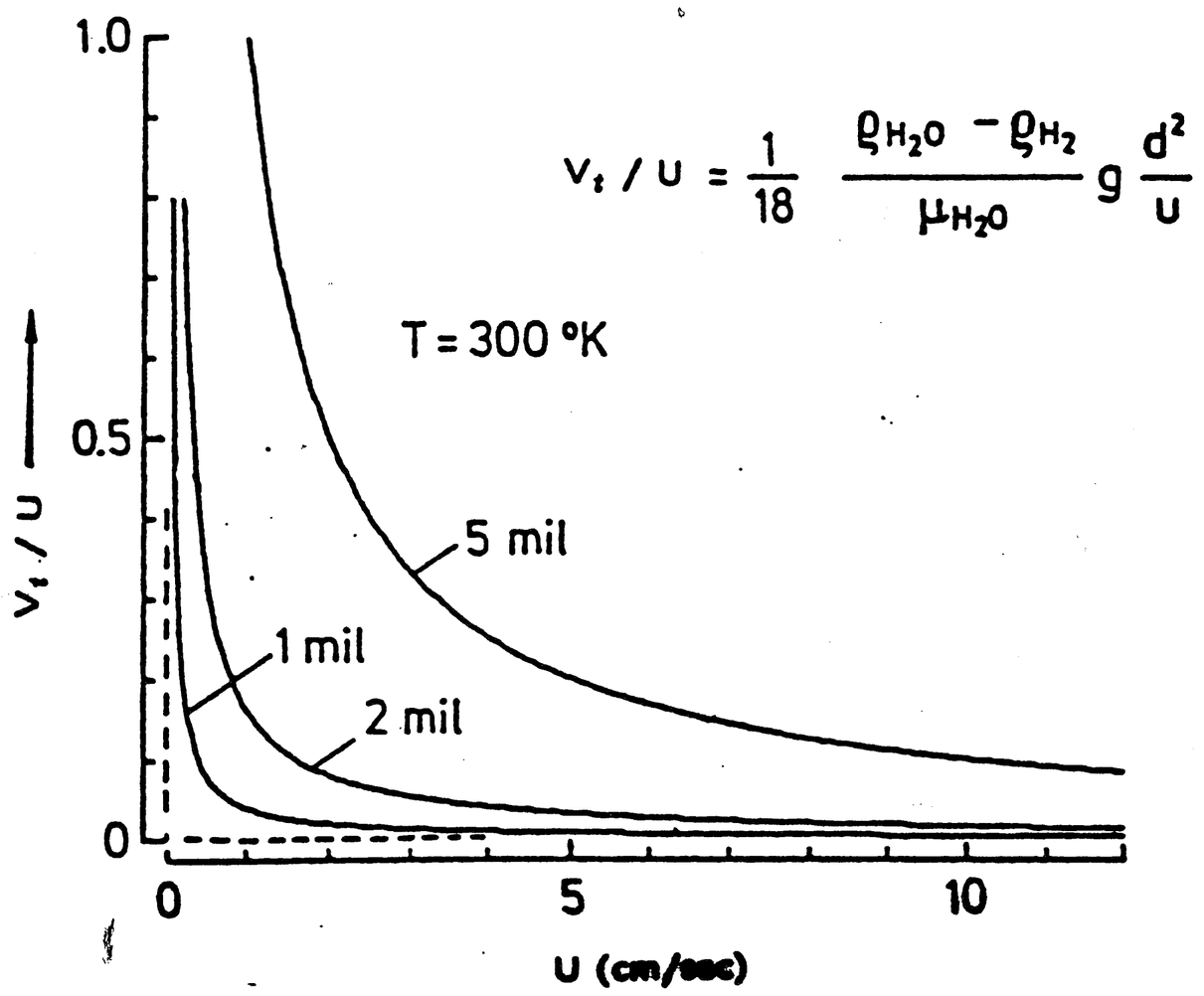

Figure 18 : Terminal rise velocity of Hydrogen bubbles from Lusseyran and Rockwell (1989).

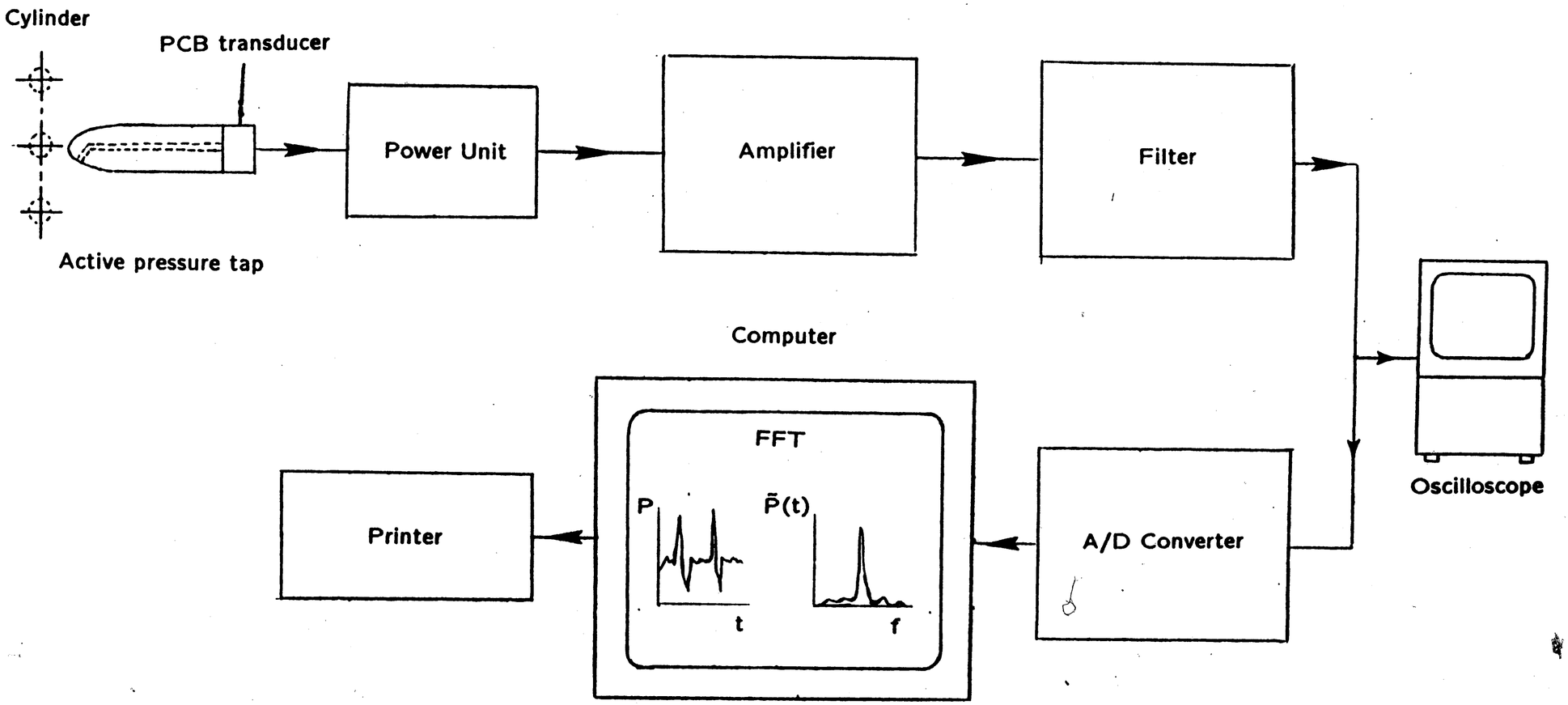

Figure 19 : Overview of pressure measurement experiments: data acquisition; cross spectral analysis.

V/U=0.043

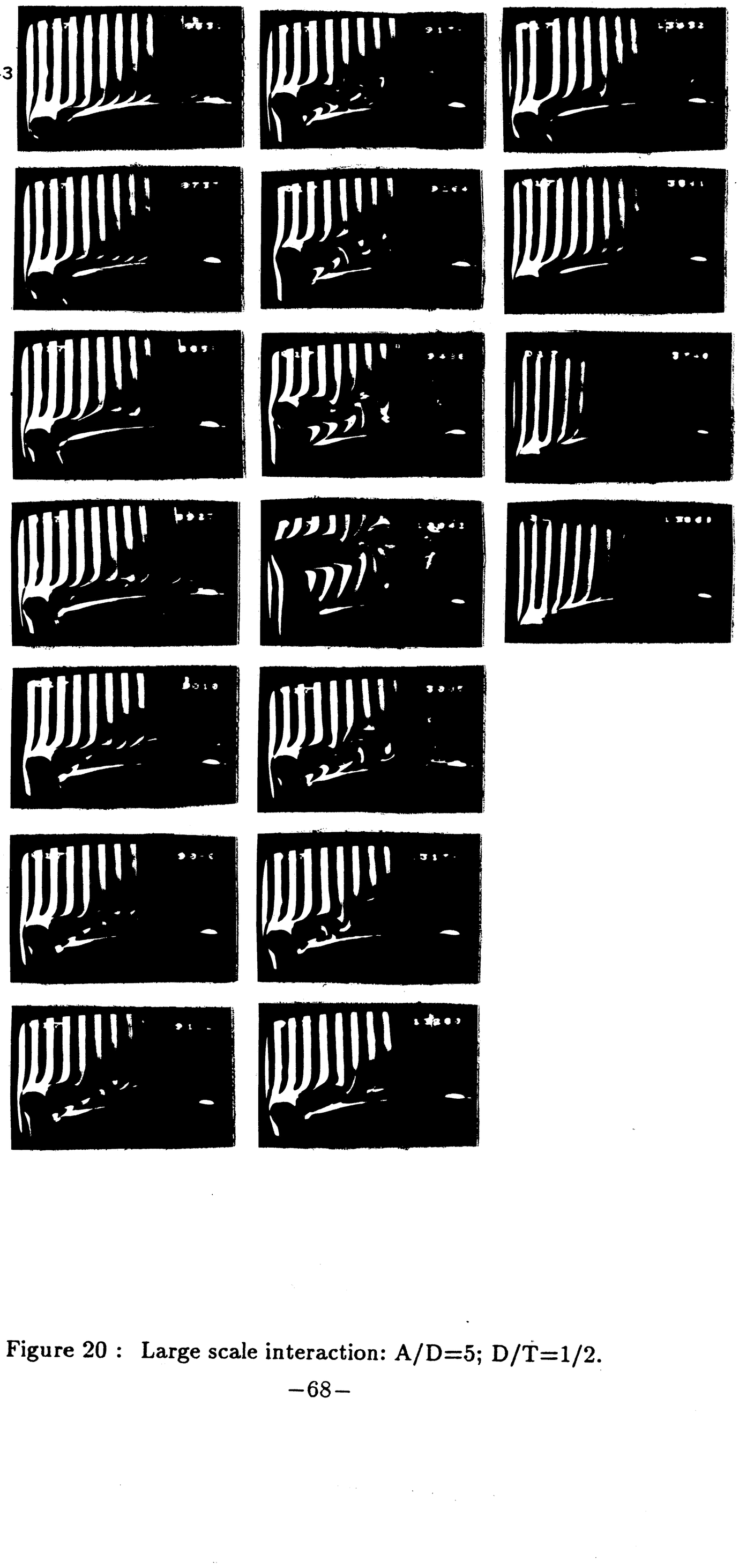

Figure 20 : Large scale interaction: A/D=5; D/T=1/2.

V/U=0.087

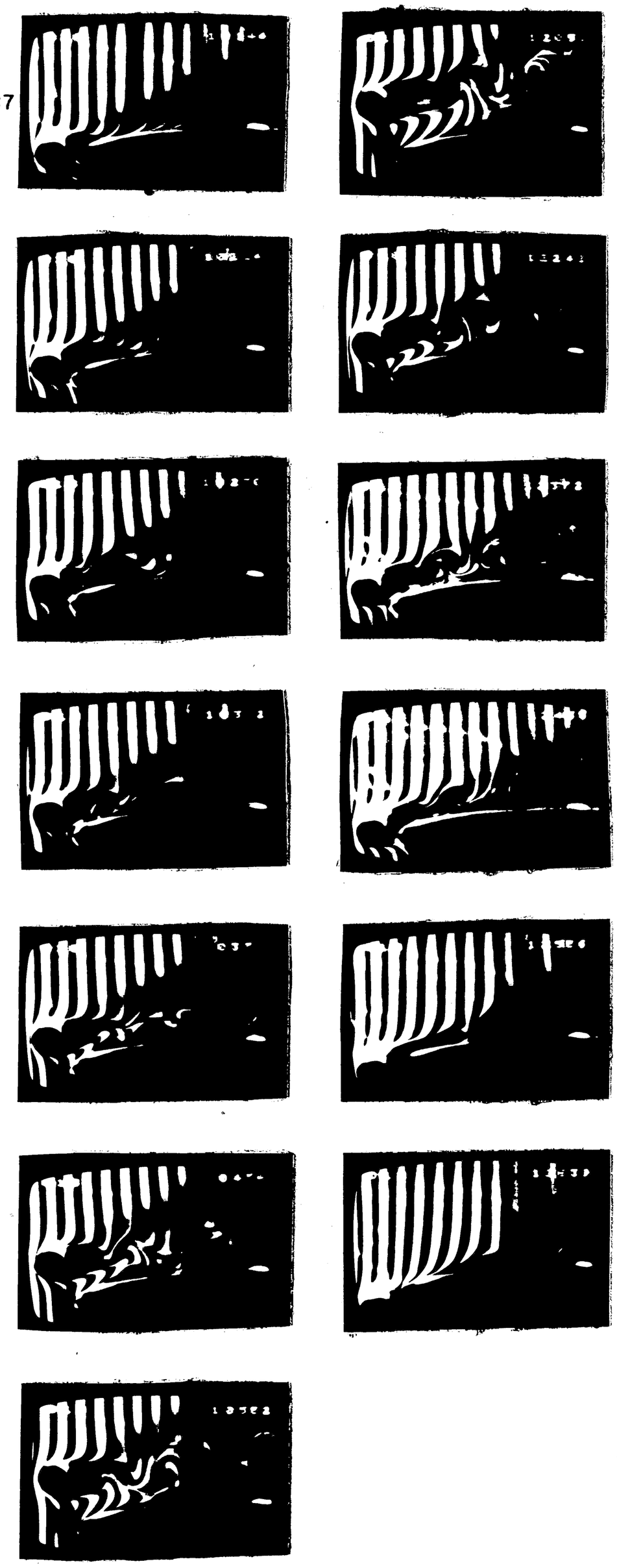

Figure 21 : Large scale interaction: A/D=5; D/T=1/2.

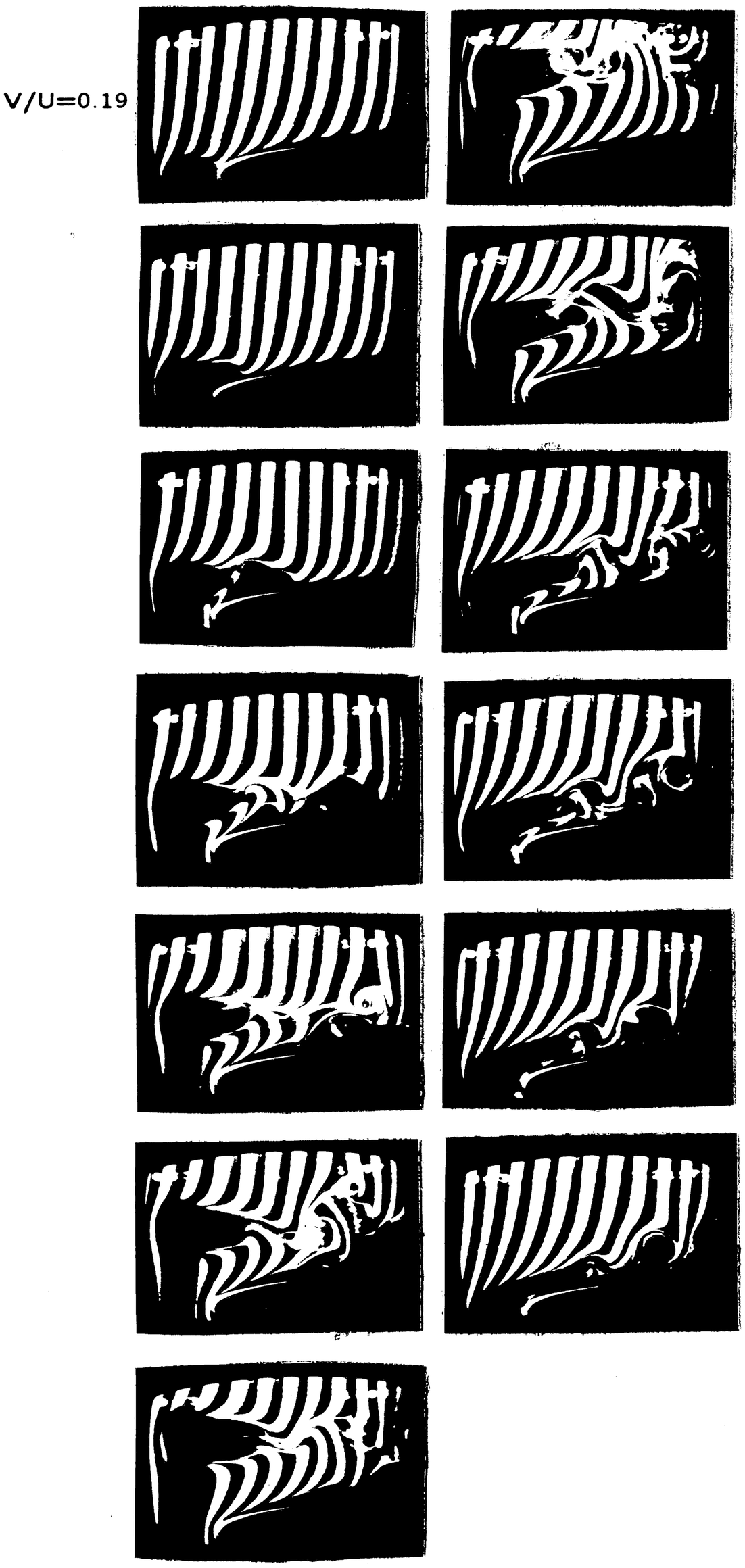

Figure 22 : Large scale interaction: A/D=5; D/T=1/2.

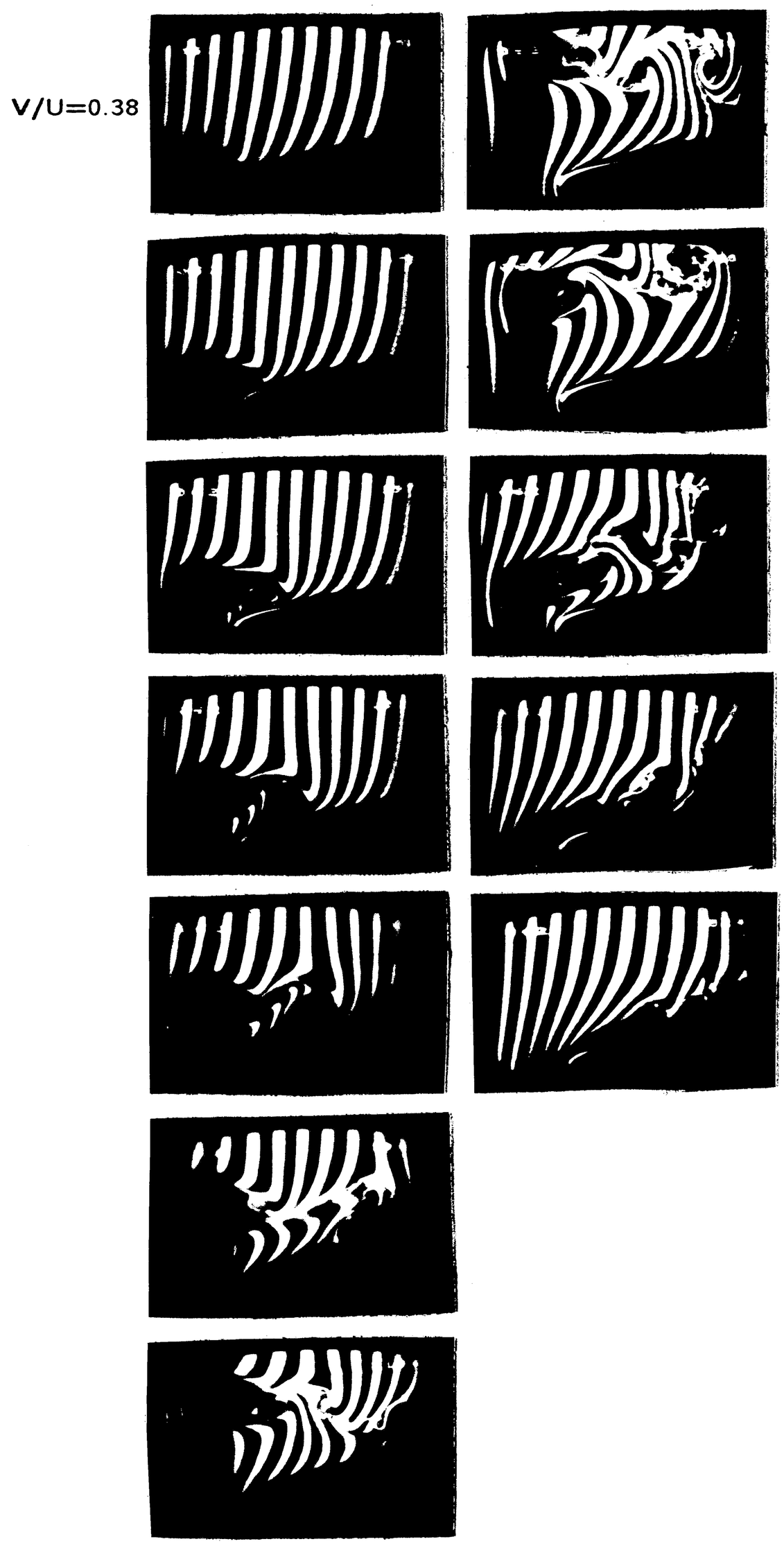

Figure 23 : Large scale interaction: A/D=5; D/T=1/2.

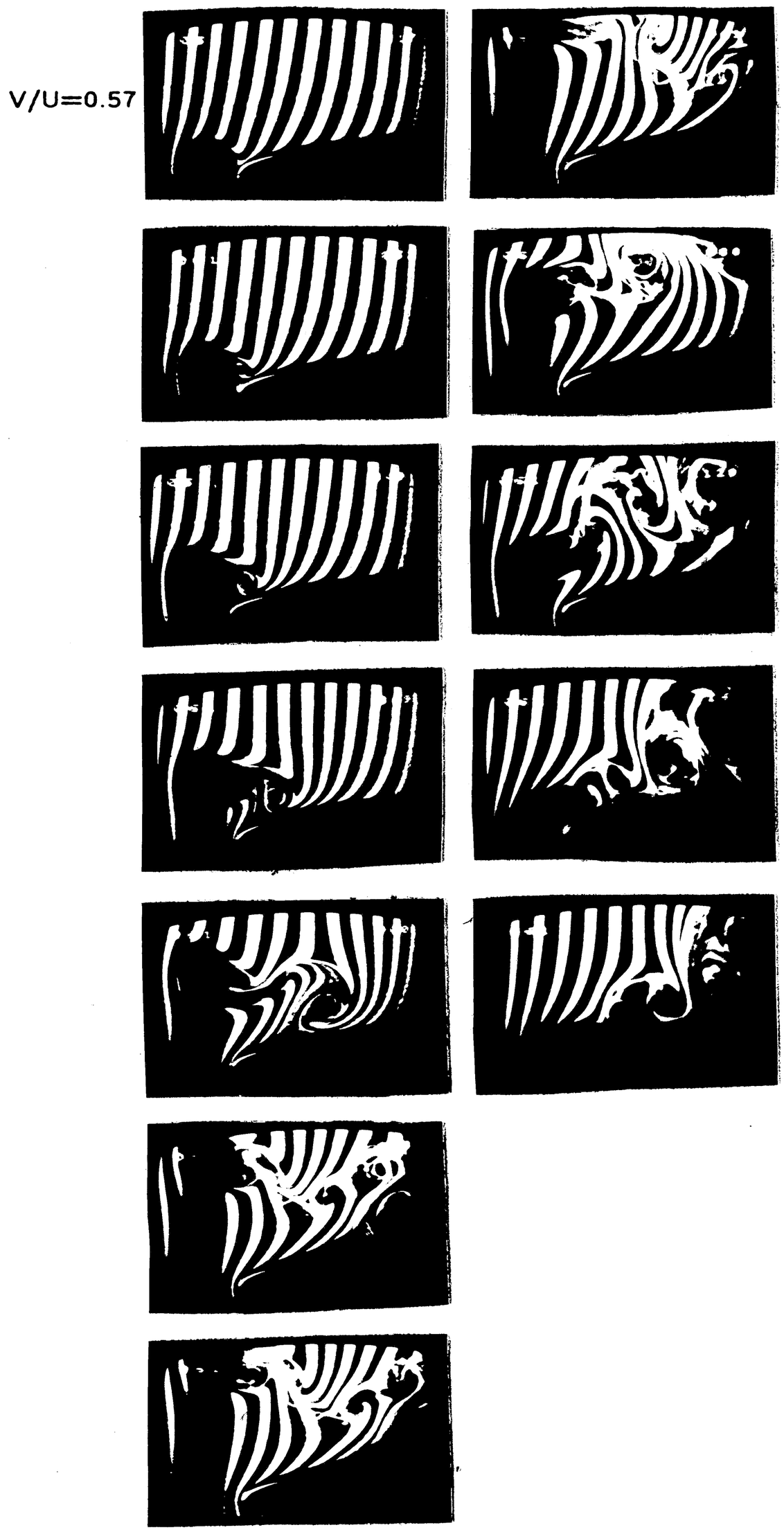

Figure 24 : Large scale interaction: A/D=5; D/T=1/2.

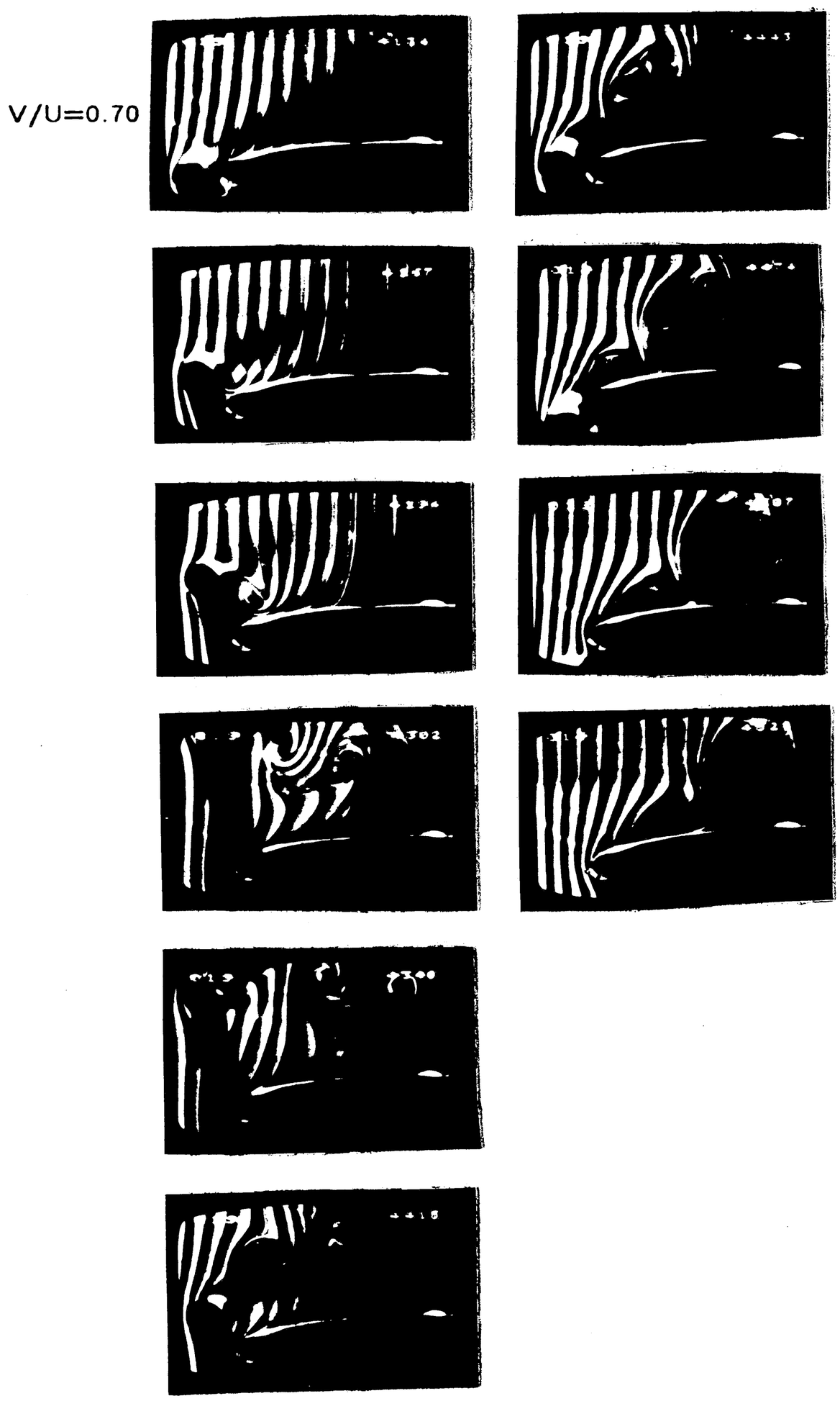

Figure 25 : Large scale interaction: A/D=5; D/T=1/2.

V/U=0.76

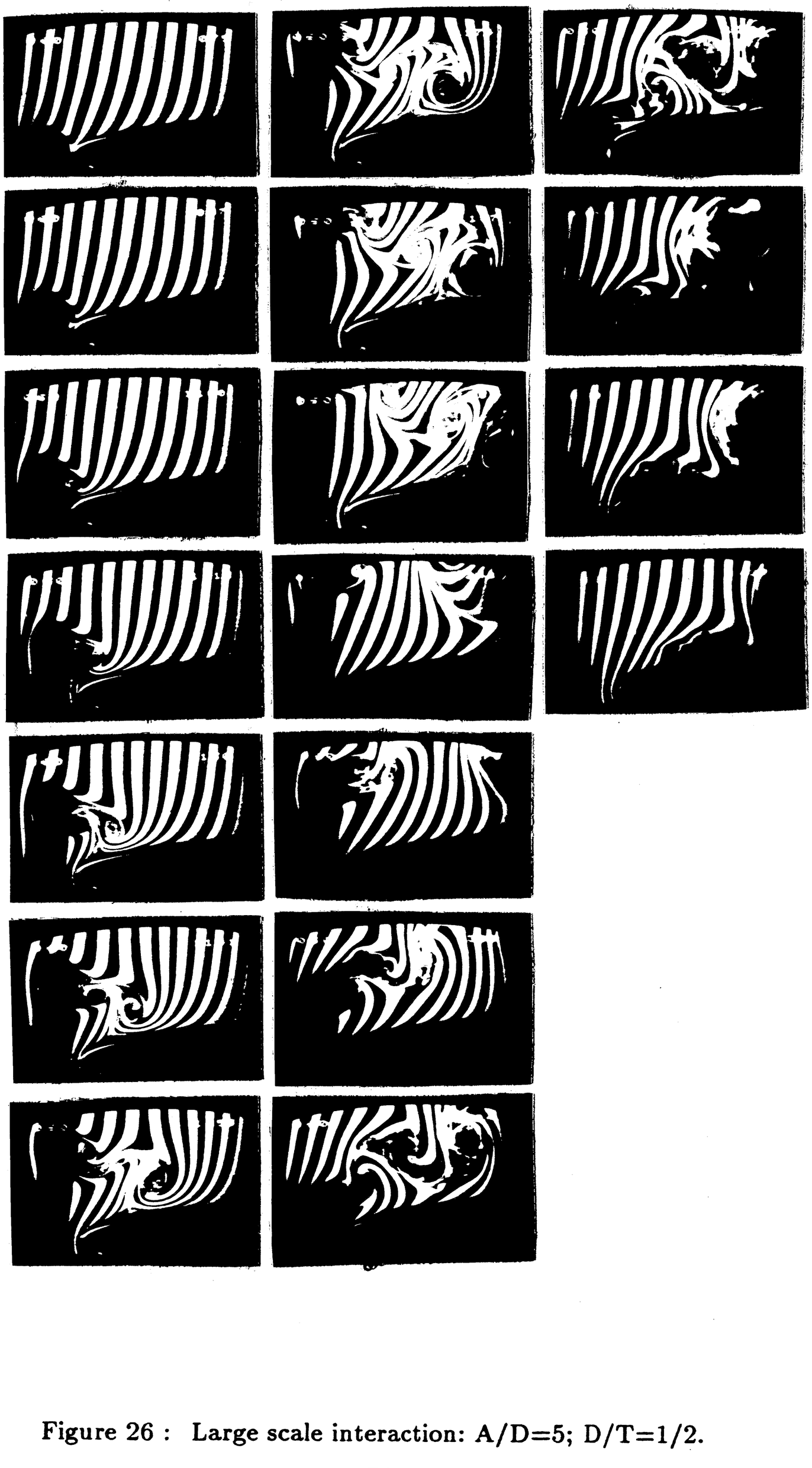

Figure 26 : Large scale interaction: A/D=5; D/T=1/2.

V/U=1.11

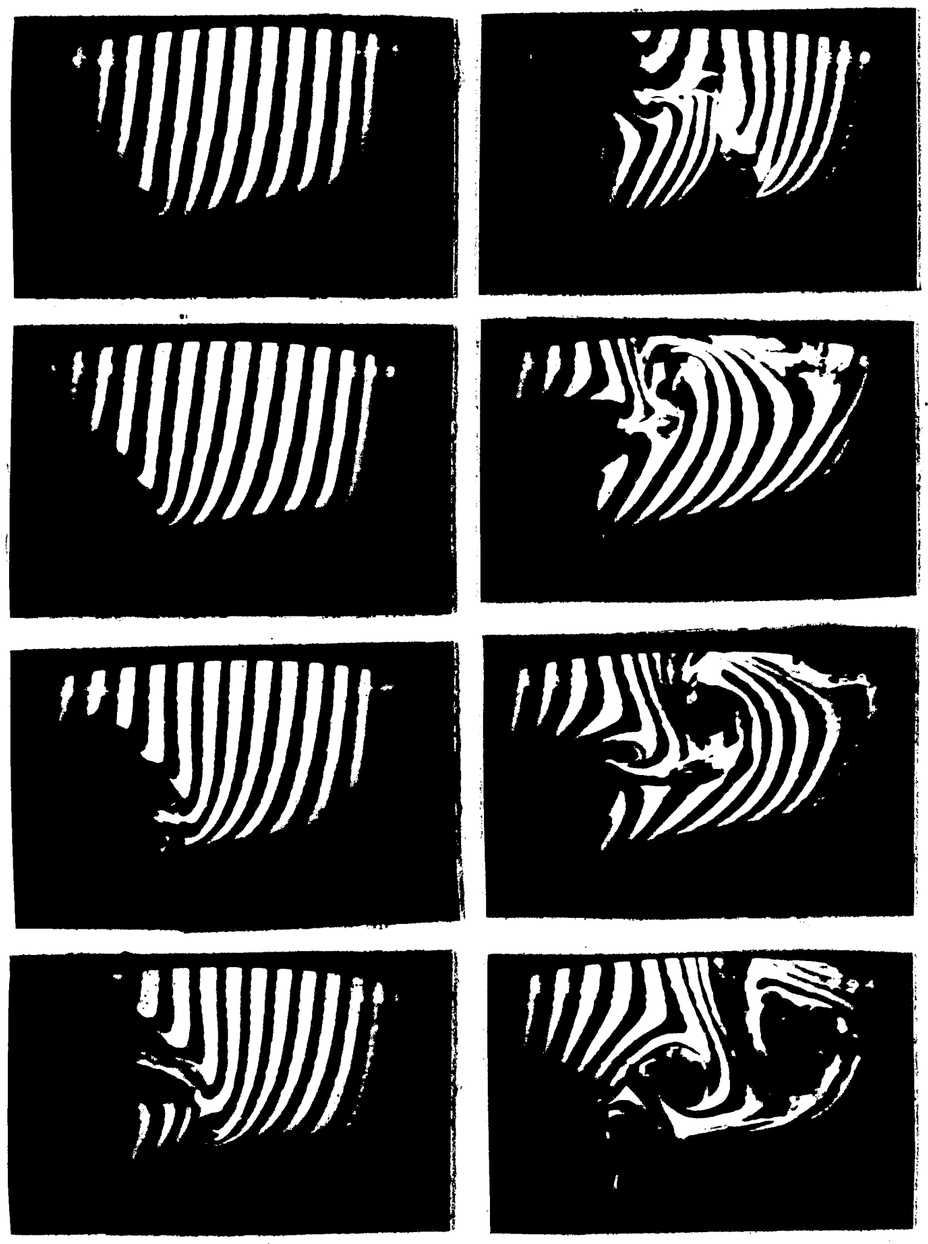

V/U=1.27

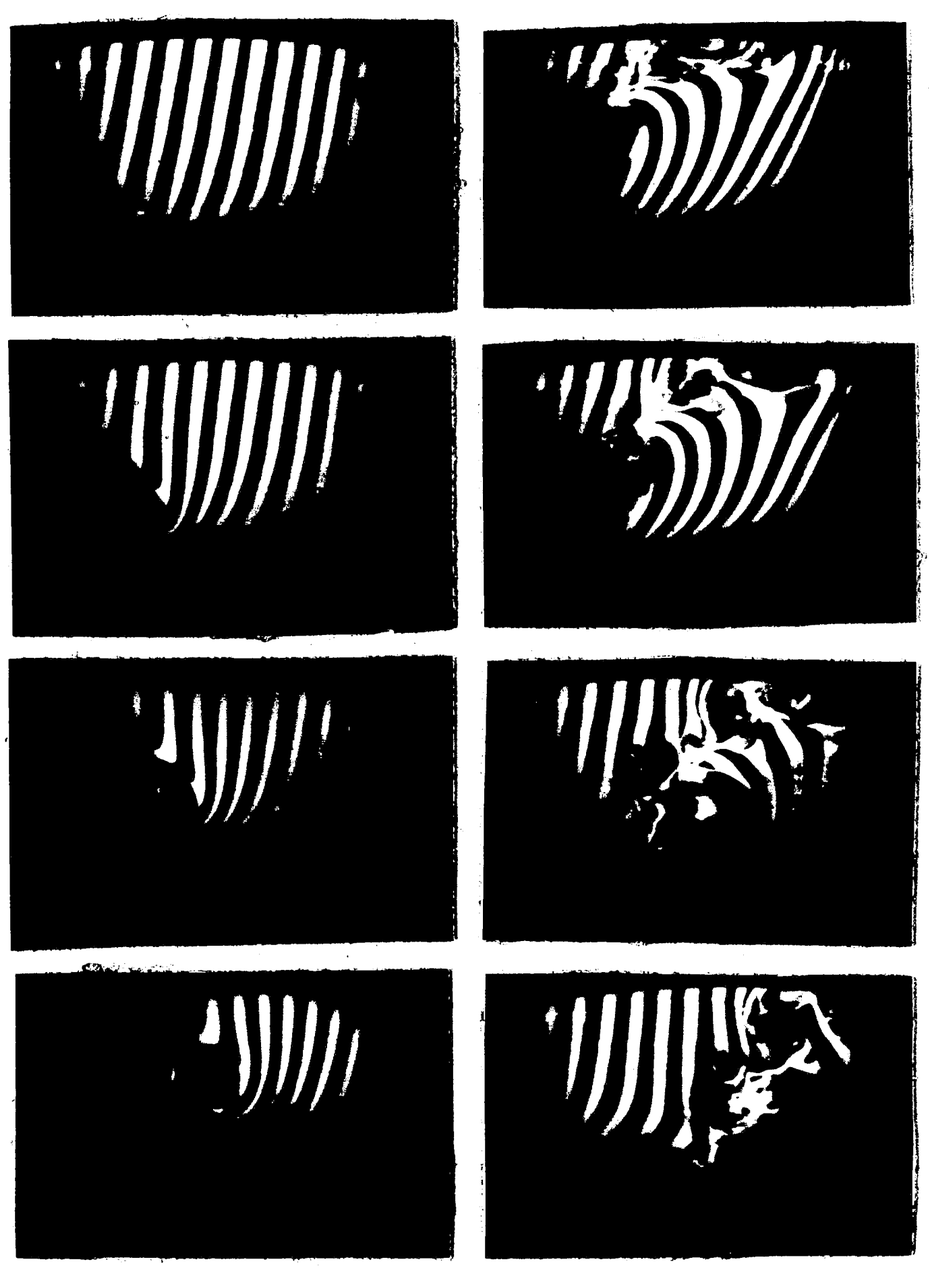

Figure 27 : Large scale interaction: A/D=5; D/T=1/2.

V/U=1.43

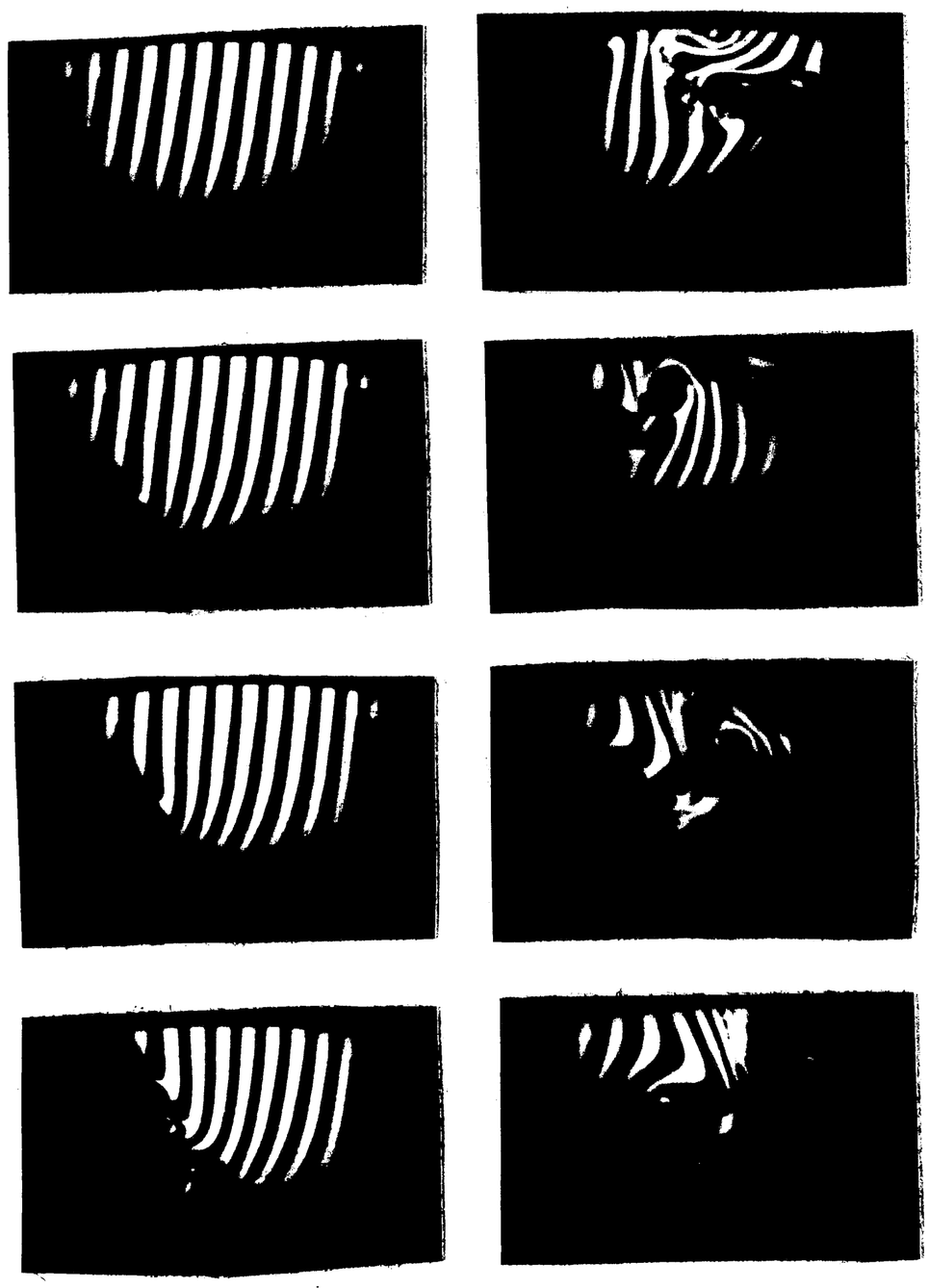

Figure 28 : Large scale interaction: A/D=5; D/T=1/2.

V/U=0.19

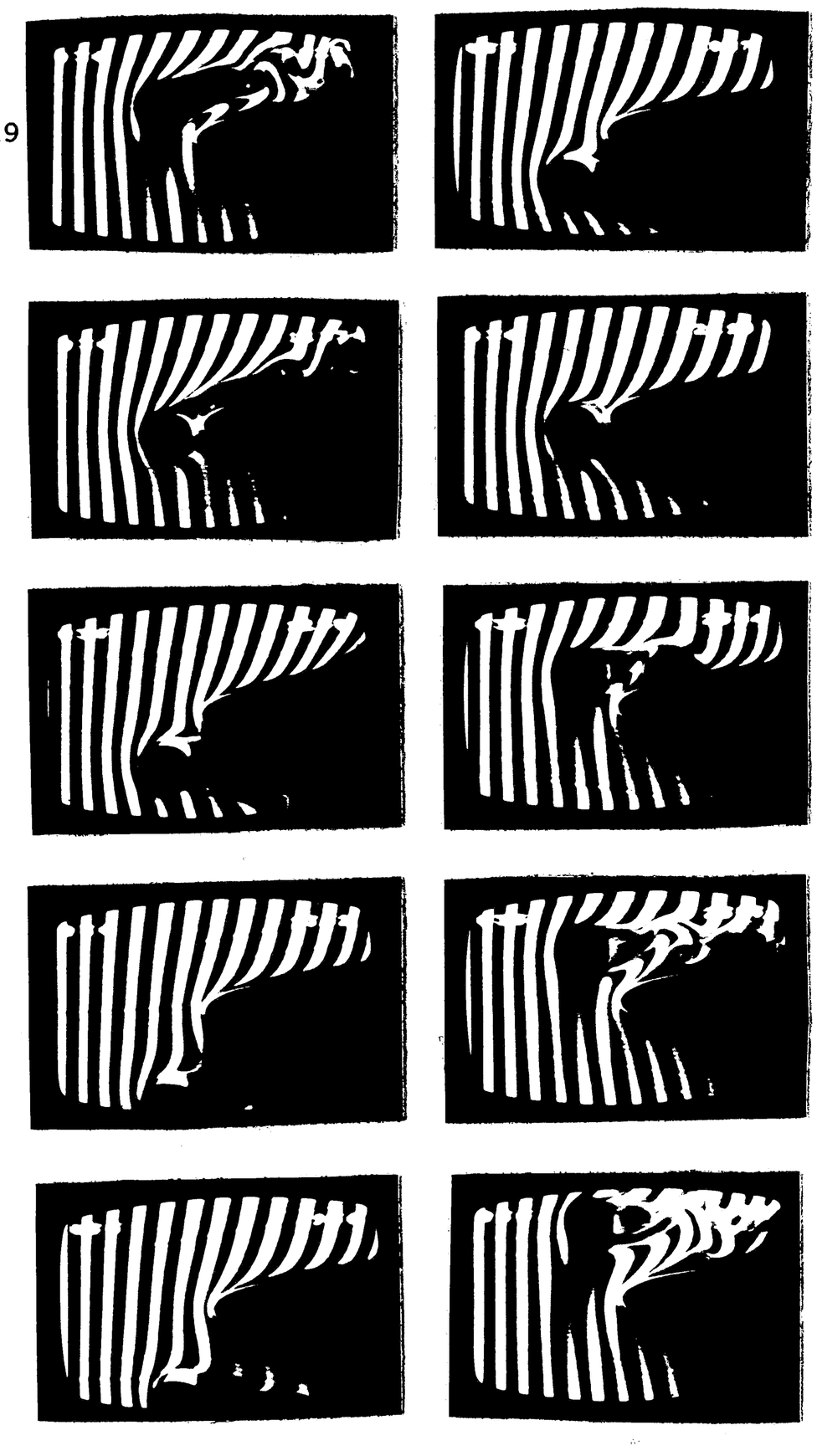

Figure 29 : Far view of the large scale interaction: A/D=5; D/T=1/2.

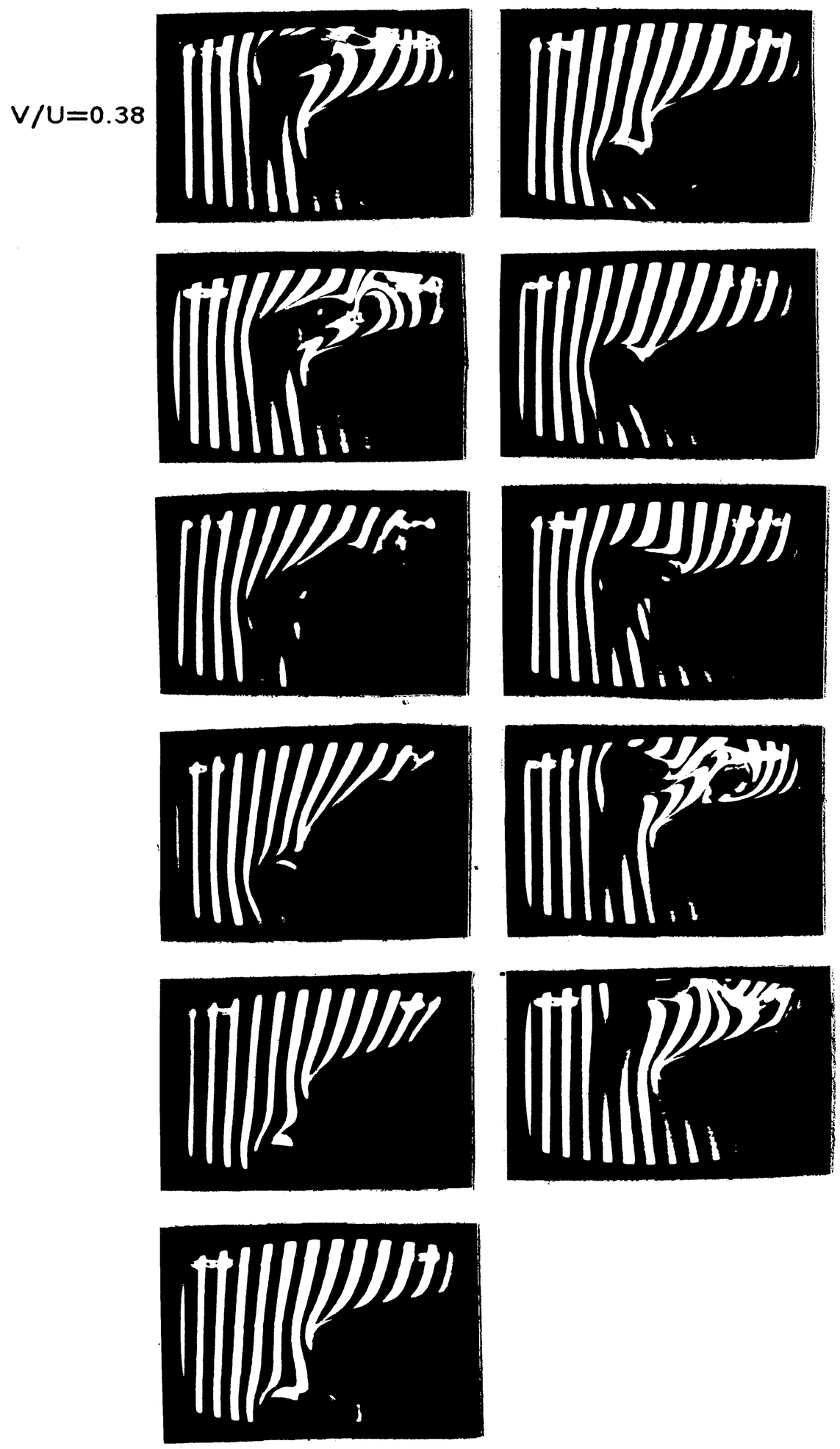

Figure 30 : Far view of the large scale interaction: A/D=5; D/T=1/2.

V/U=0.57

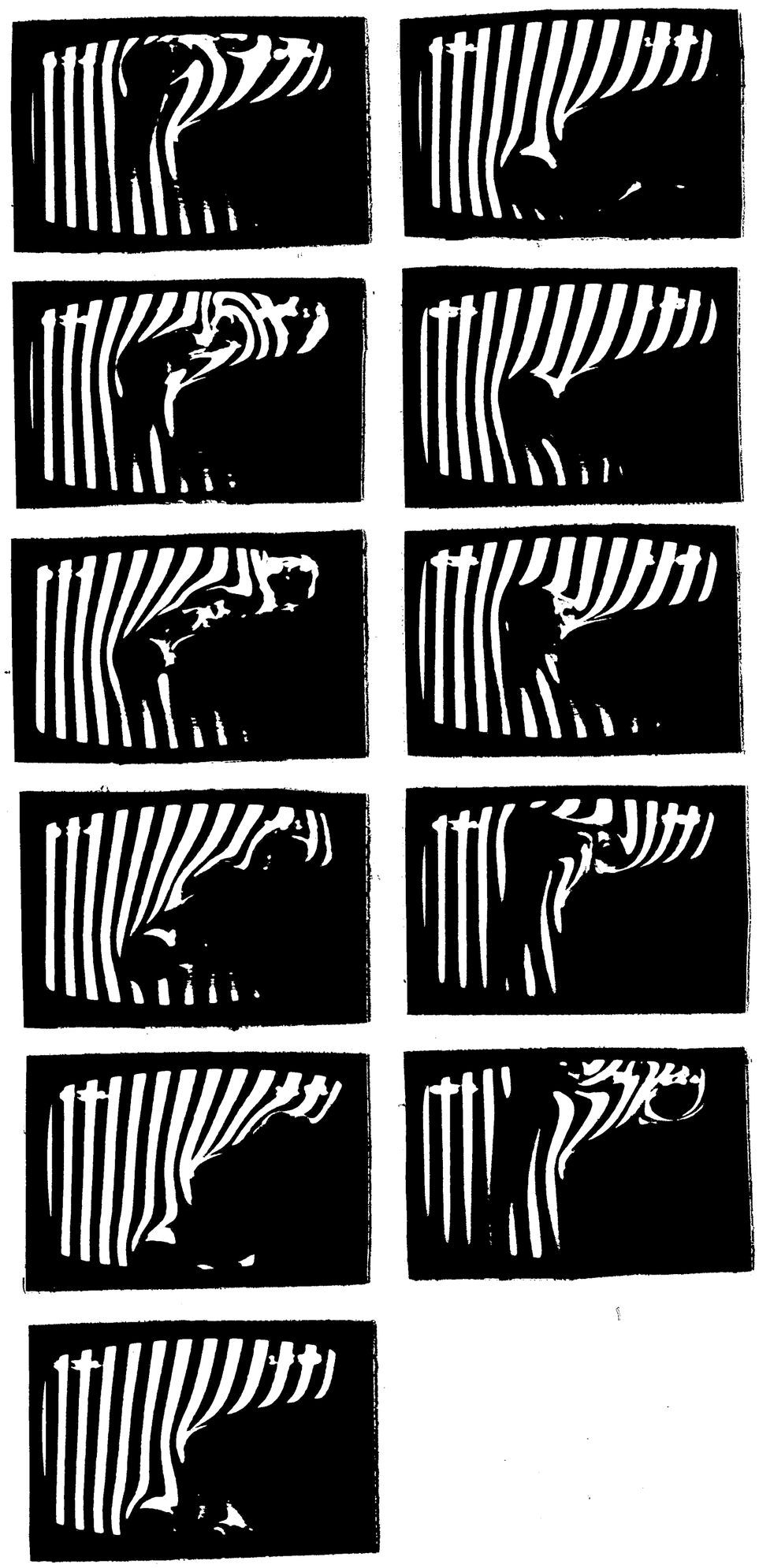

Figure 31 : Far view of the large scale interaction: A/D=5; D/T=1/2.

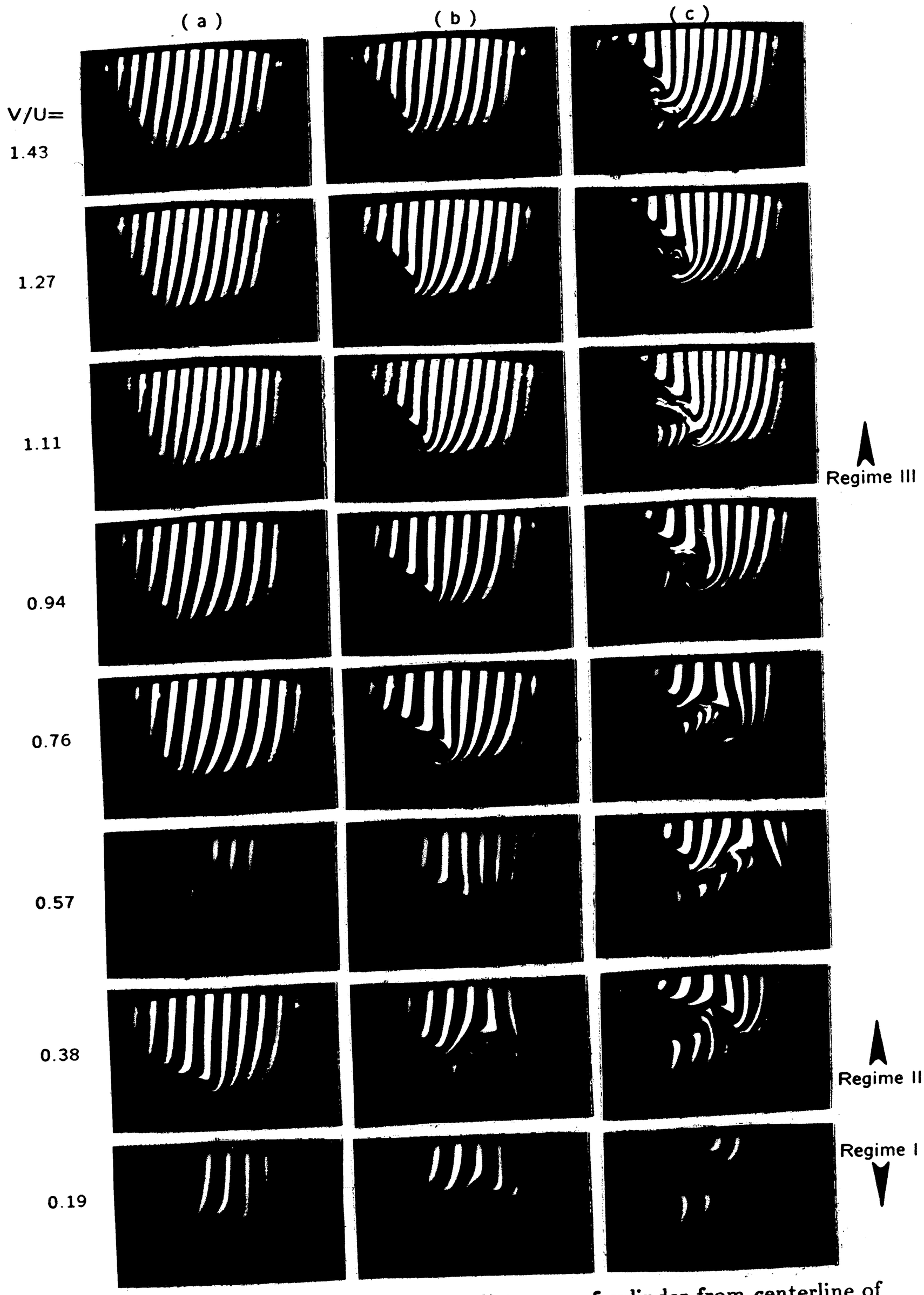

Figure 32 : Flow structure of constant distances of cylinder from centerline of elliptical leading-edge: $0.19 \leq V/U \leq 1.43$; A/D=5; D/T=1/2; (a) Y/D=1; (b) Y/D=2; (c) Y/D=3.

V/U=0.19

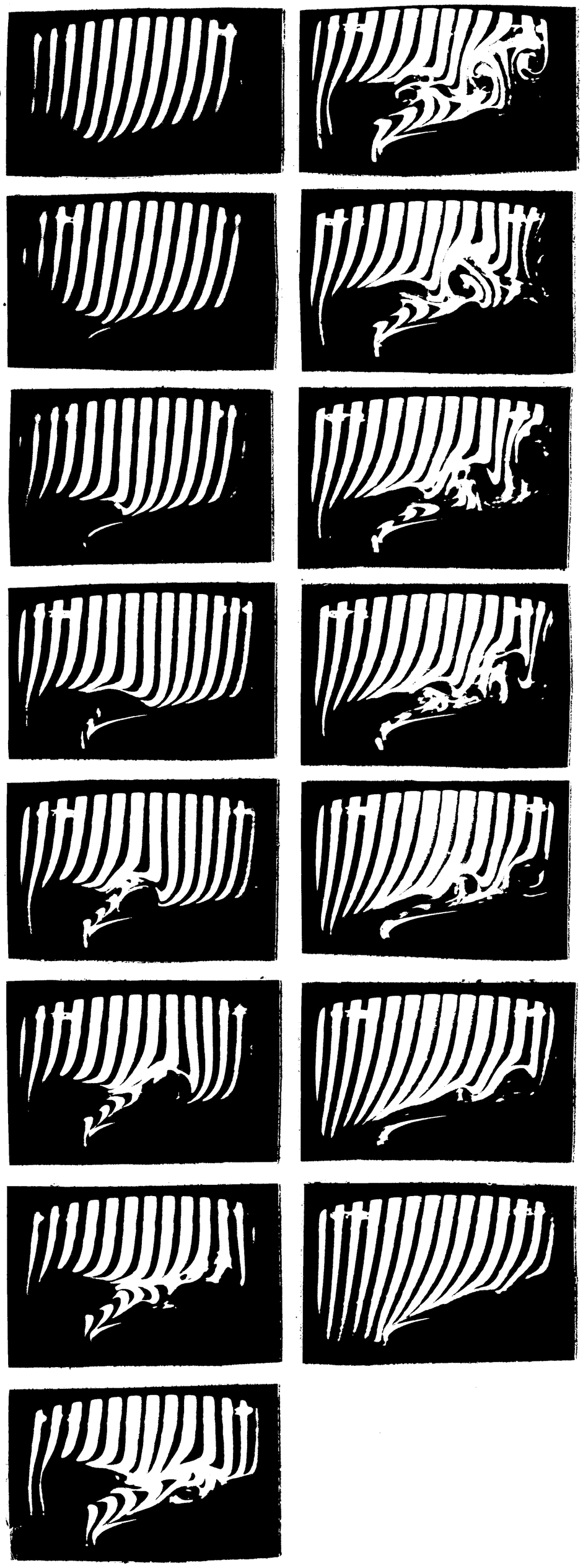

Figure 33 : Large scale interaction: A/D=2; D/T=1/2.

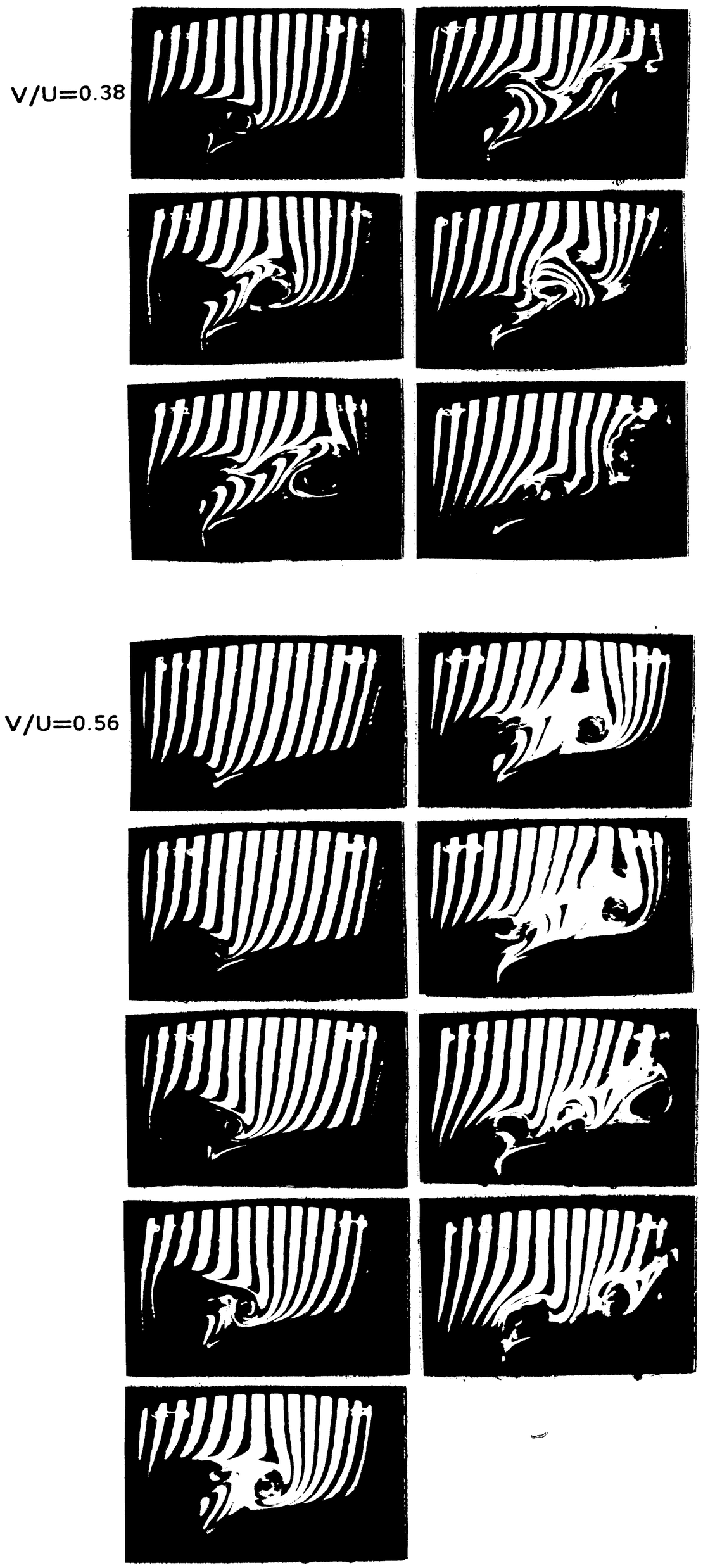

Figure 34 : Large scale interaction: A/D=2; D/T=1/2.

V/U=0.73

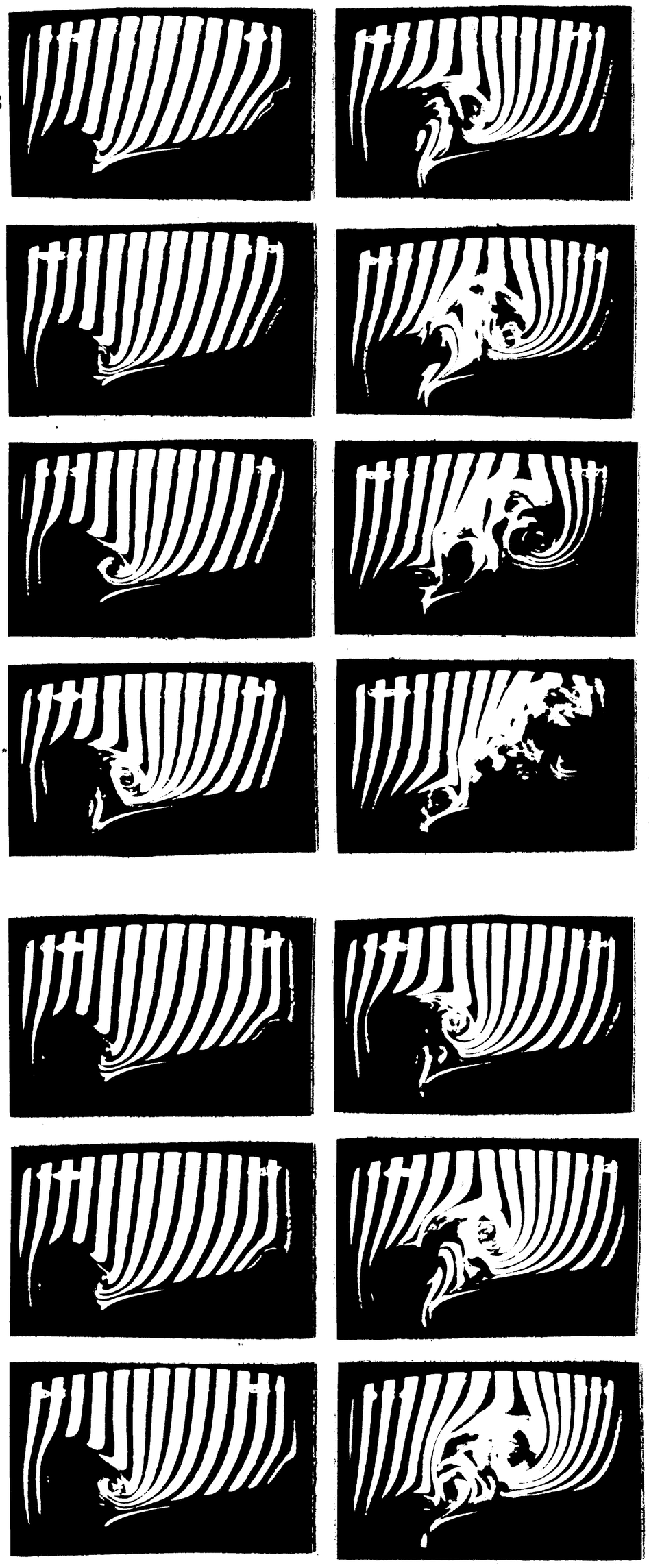

V/U=0.88

Figure 35 : Large scale interaction: A/D=2; D/T=1/2.

V/U=1.03

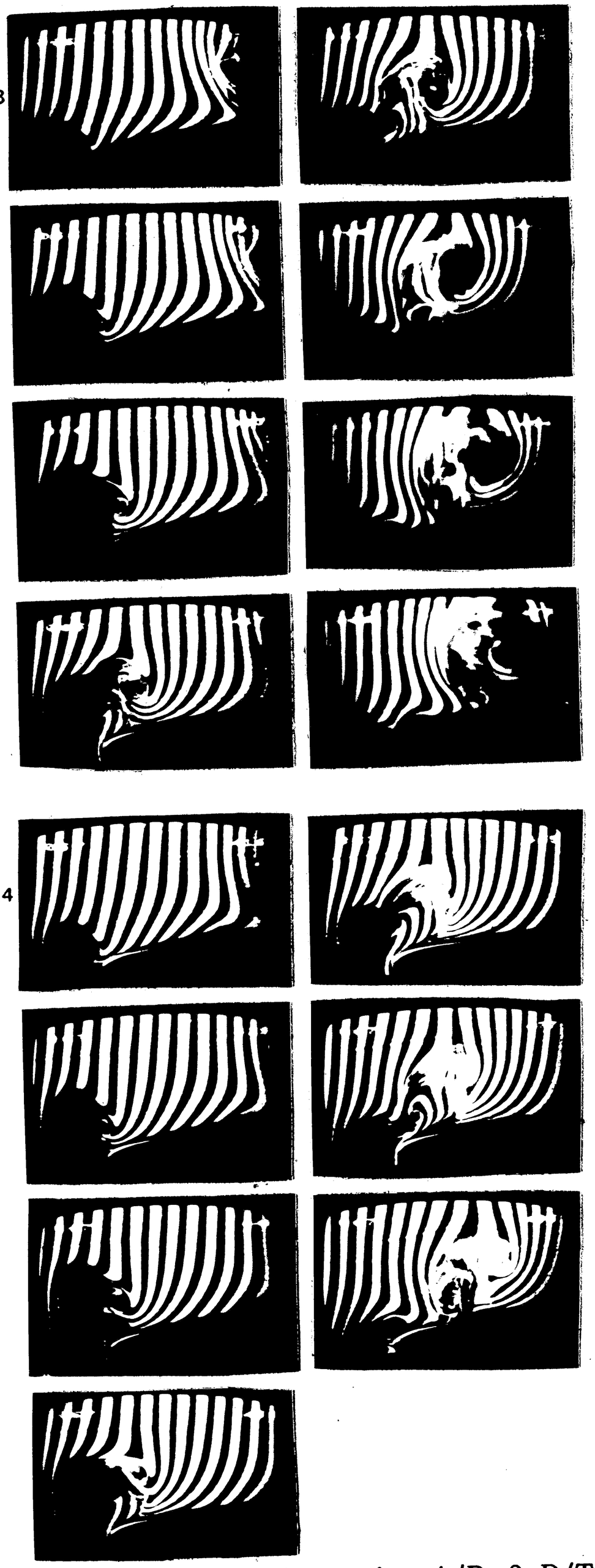

V/U=1.14

Figure 36 : Large scale interaction: A/D=2; D/T=1/2.

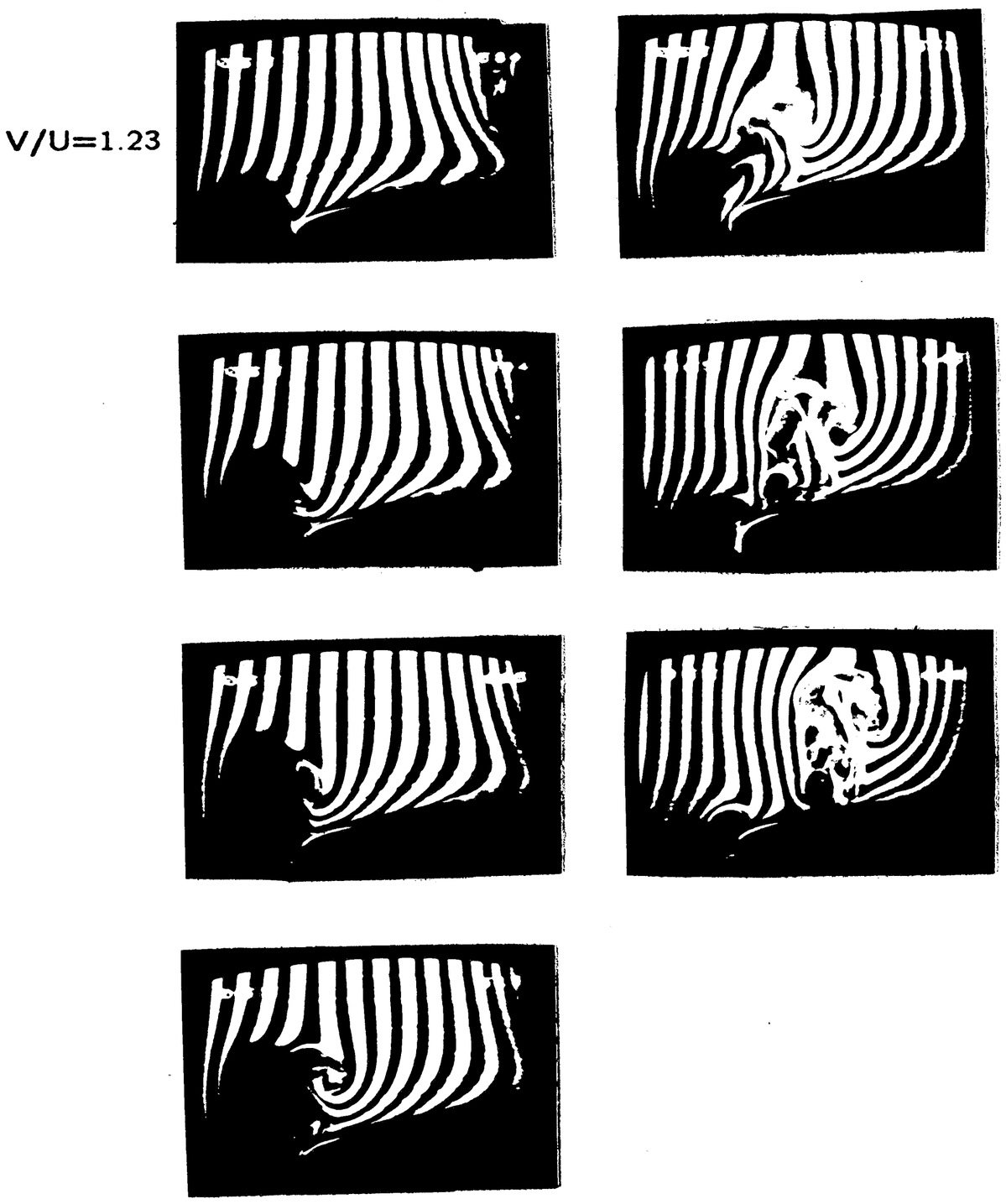

Figure 37 : Large scale interaction: A/D=2; D/T=1/2.

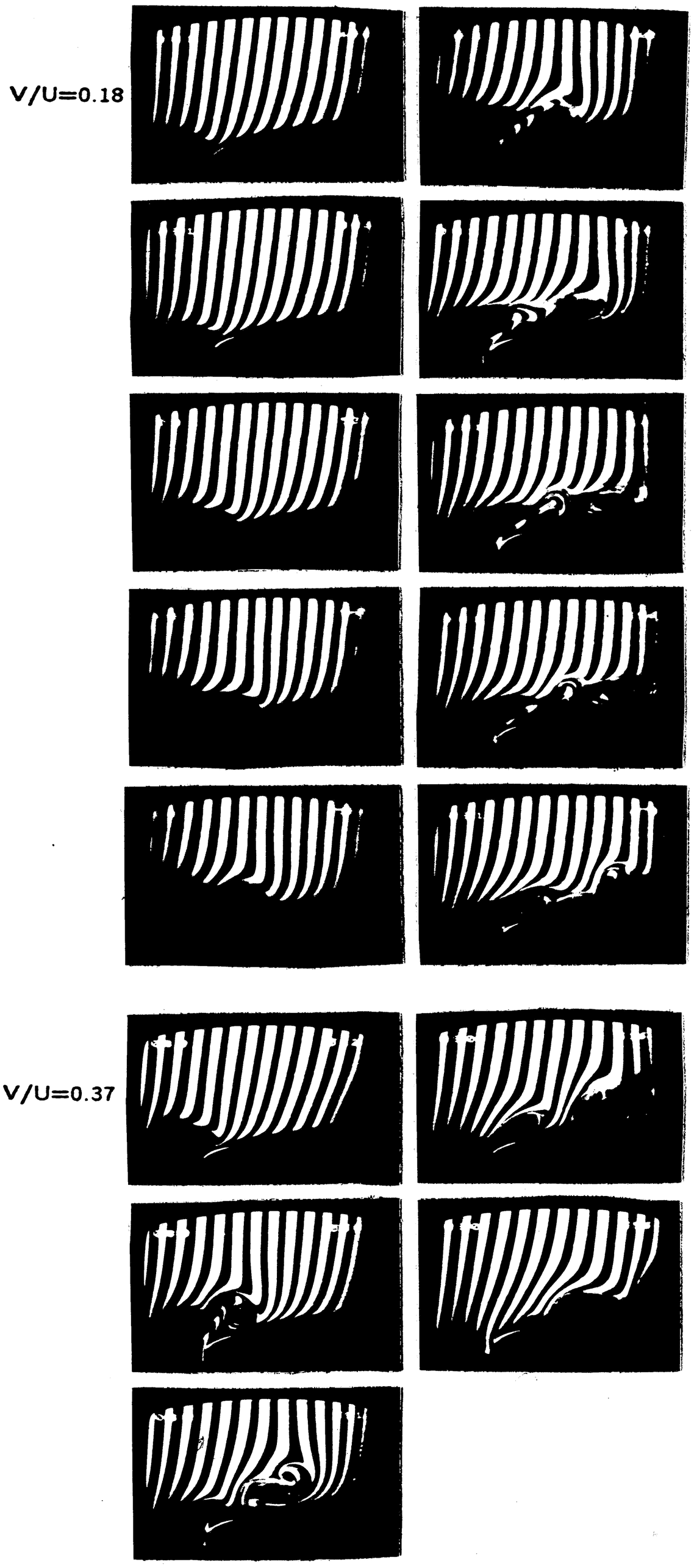

Figure 38 : Large scale interaction: A/D=1; D/T=1/2.

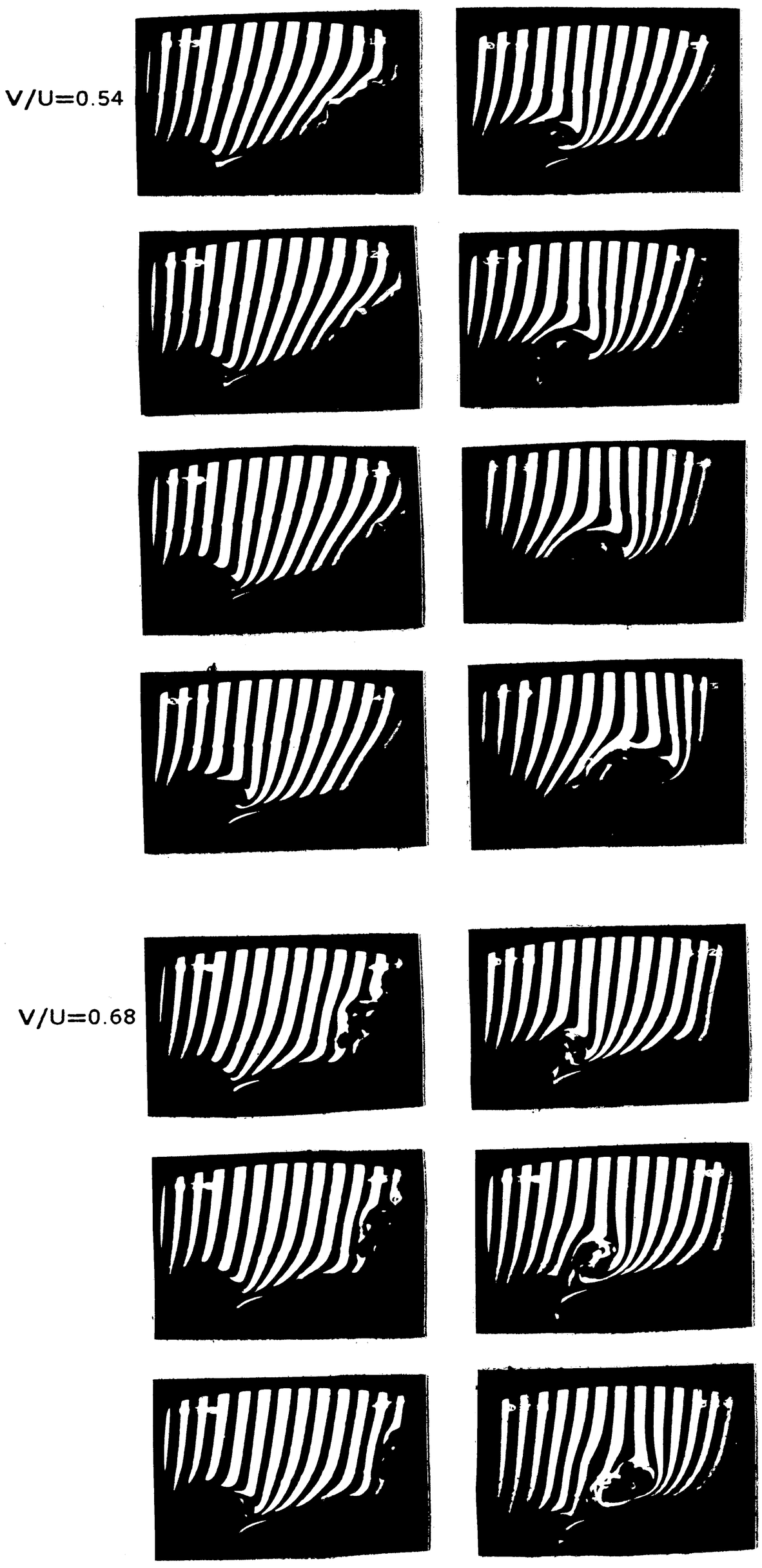

Figure 39 : Large scale interaction: A/D=1; D/T=1/2.

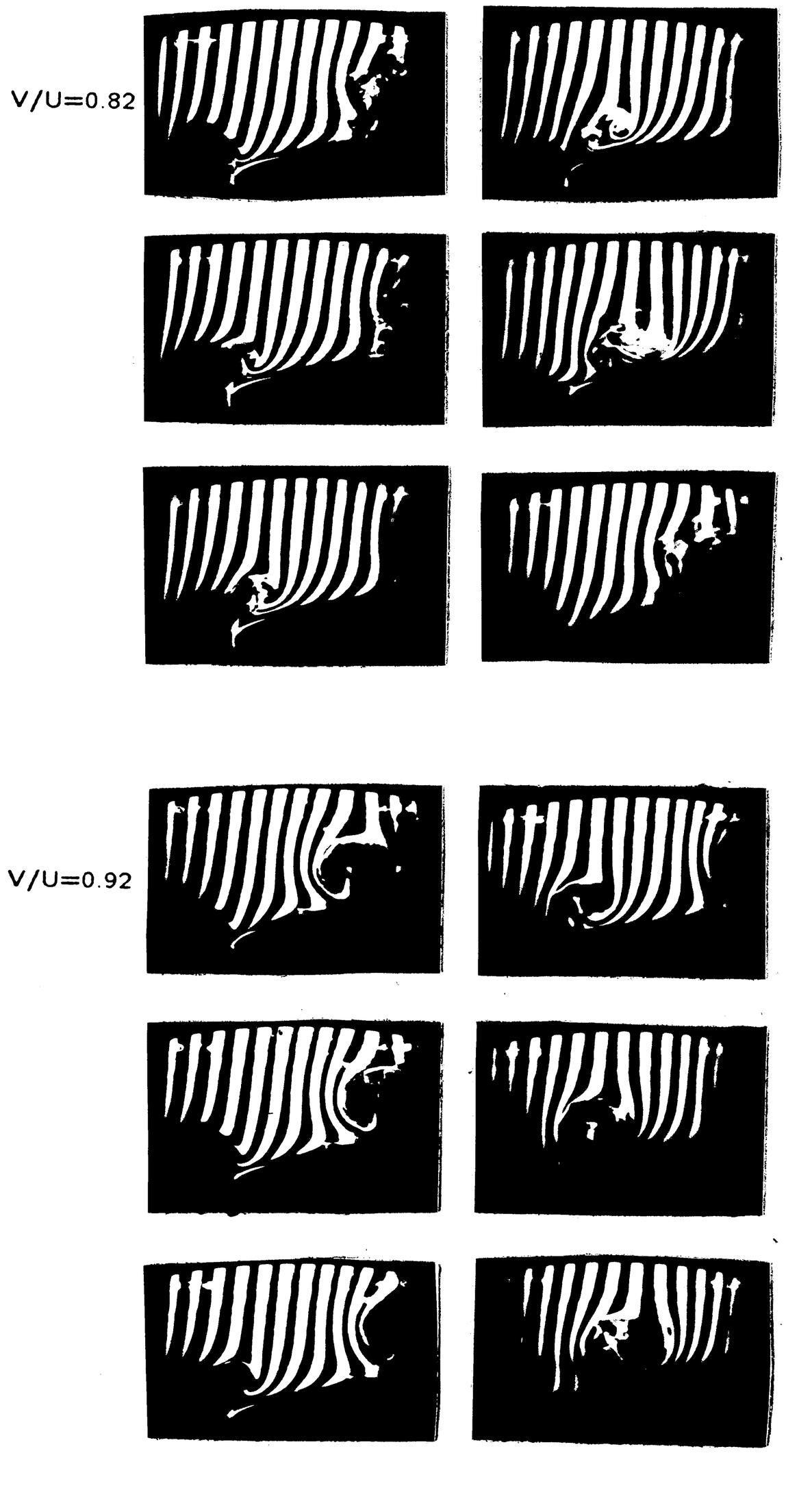

Figure 40 : Large scale interaction: A/D=1; D/T=1/2.

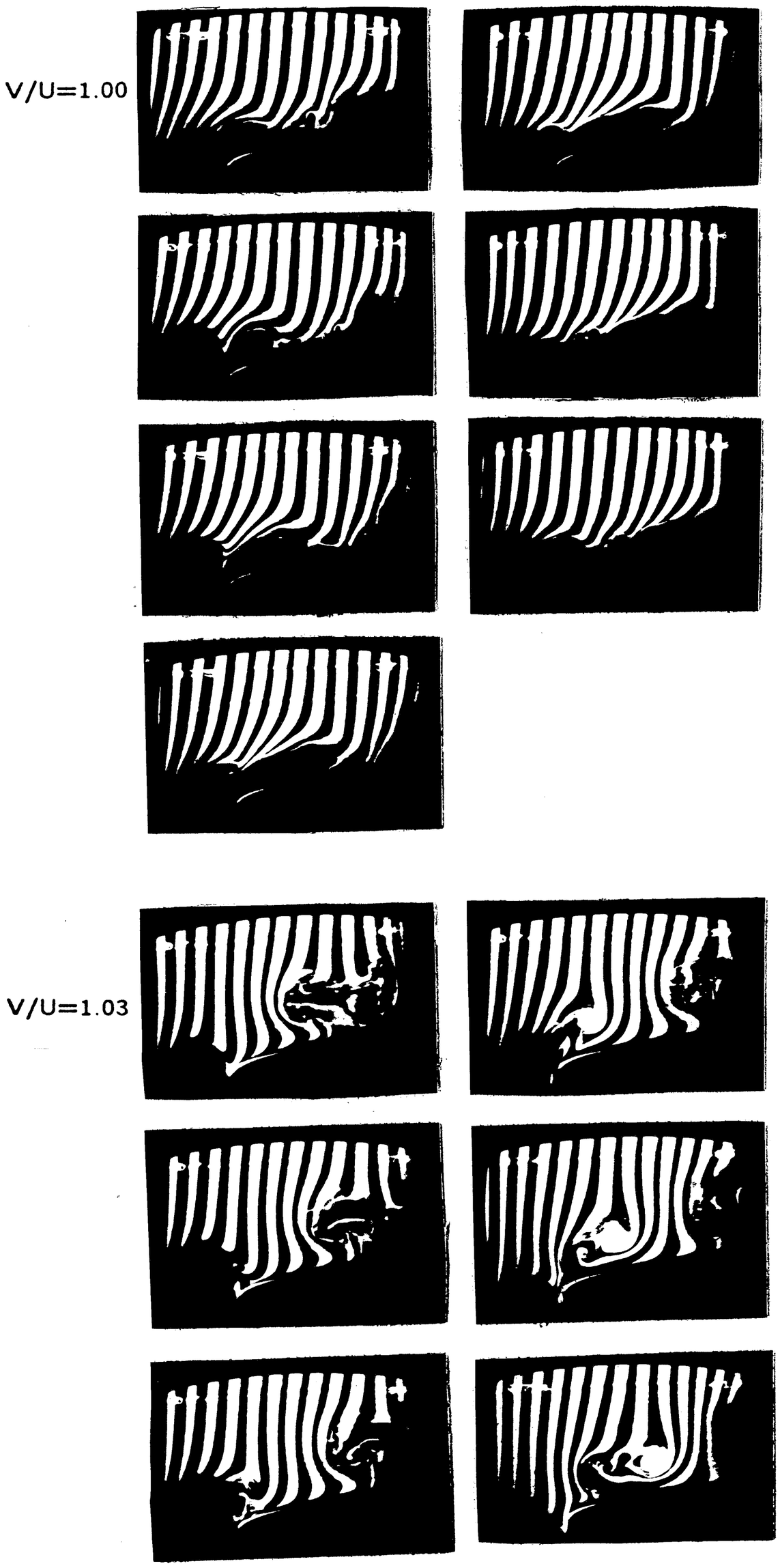

Figure 41 : Large scale interaction: A/D=1; D/T=1/2.

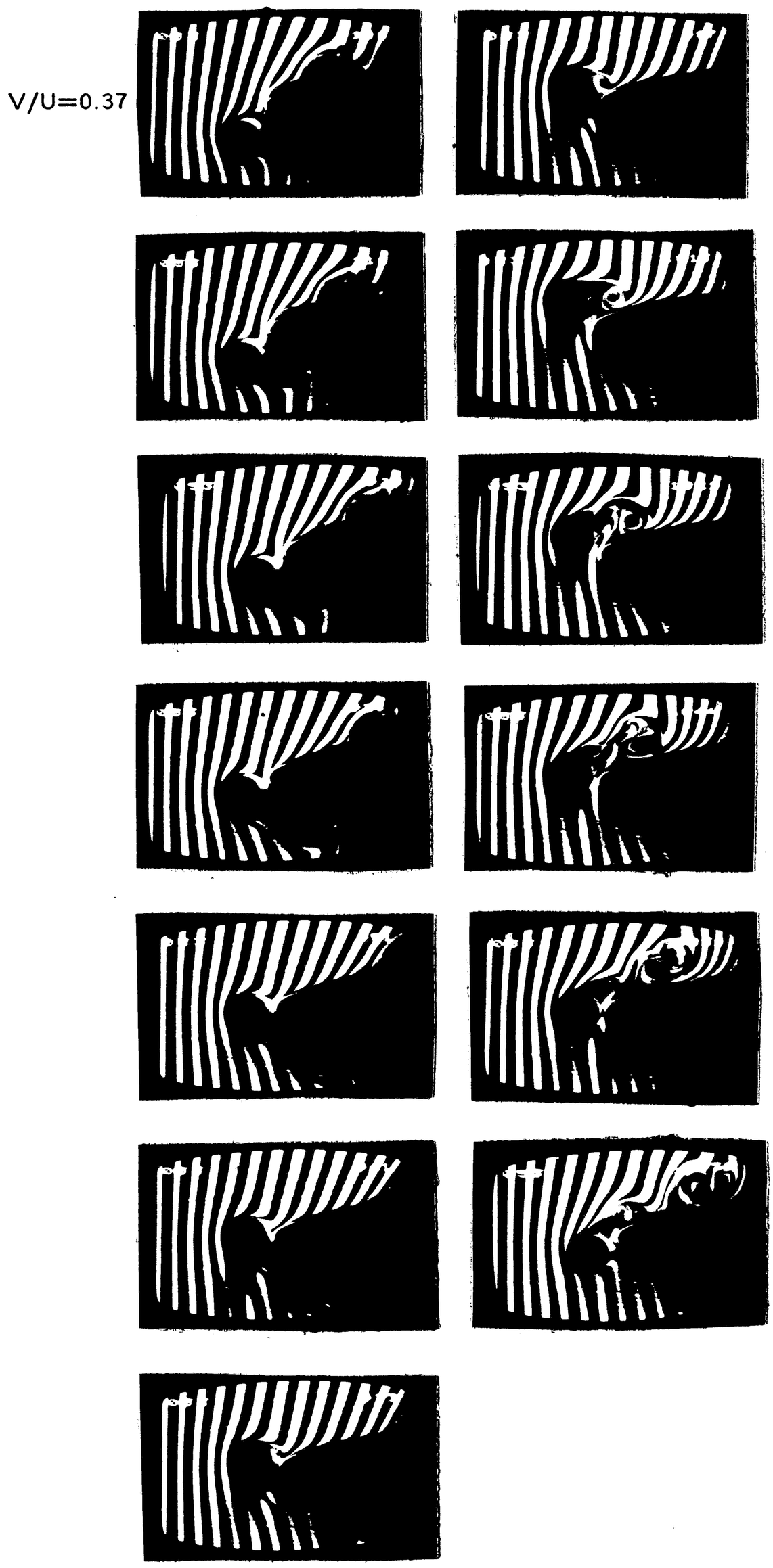

Figure 42 : Far view of the large scale interaction: A/D=1; D/T=1/2.

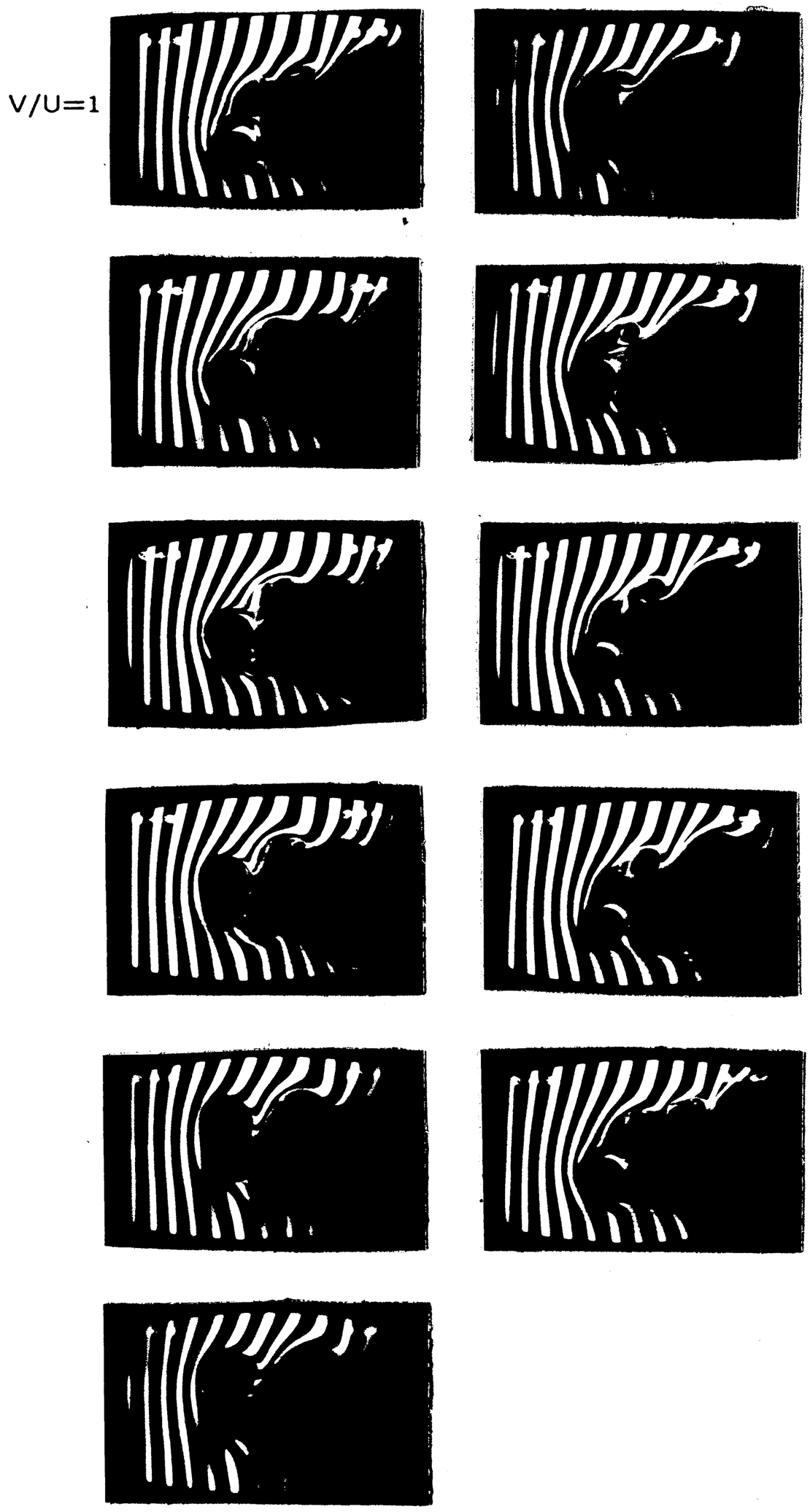

Figure 43 : Far view of the large scale interaction: A/D=1; D/T=1/2.

V/U=1.03

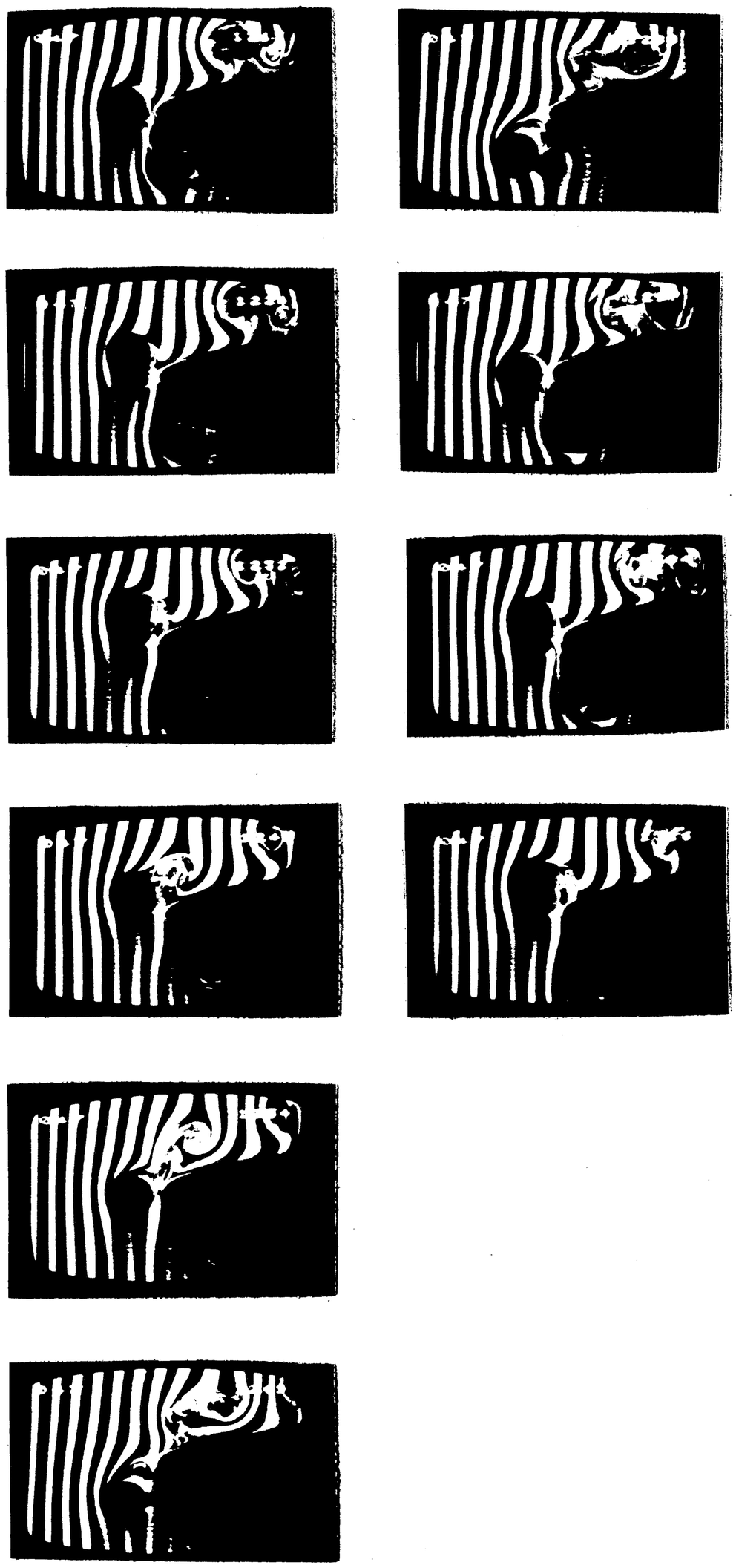

Figure 44 : Far view of the large scale interaction: A/D=1; D/T=1/2.

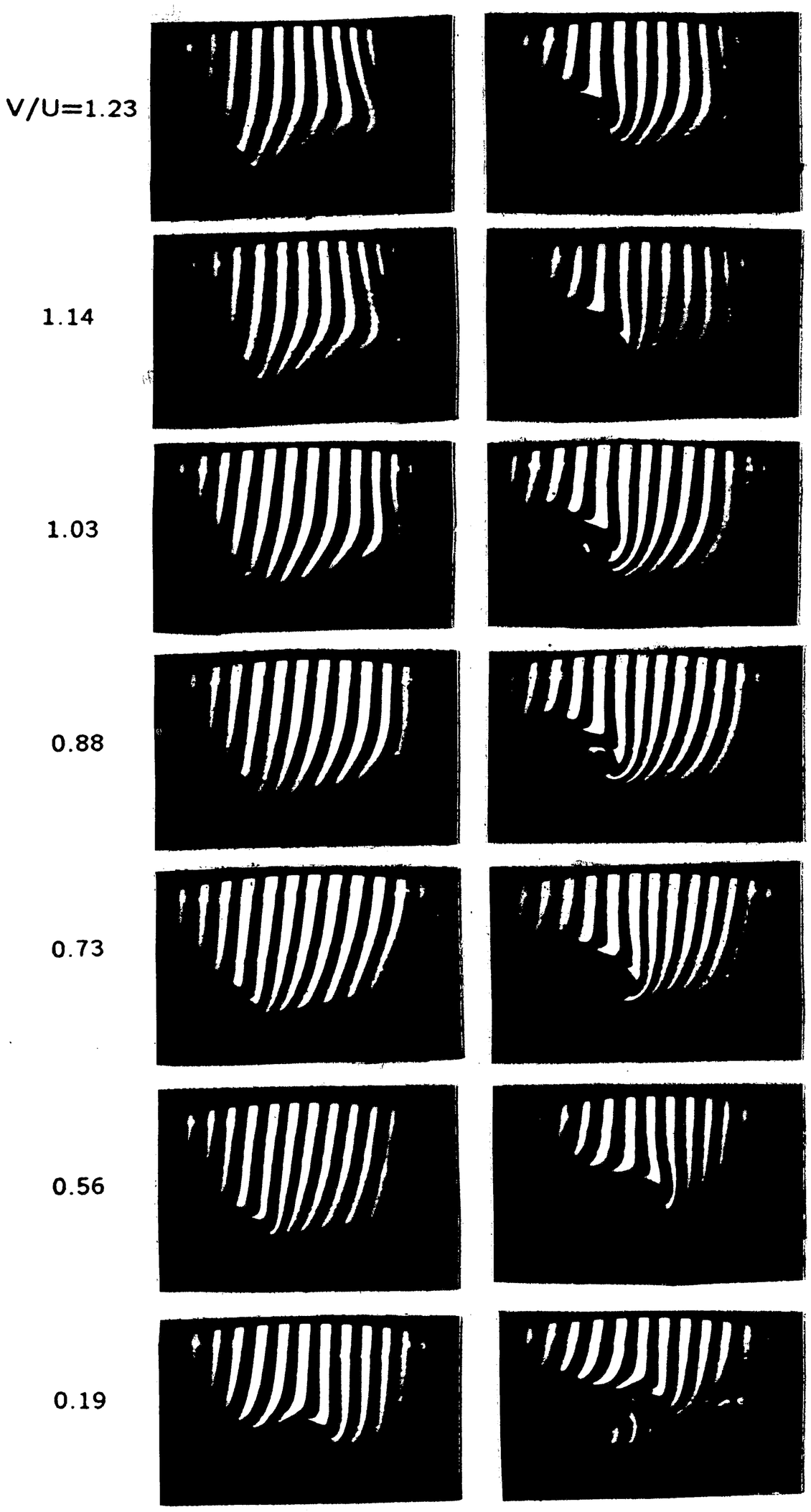

Figure 45 : Flow structure of constant distances of cylinder from centerline of elliptical edge: $0.19 \leq V/U \leq 1.23$; A/D=2; D/T=1/2; (a) Y/D=1; (b) Y/D=2.

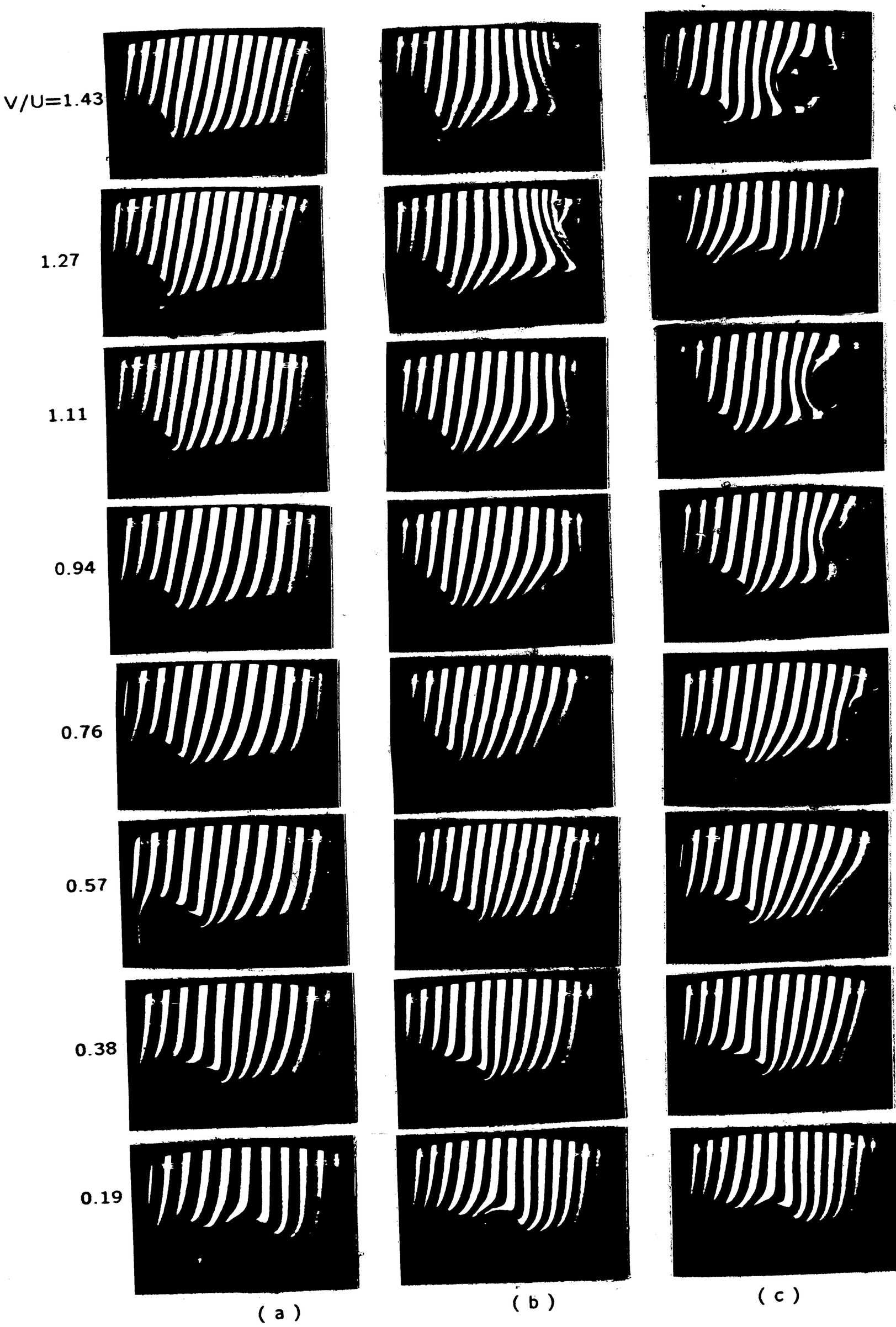

Figure 46 : Flow structure of constant distances of cylinder from centerline of elliptical edge: Y/D=1; 0.19 ≤ V/U ≤ 1.43; D/T=1/2; (a) A/D=5; (b) A/D=2; (c) A/D=1.

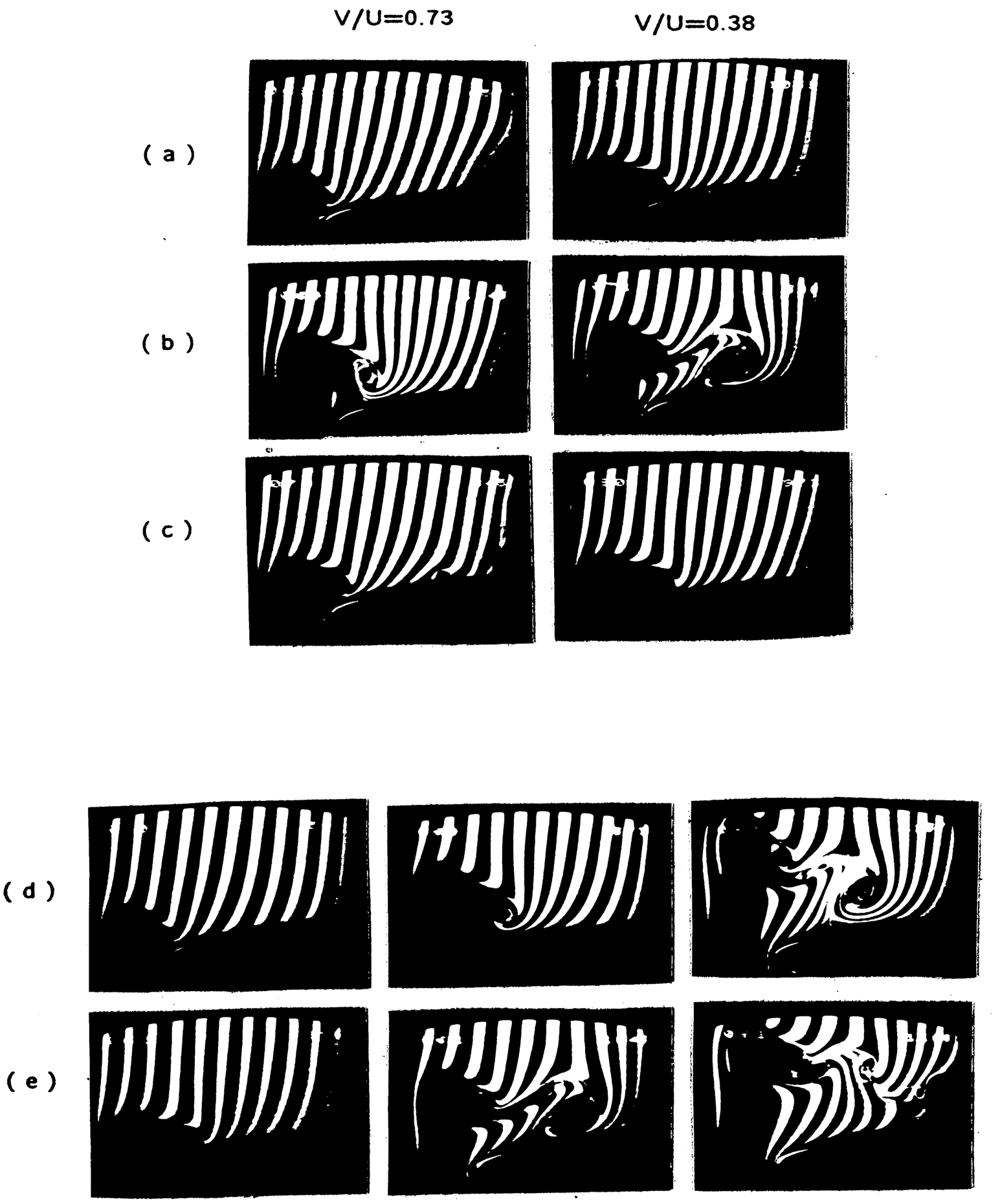

Figure 47 : Flow structure of constant distances of cylinder from centerline of elliptical edge: D/T=1/2; (a) Y/D=1; A/D=2; (b) Y/D=2; A/D=2; (c) Y/D=1; A/D=1; (d) Y/D=1; Y/D=2; Y/D=3; A/D=5; V/U=0.76; (e) Y/D=1; Y/D=2; Y/D=3; A/D=5; V/U=0.38.

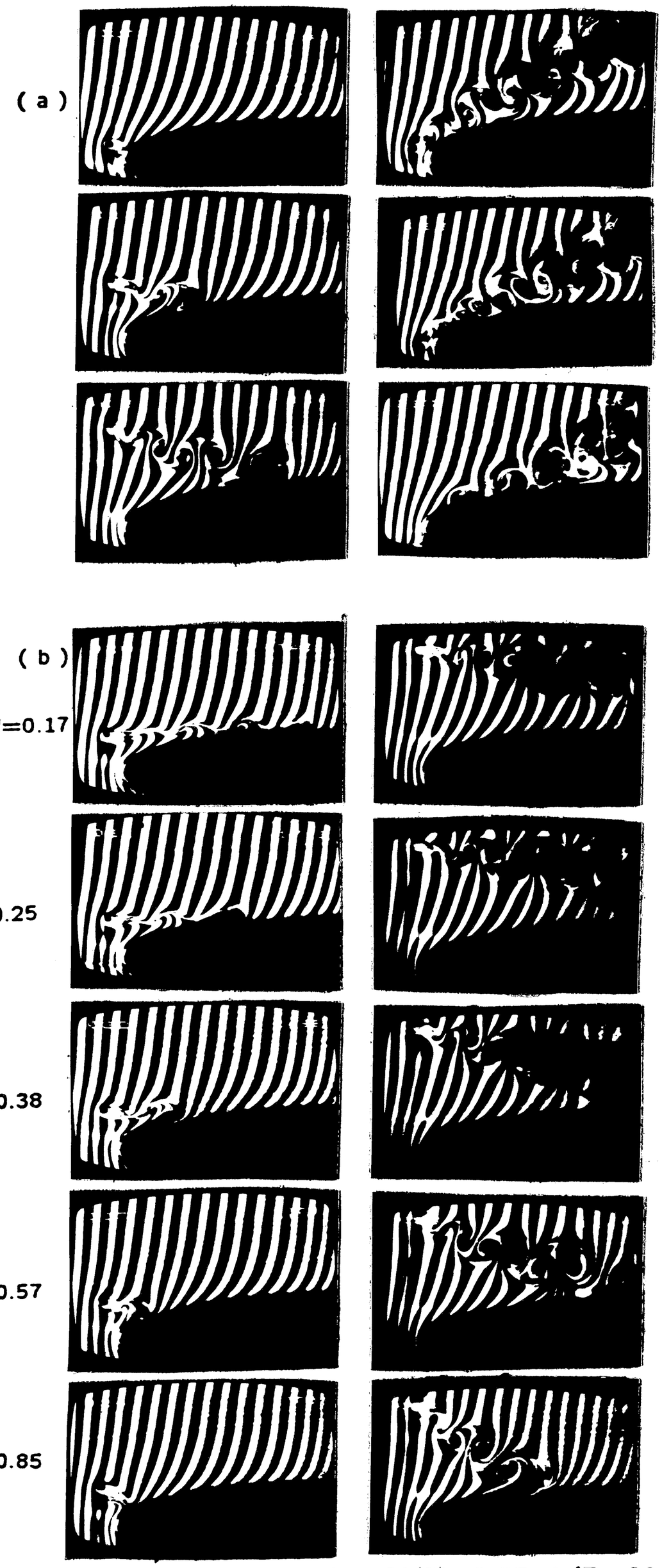

Figure 48 : (a) Small scale interaction; V/U=0.57; A/D=20; D/T=1/8; (b) Flow structure of constant distances of cylinder from centerline of elliptical edge; $0.17 \leq V/U \leq 0.85$; A/D=20; D/T=1/8; Y/D=4 (First column): Y/D=12 (Second column).

V/U=0.55

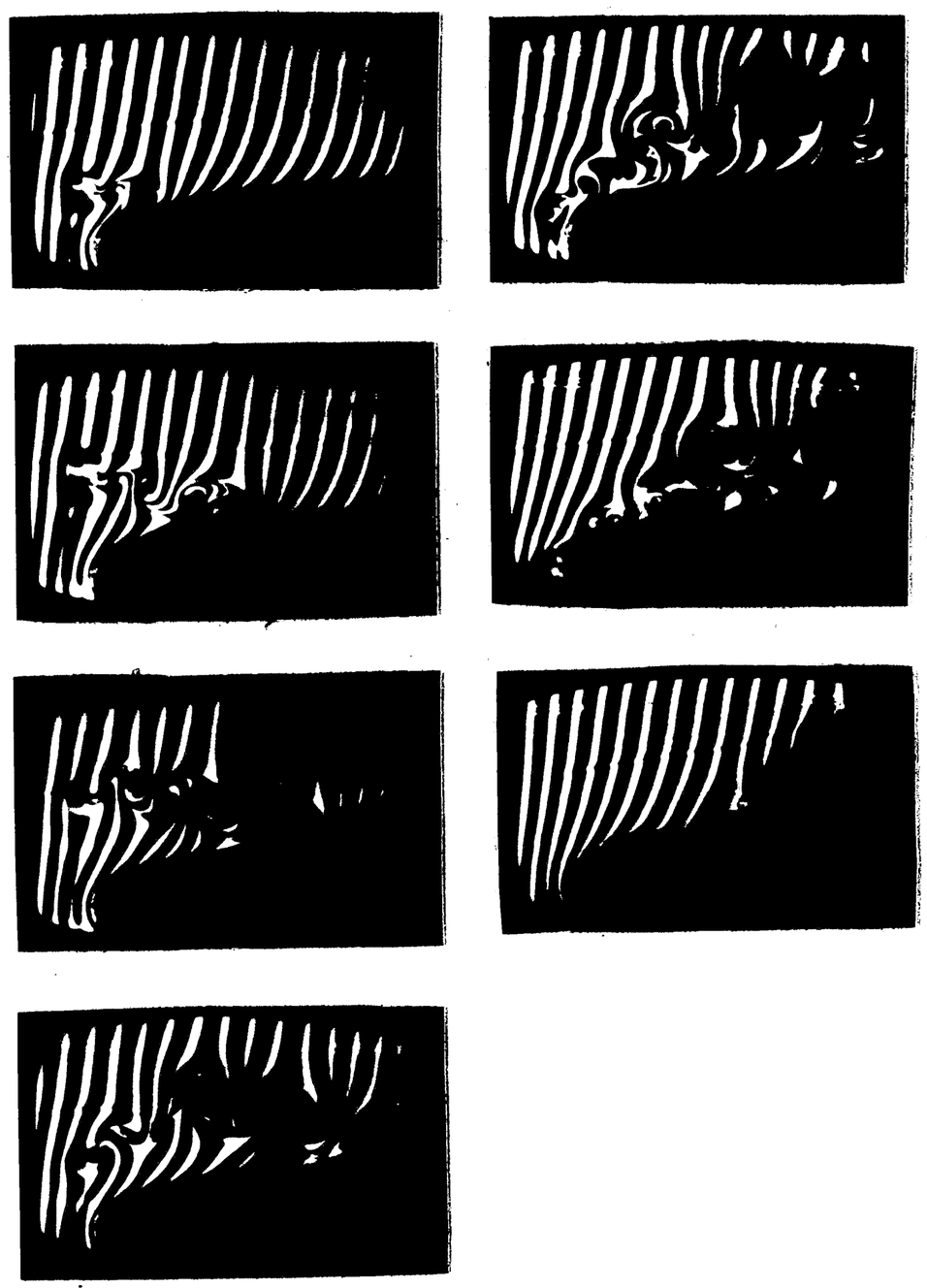

Figure 49 : Small scale interaction: D/T=1/8.

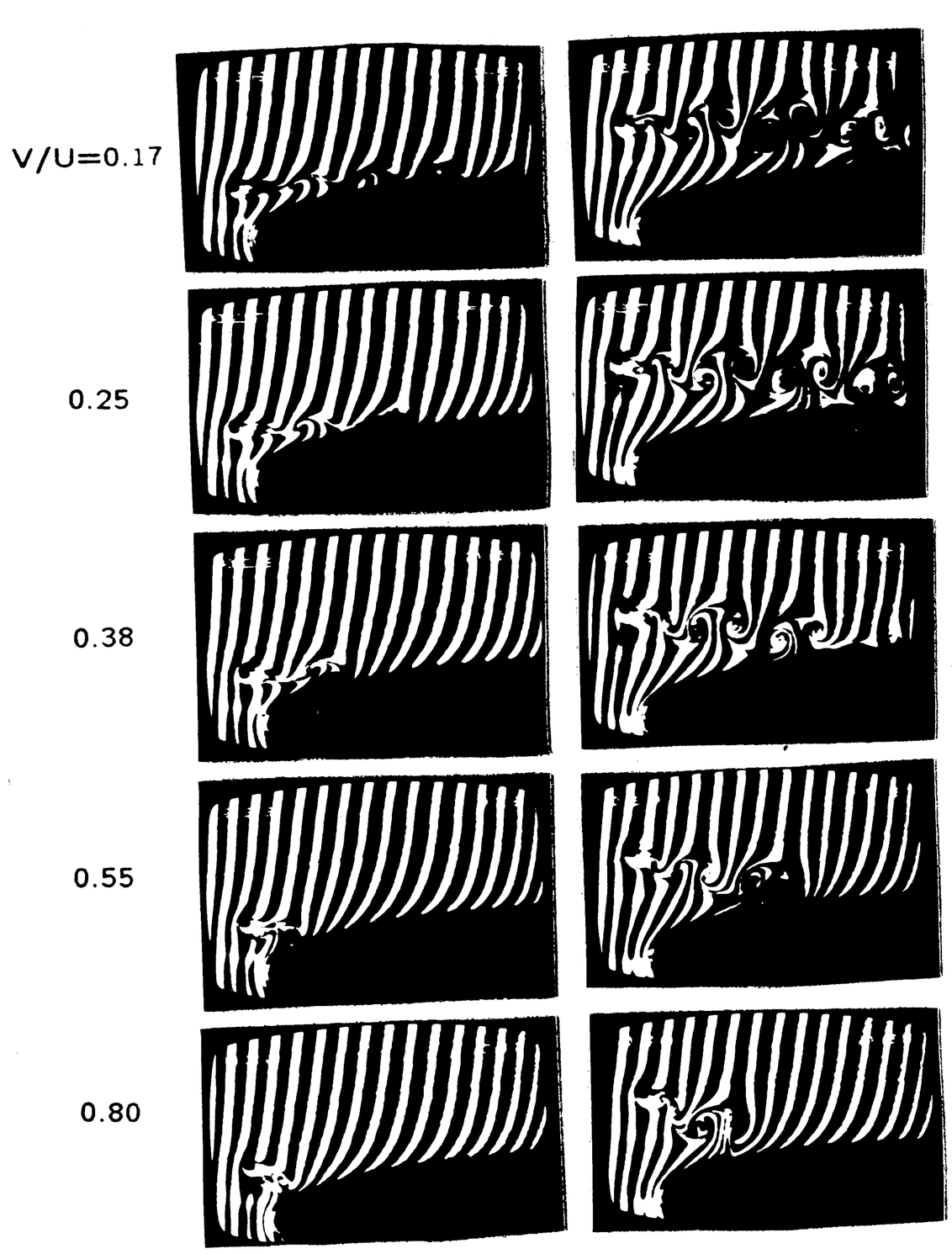

Figure 50 : Flow structure of constant distances of cylinder from centerline of elliptical edge: $0.17 \leq V/U \leq 0.80$; A/D=8; D/T=1/8; (a) Y/D=4; (b) Y/D=8.

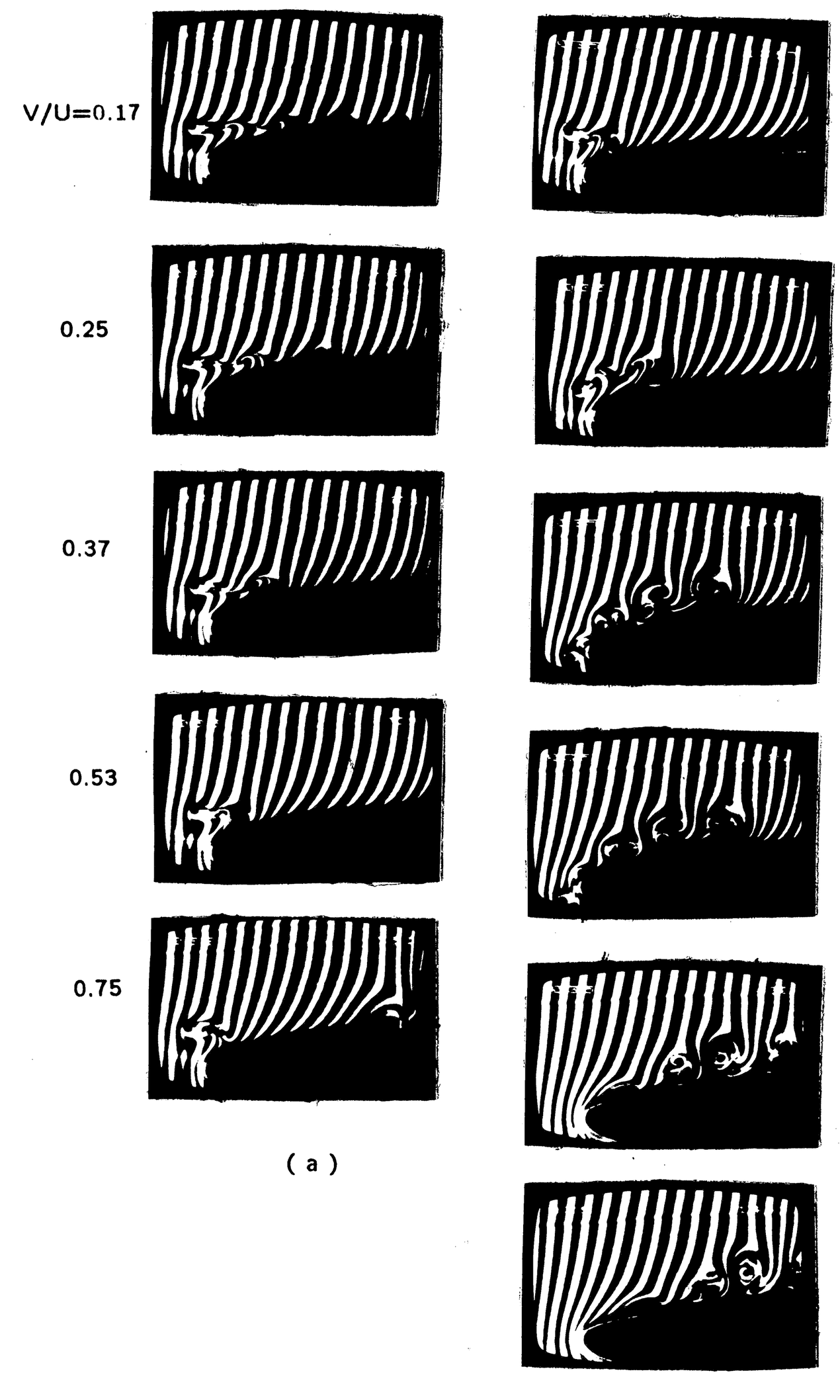

Figure 51 : (a) Flow structure of constant distances of cylinder from centerline of elliptical edge: $0.17 \leq V/U \leq 0.75$; A/D=4; D/T=1/8; Y/D=4; (b) Small scale interaction: V/U=0.53; A/D=4; D/T=1/8.

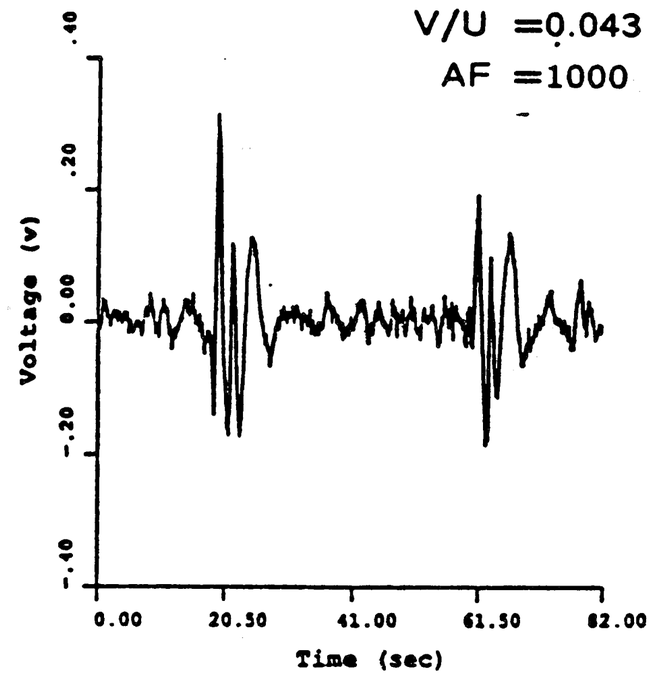

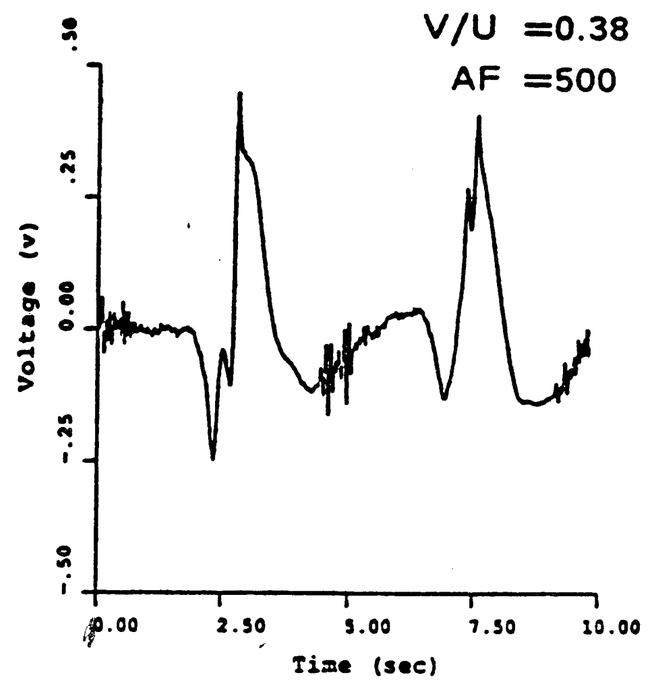

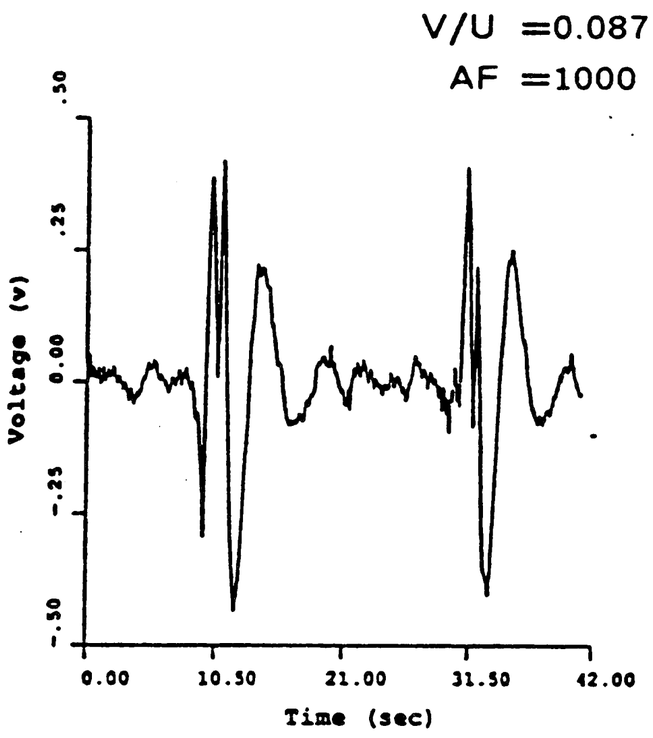

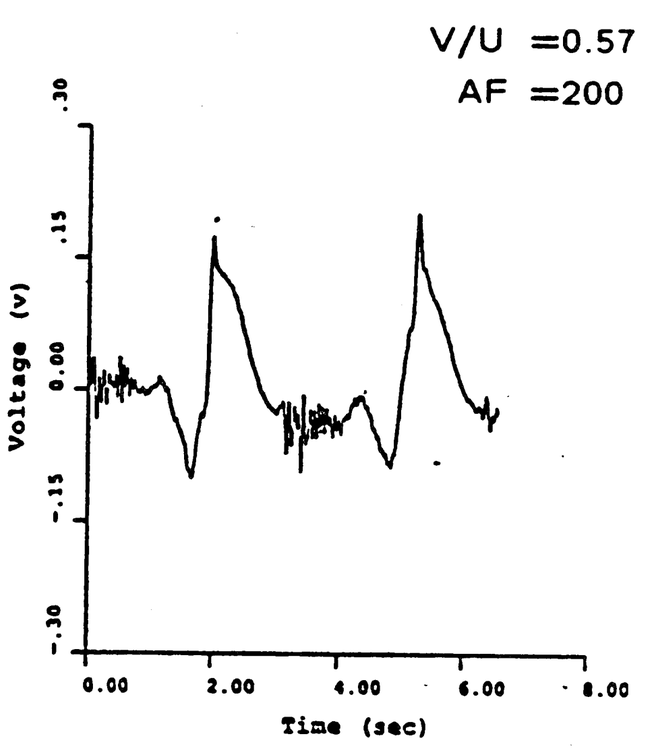

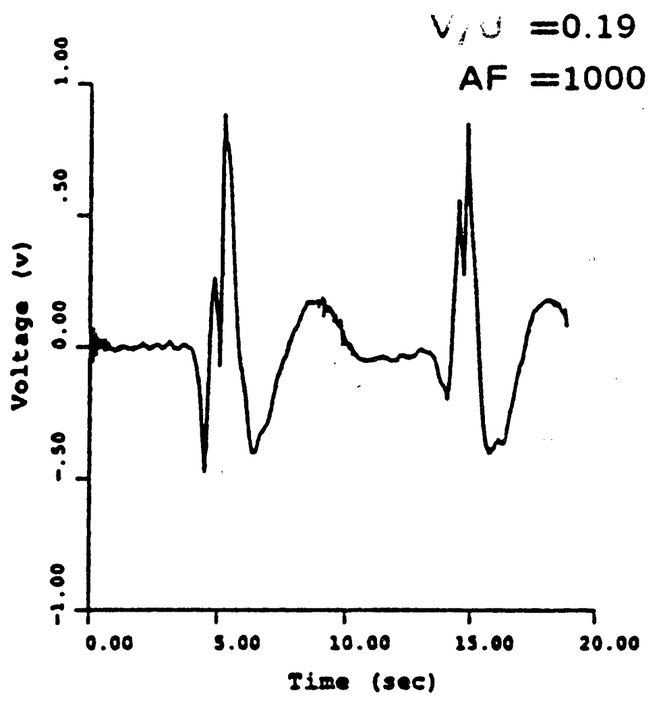

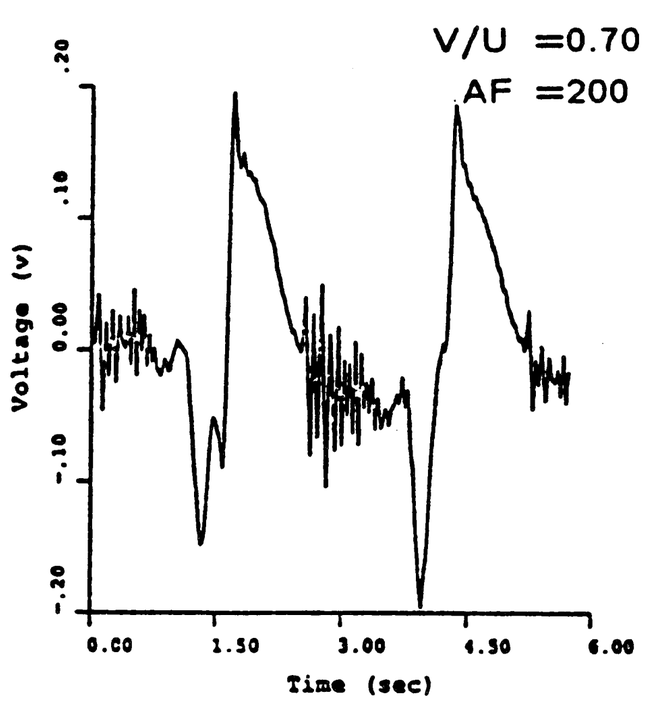

Figure 52 : Instantaneous pressure signals at tip of edge (Tap No. 13) for various values of cylinder velocity V/U at dimensionless diameter D/T=1/2 and amplitude-edge spacing A/D=5.

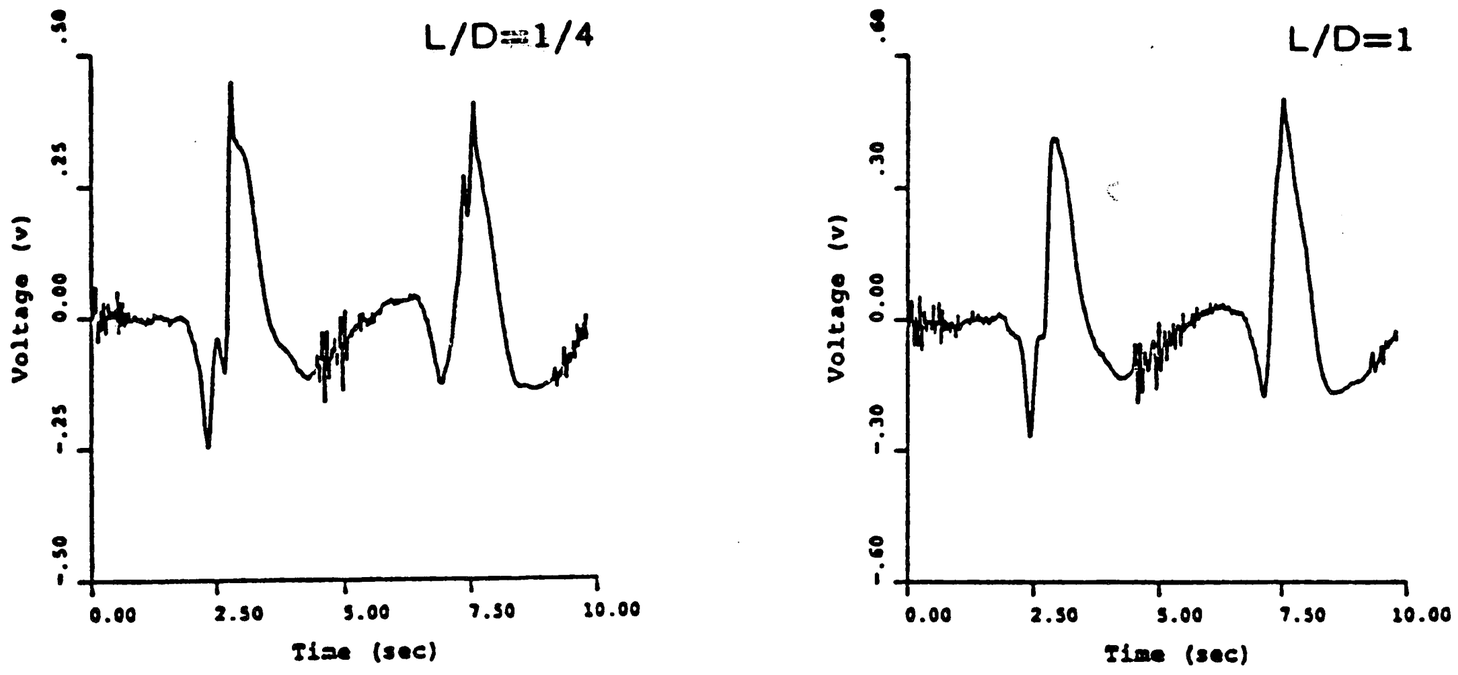

Figure 53 : Instantaneous pressure signals at tip of edge (Tap No. 13) for various values of L/D at dimensionless cylinder velocity of V/U=0.38, diameter D/T=1/2 and amplitude-edge spacing A/D=5.

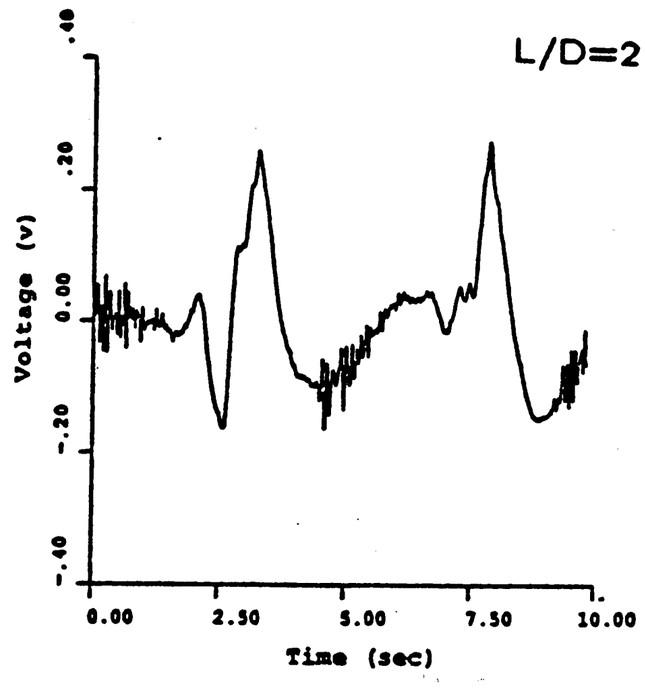

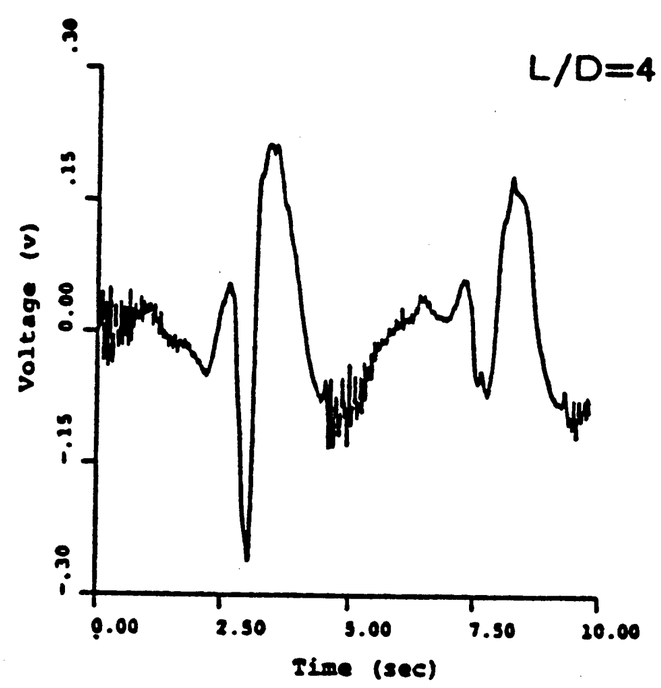

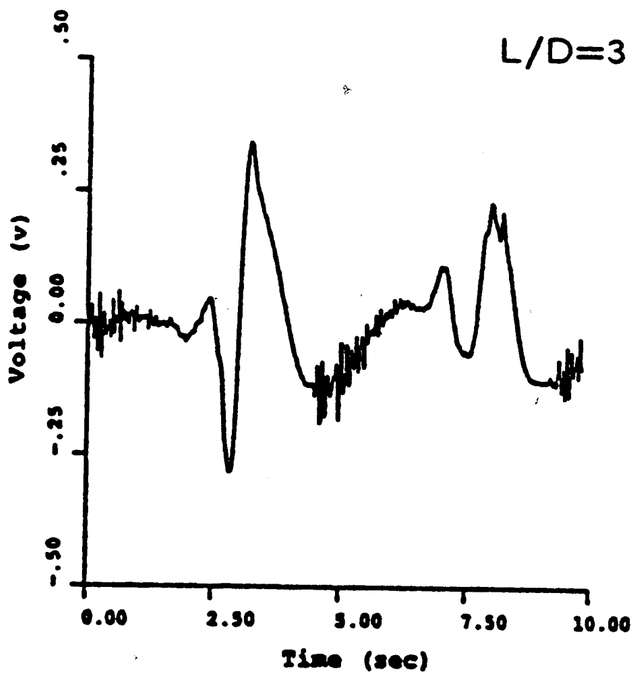

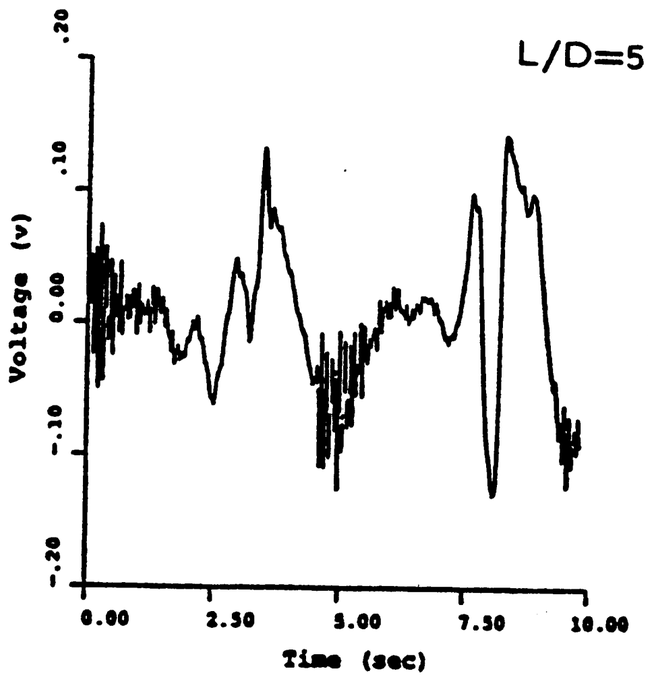

Figure 54 : **Instantaneous pressure signals at tip of edge (Tap No. 13) for various values of L/D at dimensionless cylinder velocity of V/U=0.38, diameter D/T=1/2 and amplitude-edge spacing A/D=5.**

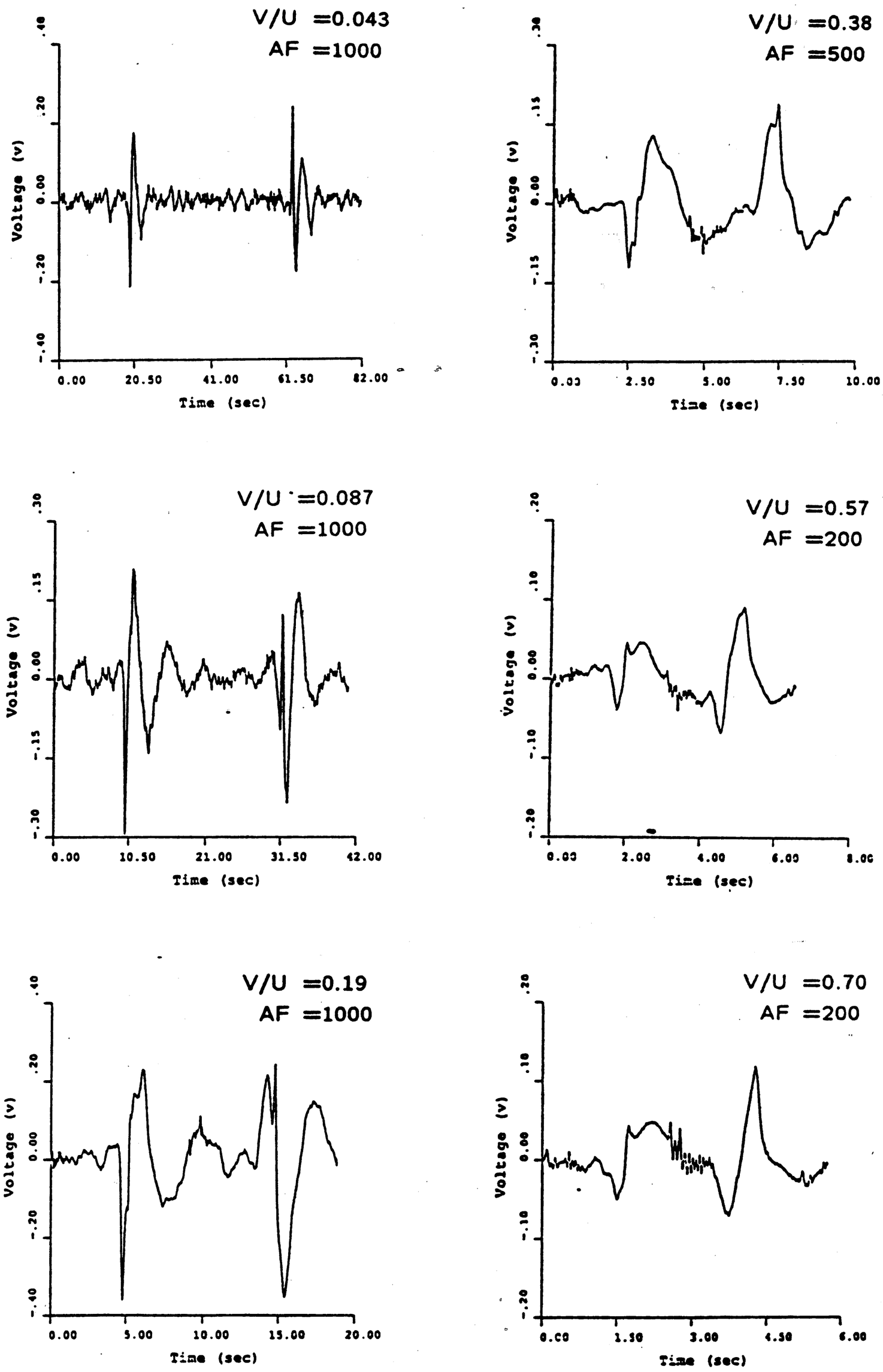

Figure 55 : Instantaneous pressure signals at downstream of tip of edge (Tap No. 14) for various values of cylinder velocity V/U at dimensionless diameter D/T=1/2 and amplitude-edge spacing A/D=5.

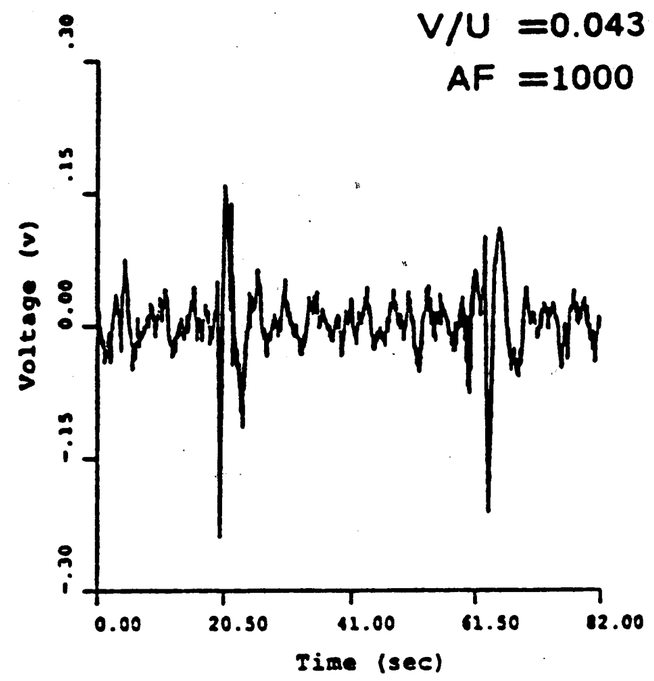

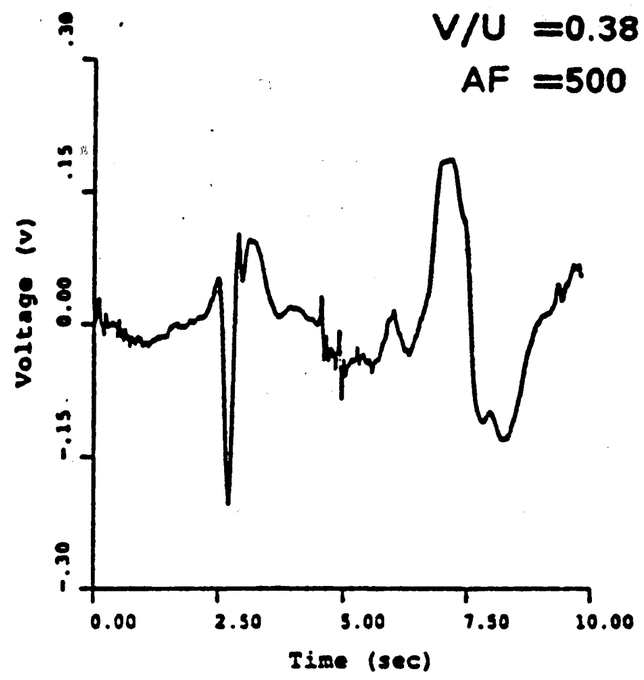

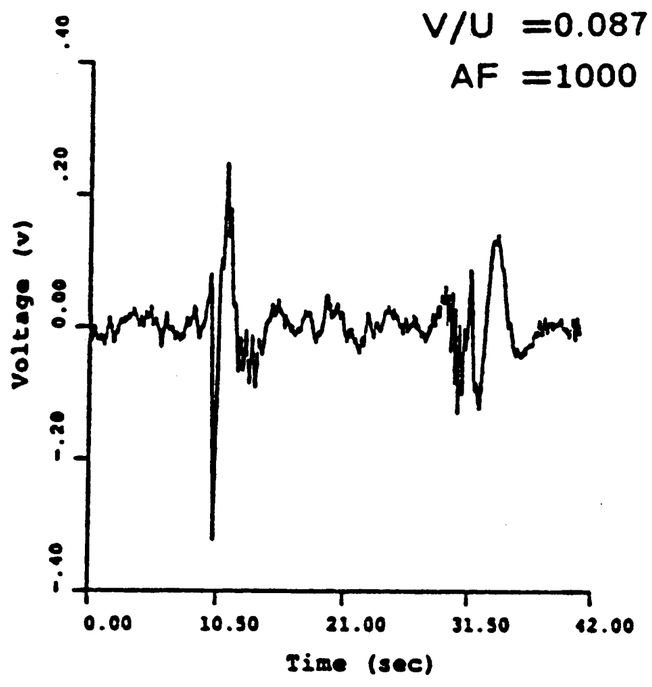

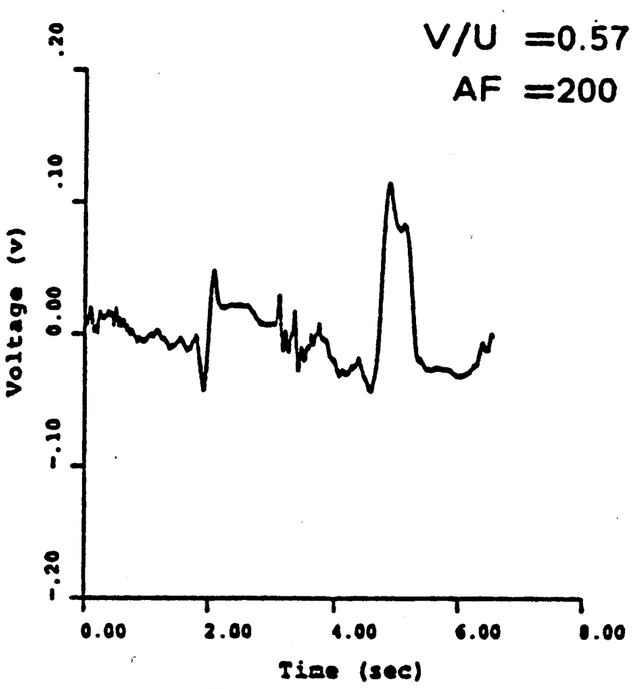

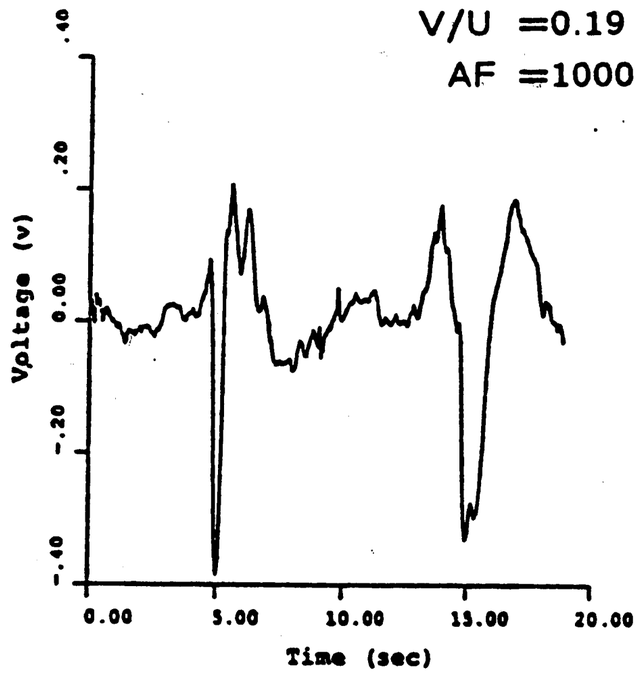

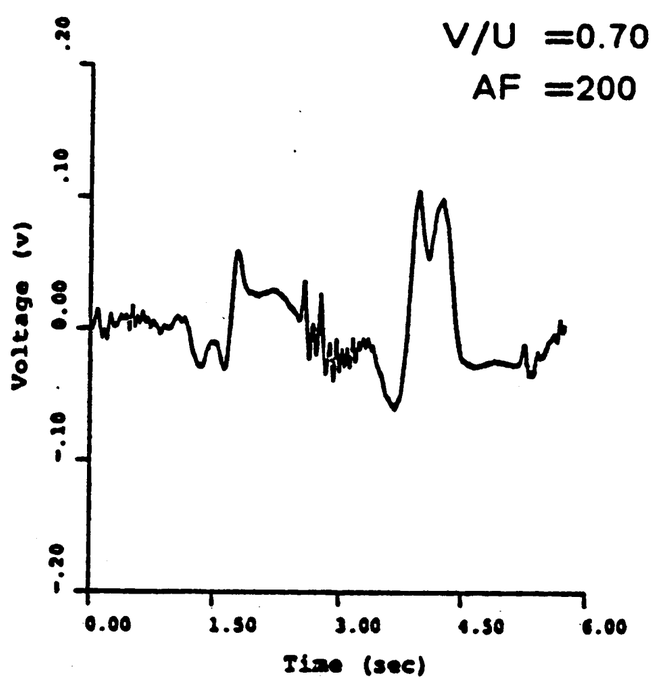

Figure 56 : Instantaneous pressure signals at downstream of tip of edge (Tap No. 15) for various values of cylinder velocity V/U at dimensionless diameter D/T=1/2 and amplitude-edge spacing A/D=5.

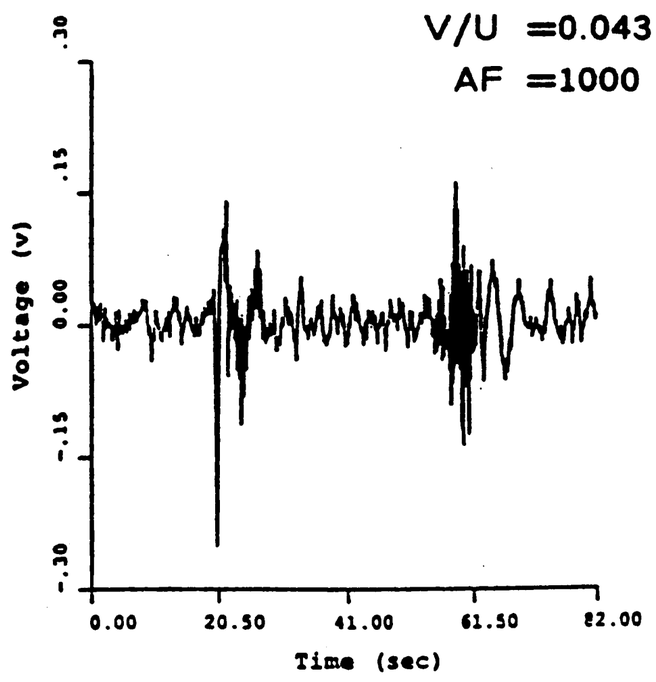

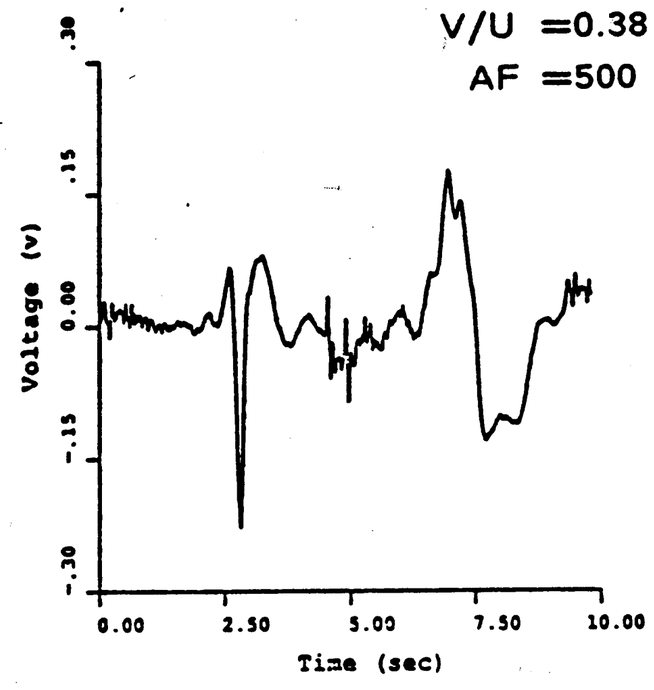

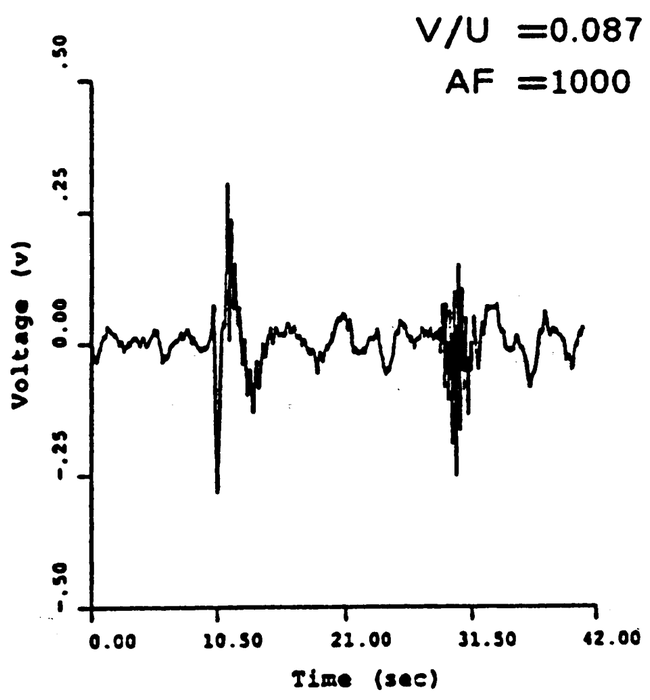

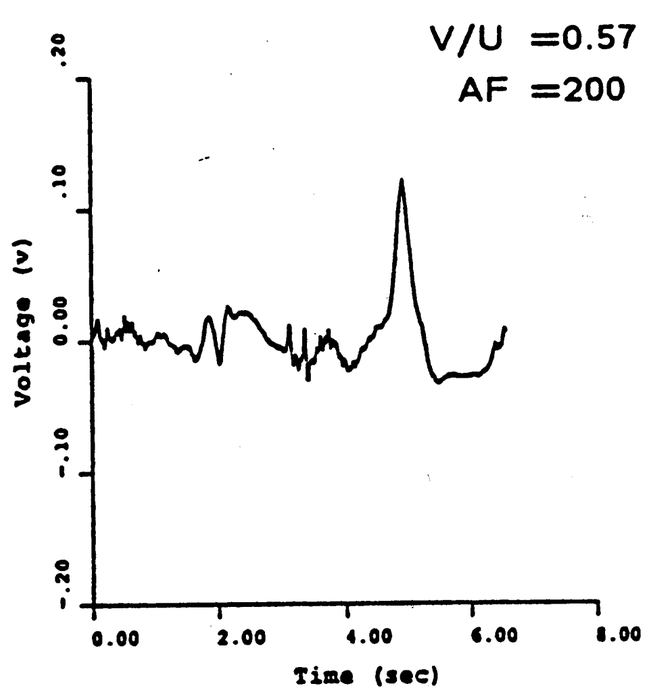

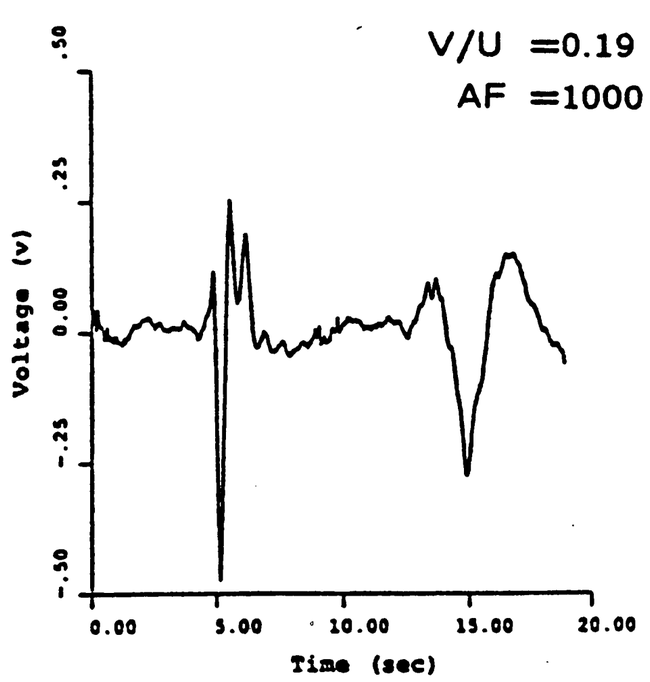

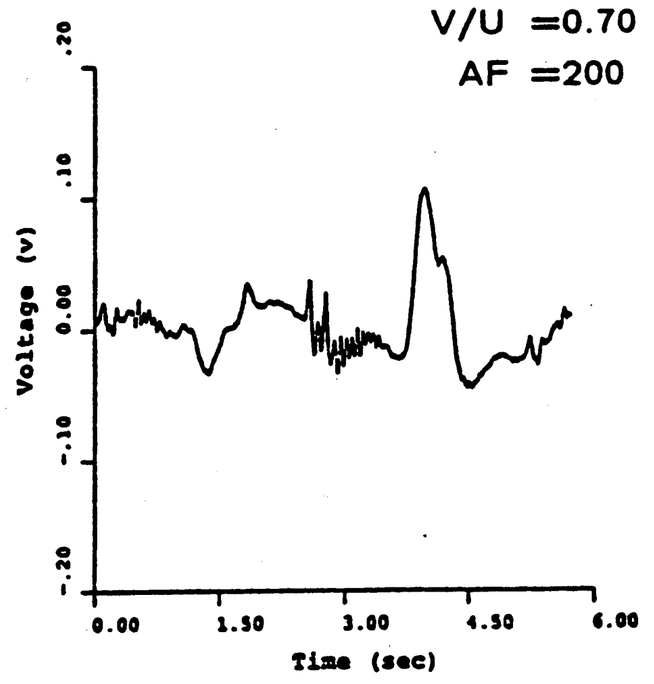

Figure 57 : Instantaneous pressure signals at downstream of tip of edge (Tap No. 16) for various values of cylinder velocity V/U at dimensionless diameter D/T=1/2 and amplitude-edge spacing A/D=5.

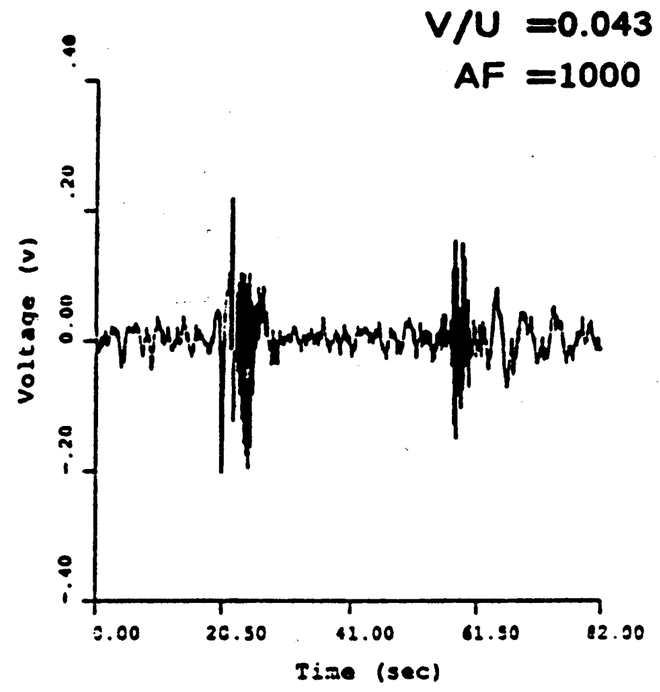

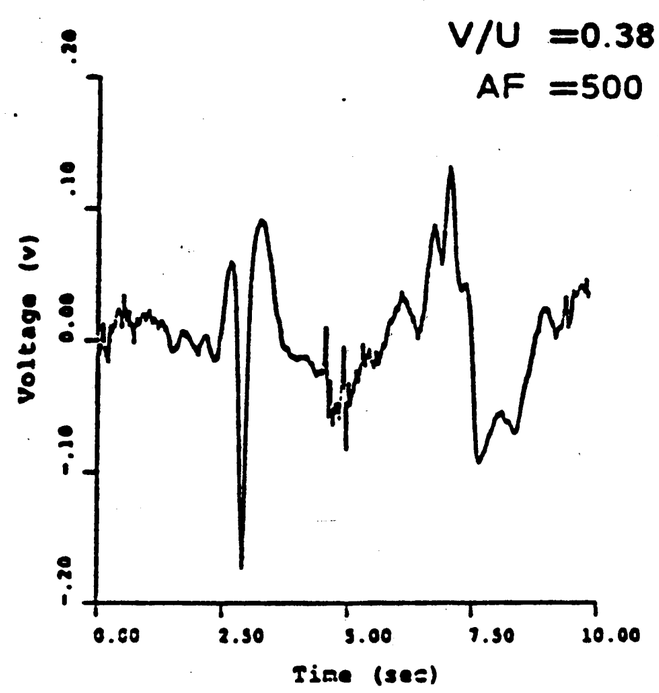

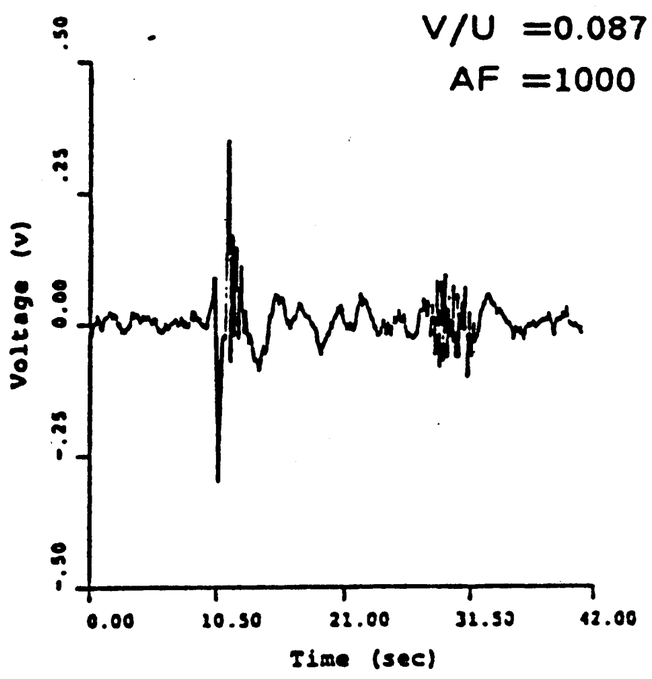

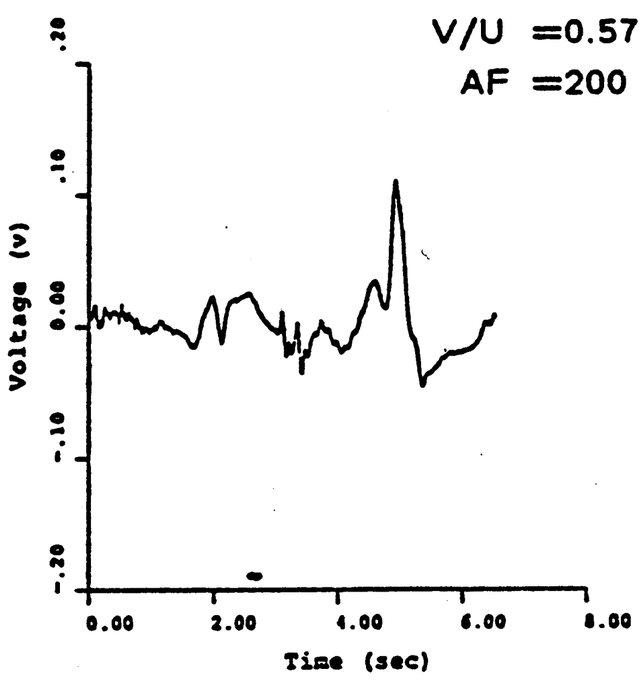

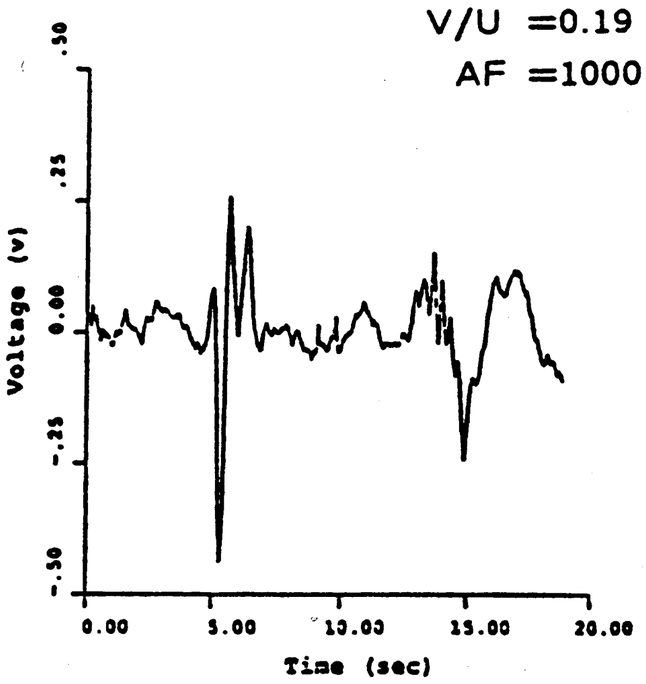

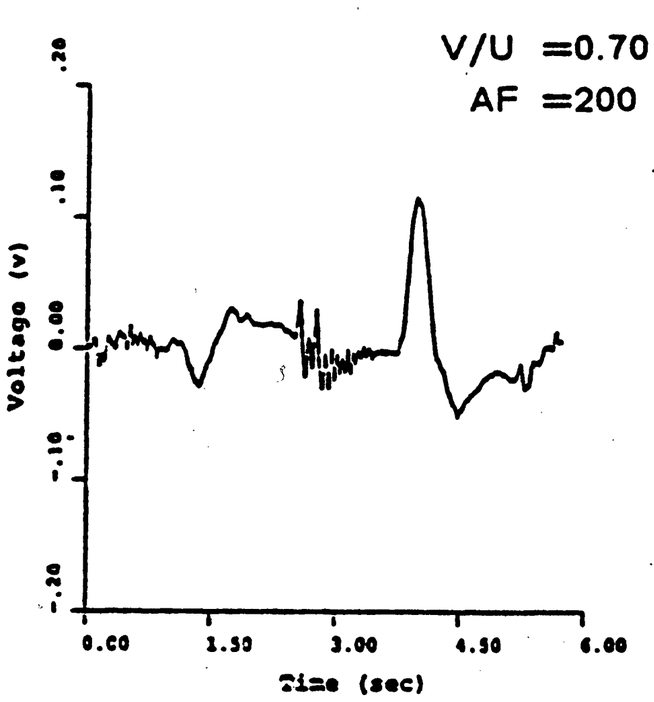

Figure 58 : Instantaneous pressure signals at downstream of tip of edge (Tap No. 17) for various values of cylinder velocity V/U at dimensionless diameter D/T=1/2 and amplitude-edge spacing A/D=5.

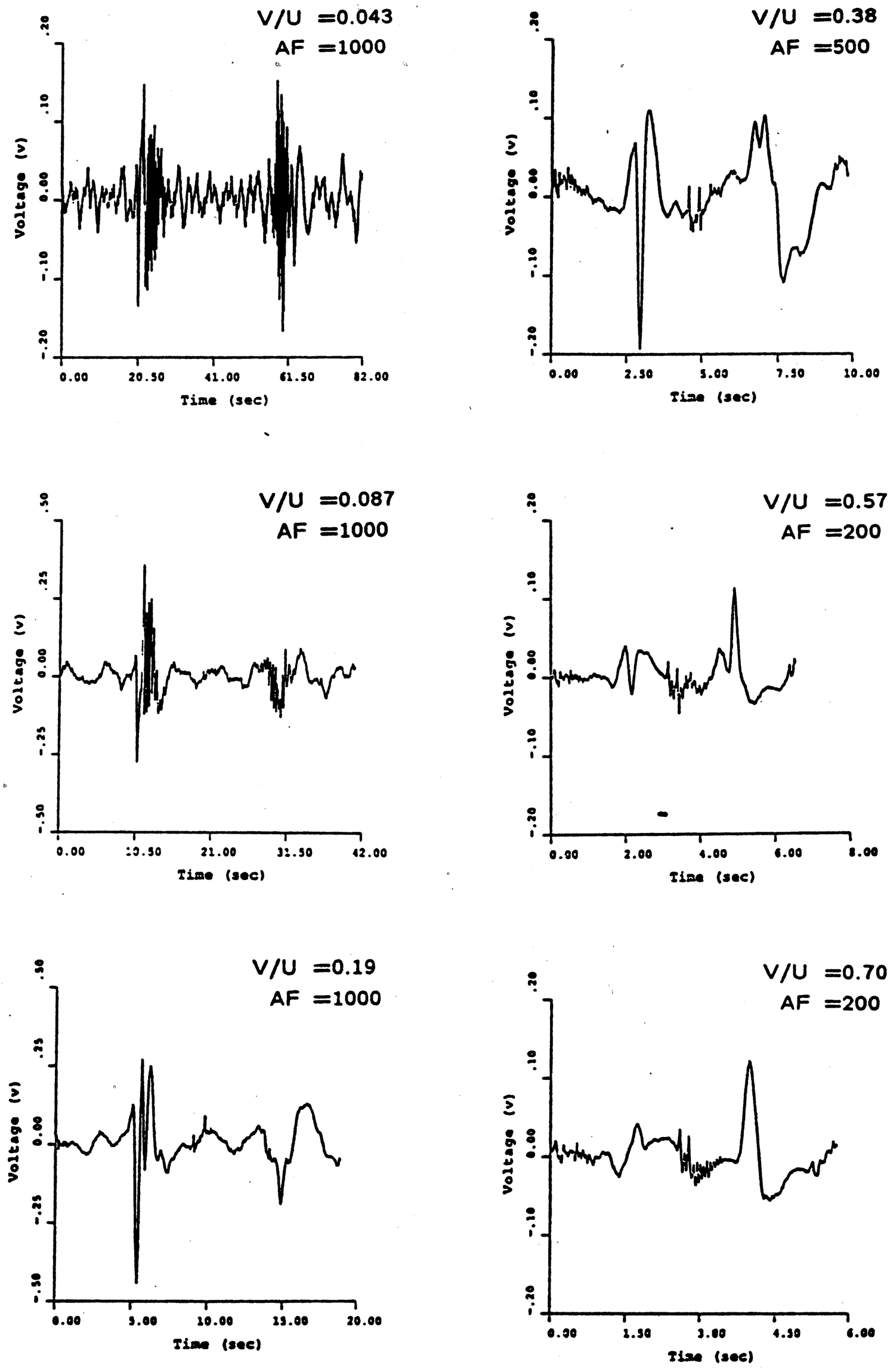

Figure 59 : Instantaneous pressure signals at downstream of tip of edge (Tap No. 18) for various values of cylinder velocity V/U at dimensionless diameter D/T=1/2 and amplitude-edge spacing A/D=5.

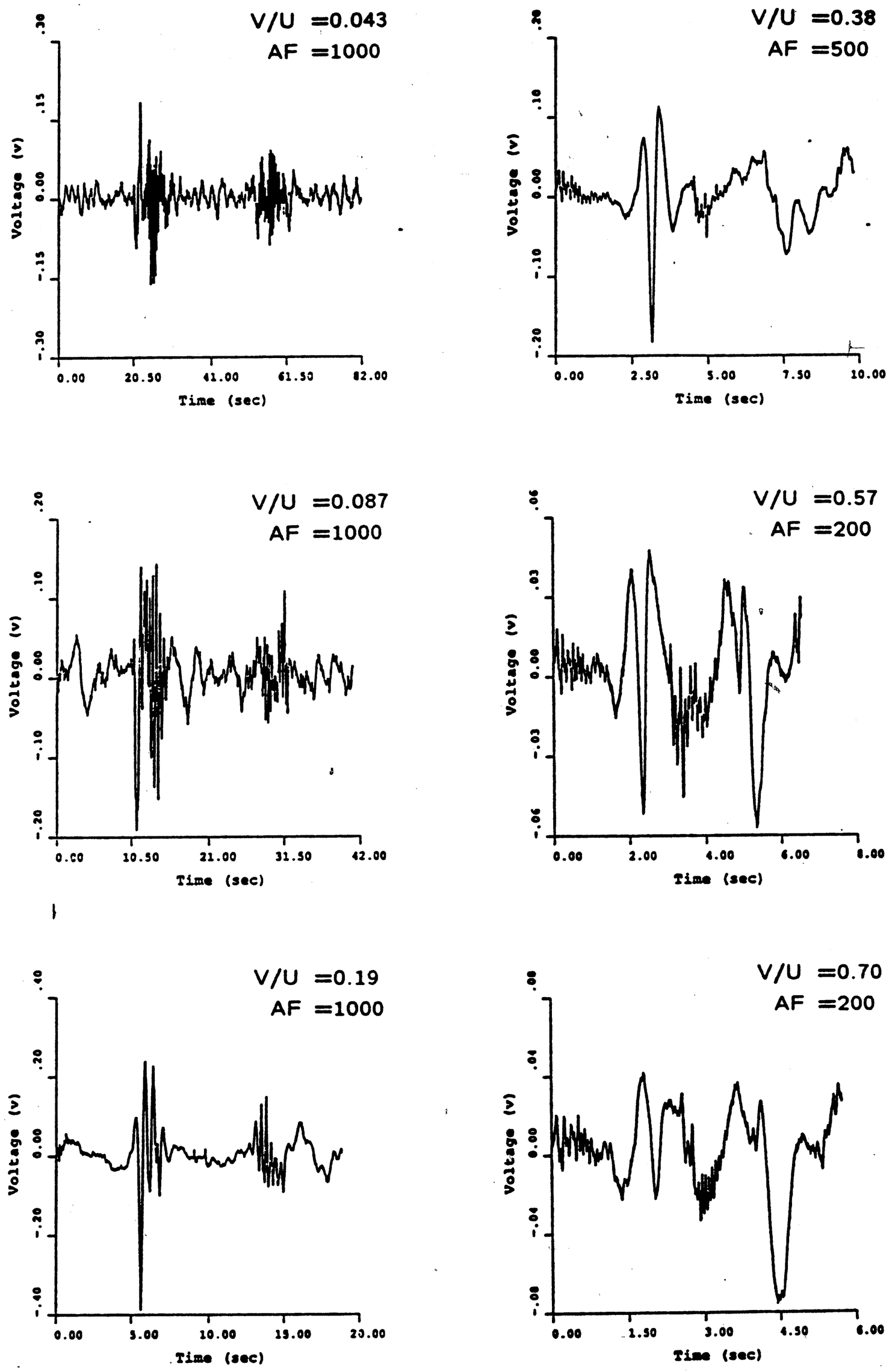

Figure 60 : Instantaneous pressure signals at downstream of tip of edge (Tap No. 20) for various values of cylinder velocity V/U at dimensionless diameter D/T=1/2 and amplitude-edge spacing A/D=5.

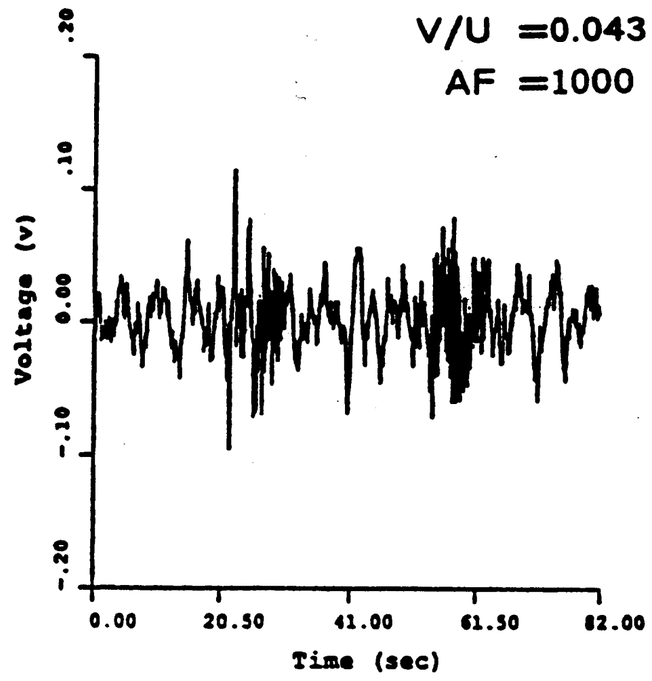

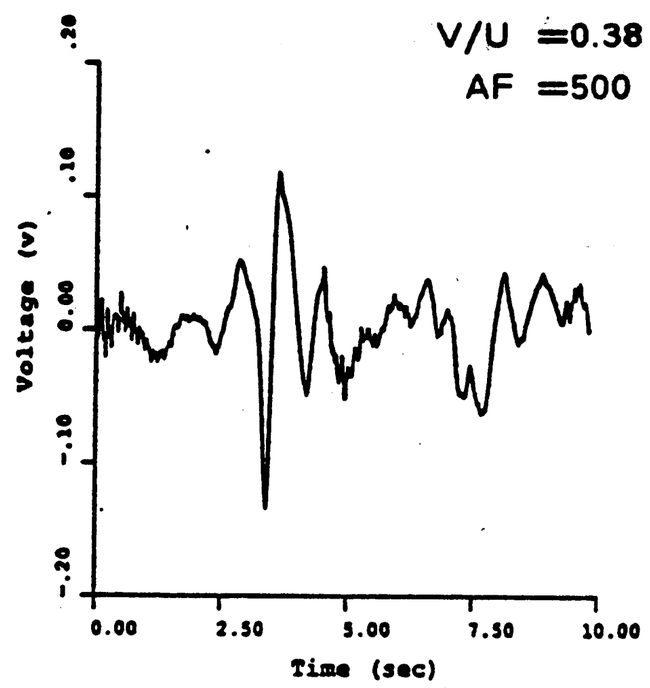

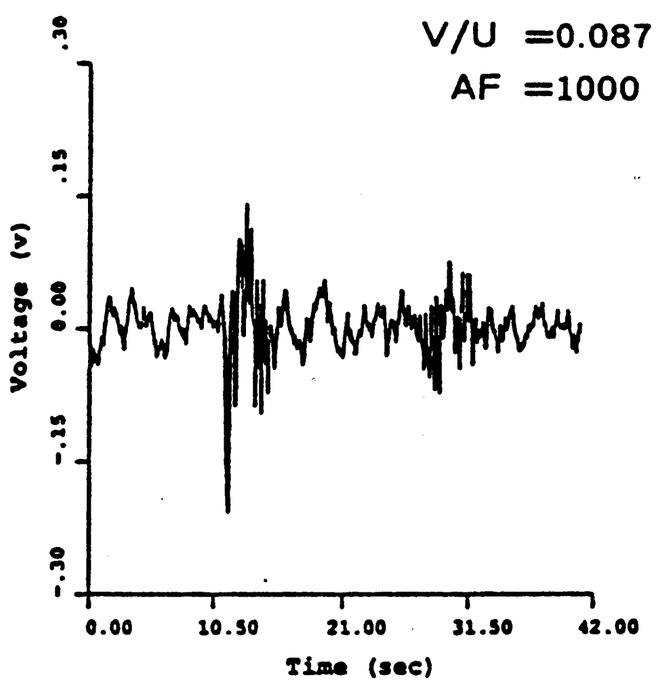

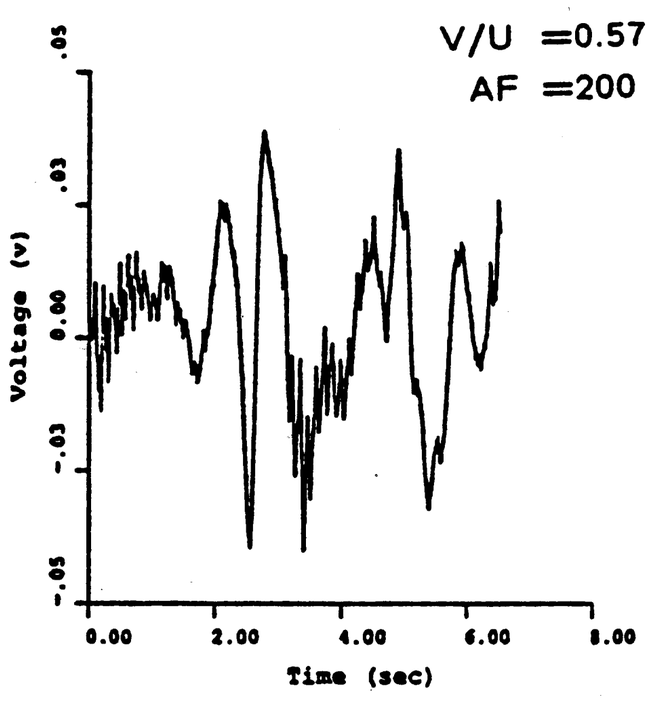

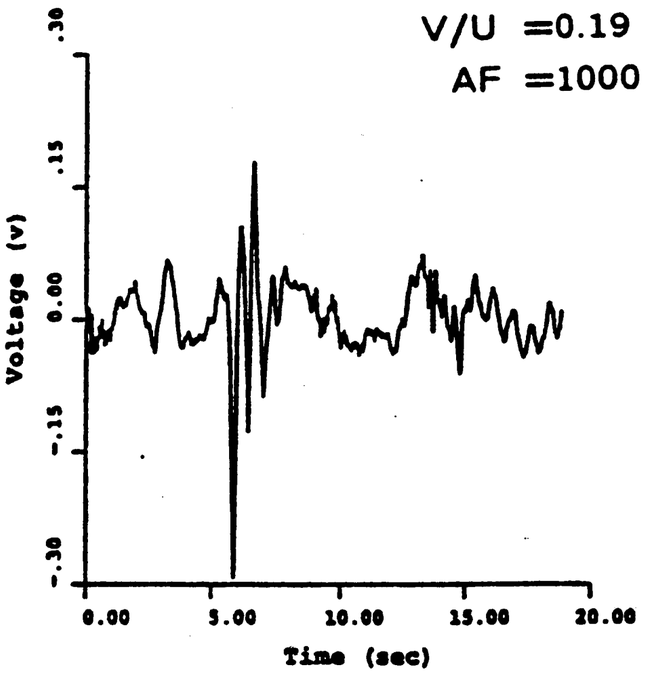

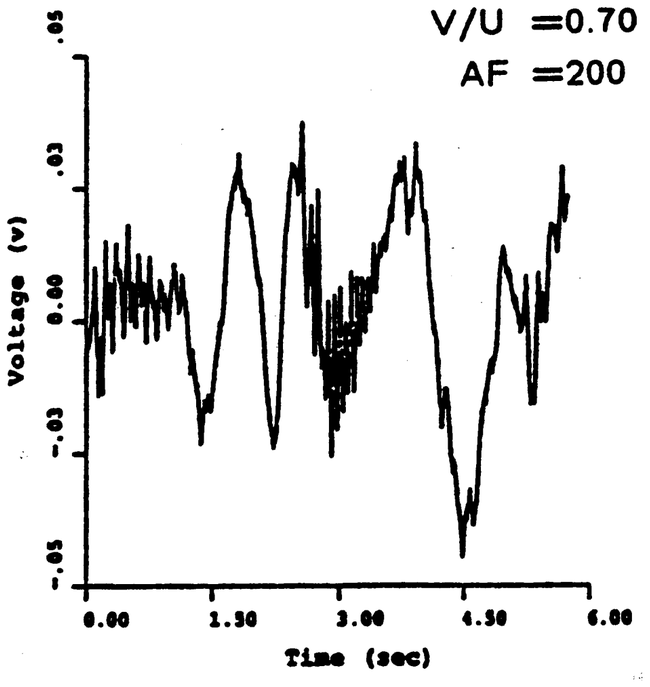

Figure 61 : Instantaneous pressure signals at downstream of tip of edge (Tap No. 22) for various values of cylinder velocity V/U at dimensionless diameter D/T=1/2 and amplitude-edge spacing A/D=5.

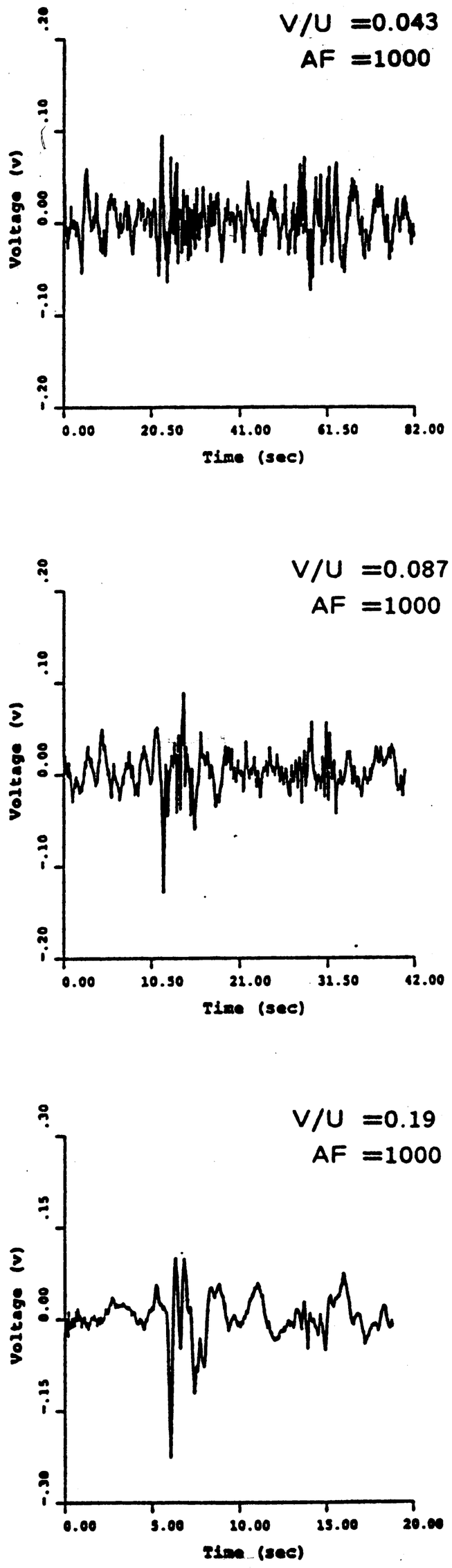

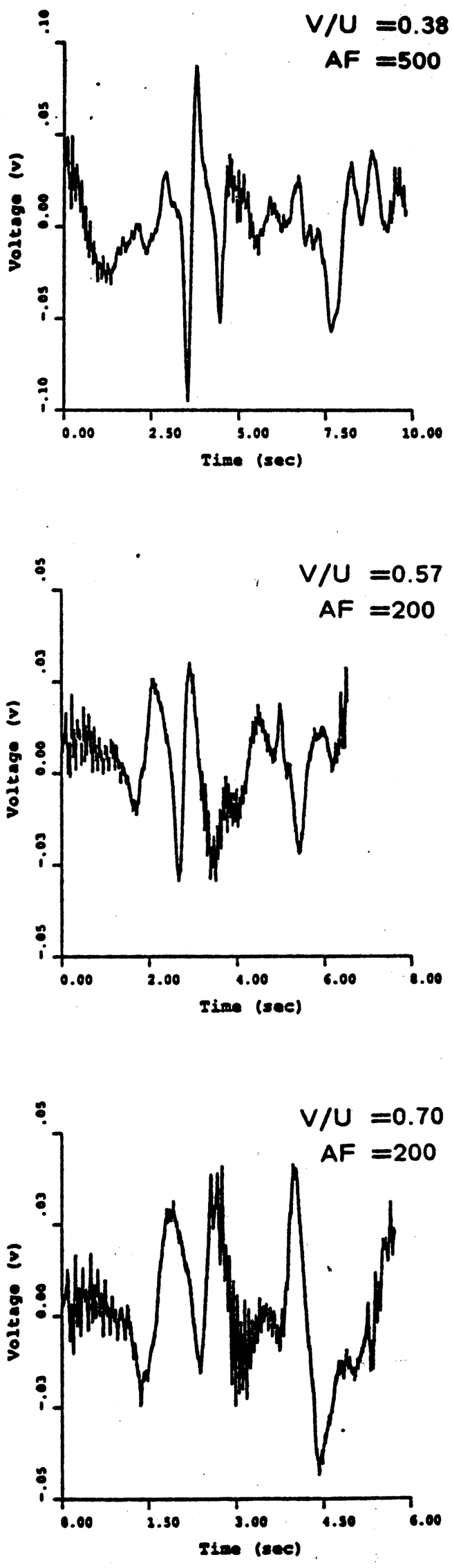

Figure 62 : Instantaneous pressure signals at downstream of tip of edge (Tap No. 24) for various values of cylinder velocity V/U at dimensionless diameter D/T=1/2 and amplitude-edge spacing A/D=5.

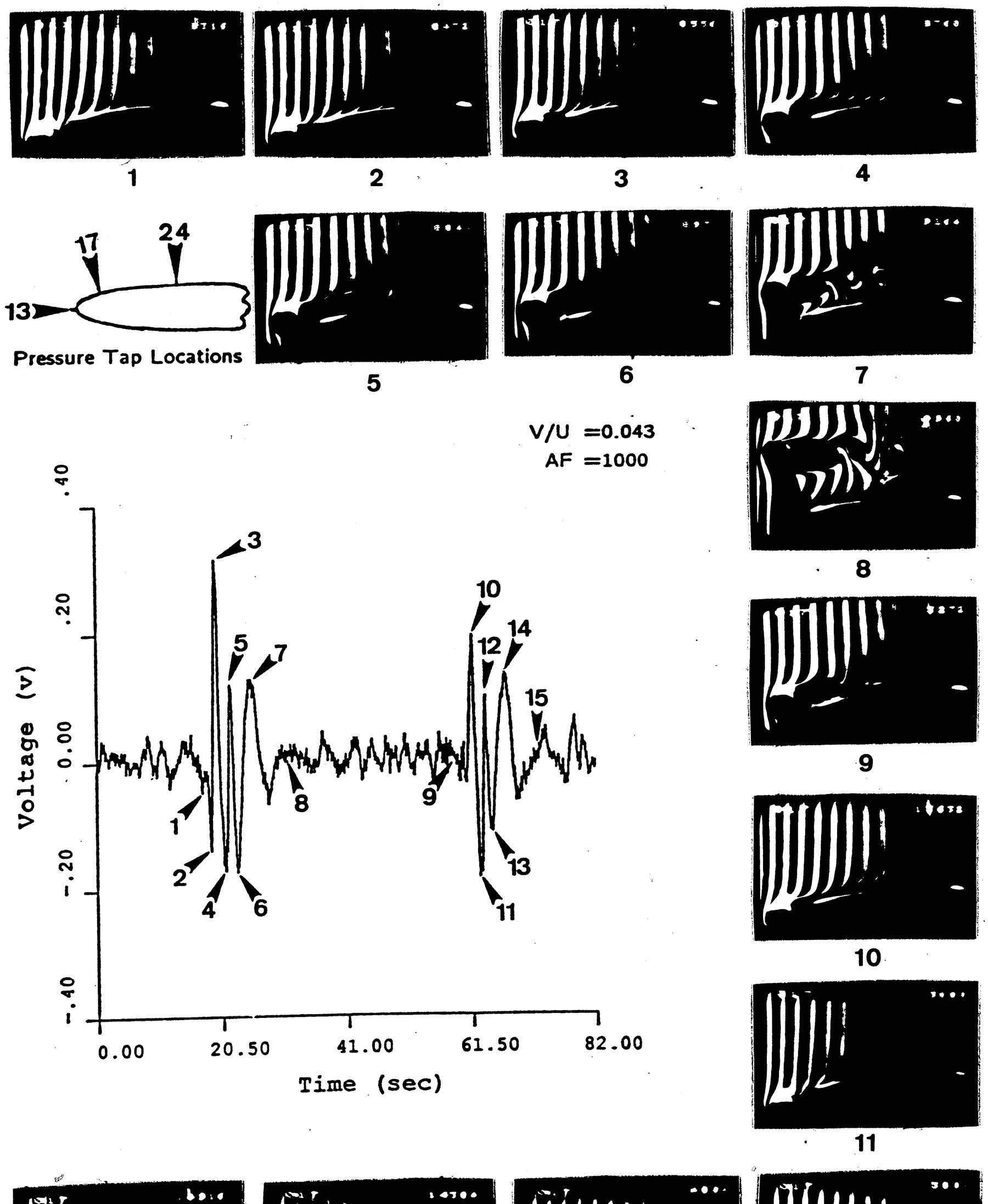

Figure 63 : Correlation between the instantaneous pressure signal and the unsteady flow structure at the tip of the edge.

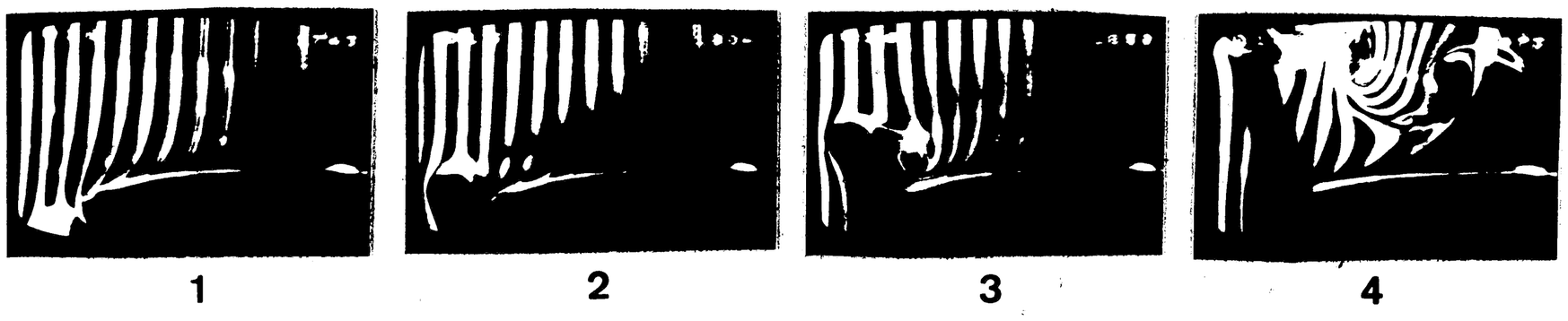

Figure 64 : Correlation between the instantaneous pressure signal and the unsteady flow structure at the tip of the edge.

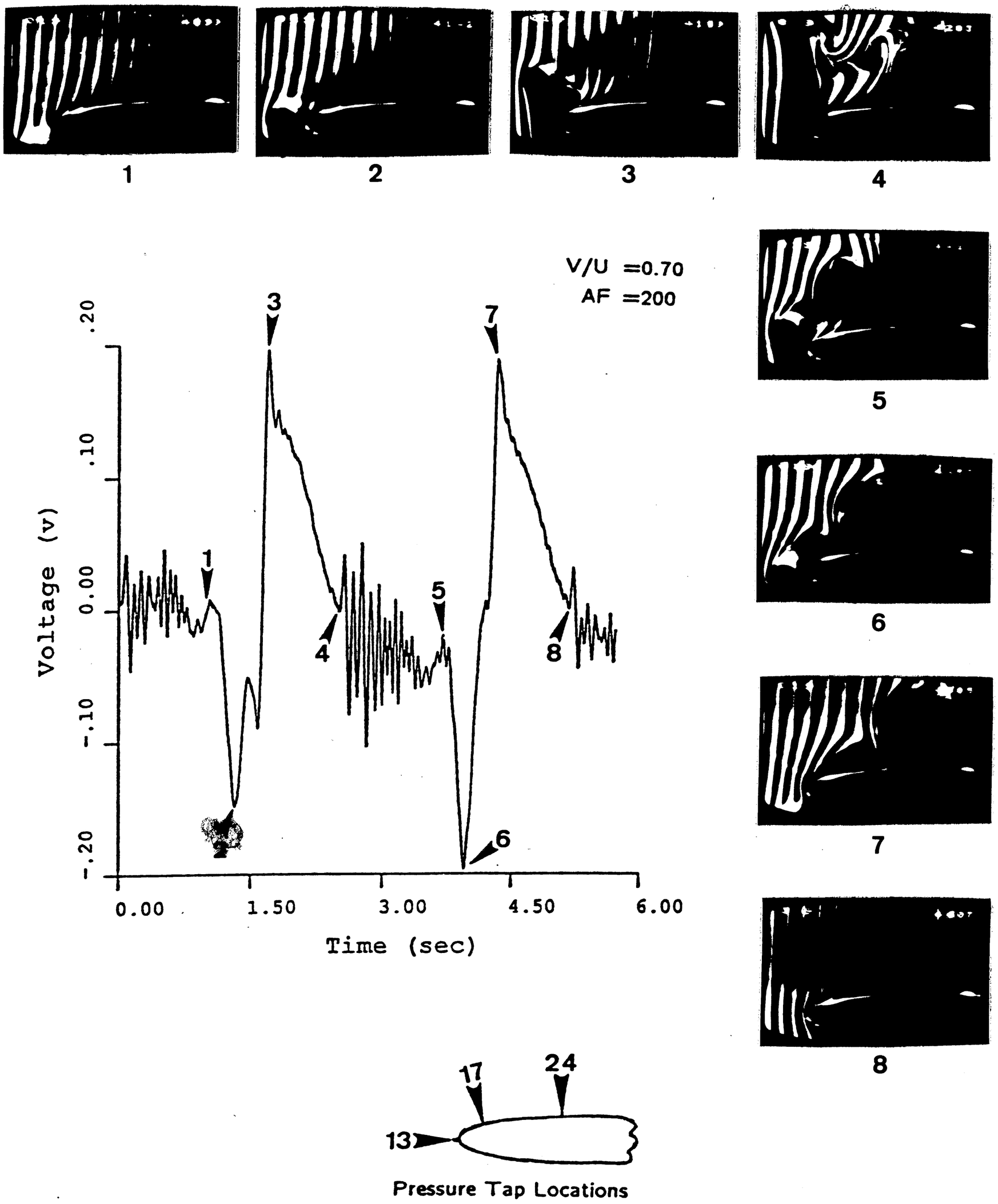

Figure 65 : Correlation between the instantaneous pressure signal and the unsteady flow structure at the tip of the edge.

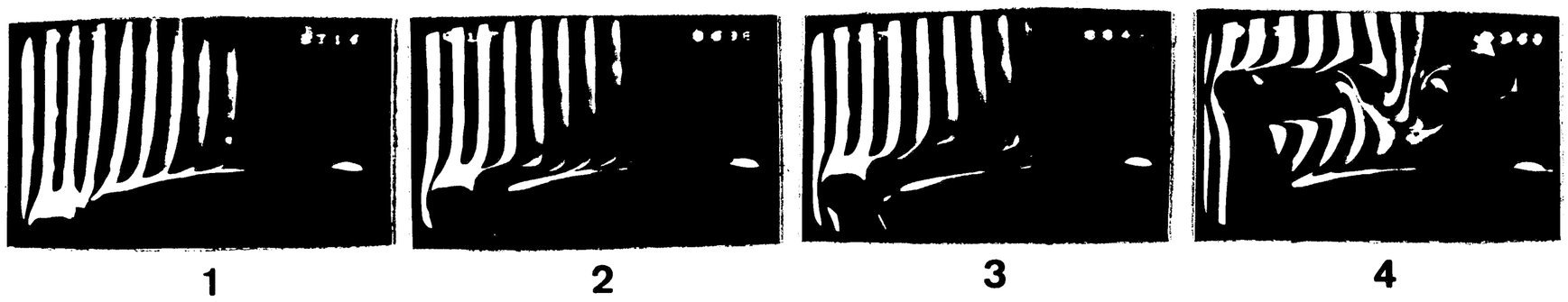

1 2 3 4

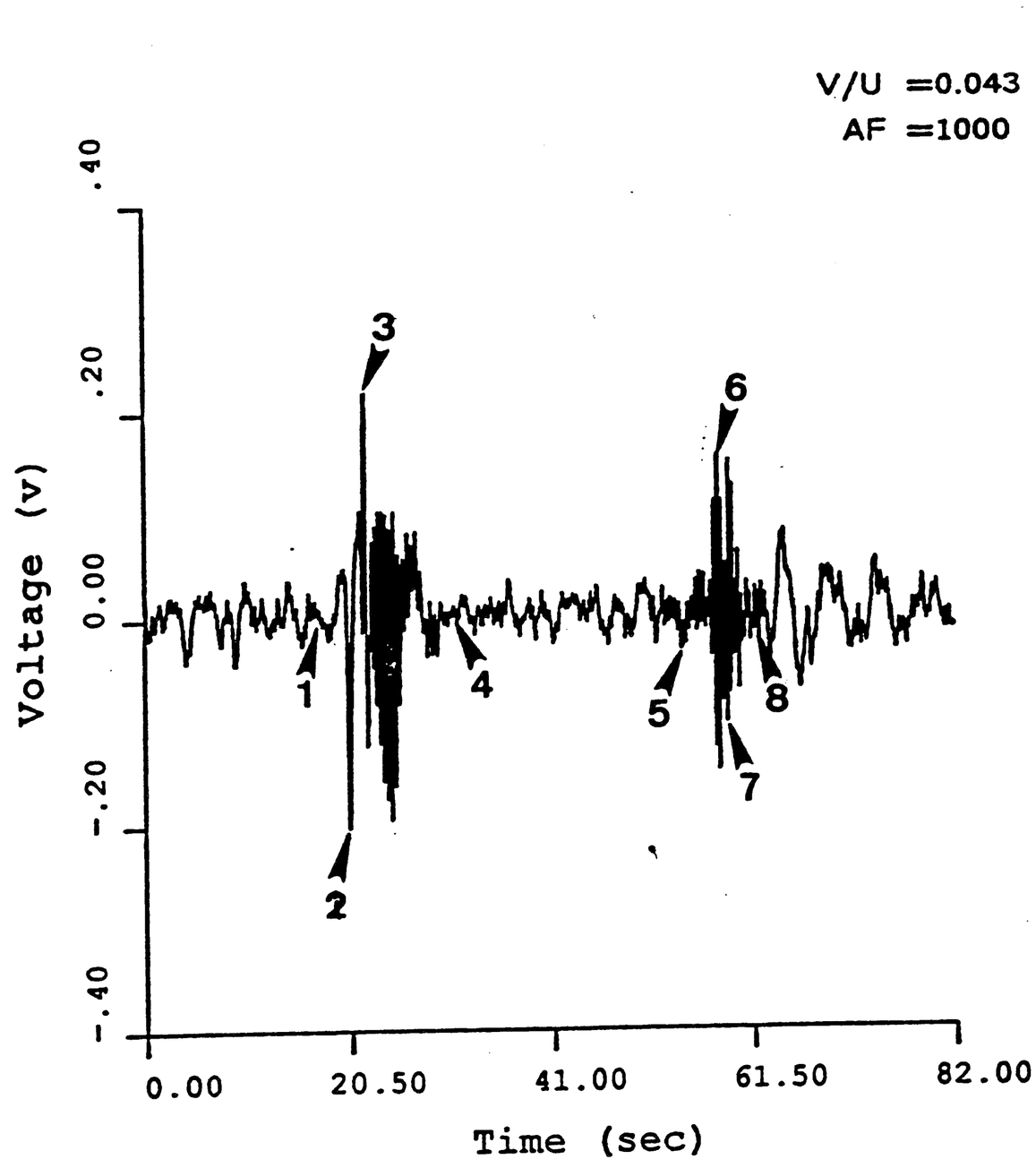

5

6

7

8

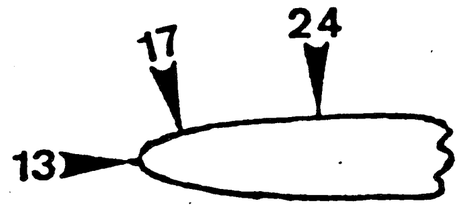

Pressure Tap Locations

Figure 66 : Correlation between the instantaneous pressure signal and the unsteady flow structure along the edge (Tap No. 17).

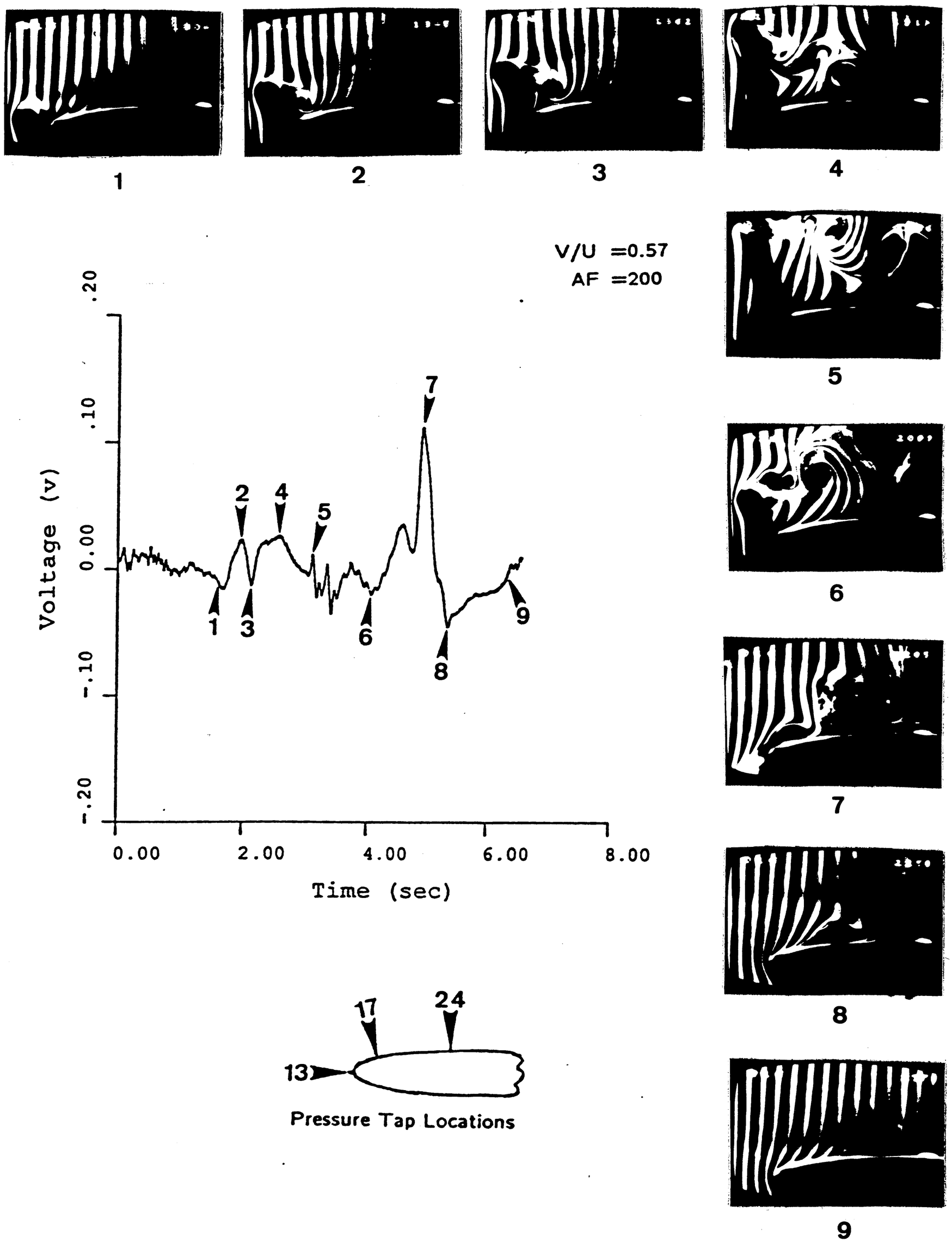

Figure 67 : Correlation between the instantaneous pressure signal and the unsteady flow structure along the edge (Tap No. 17).

Figure 68 : Correlation between the instantaneous pressure signal and the unsteady flow structure along the edge (Tap No. 17).

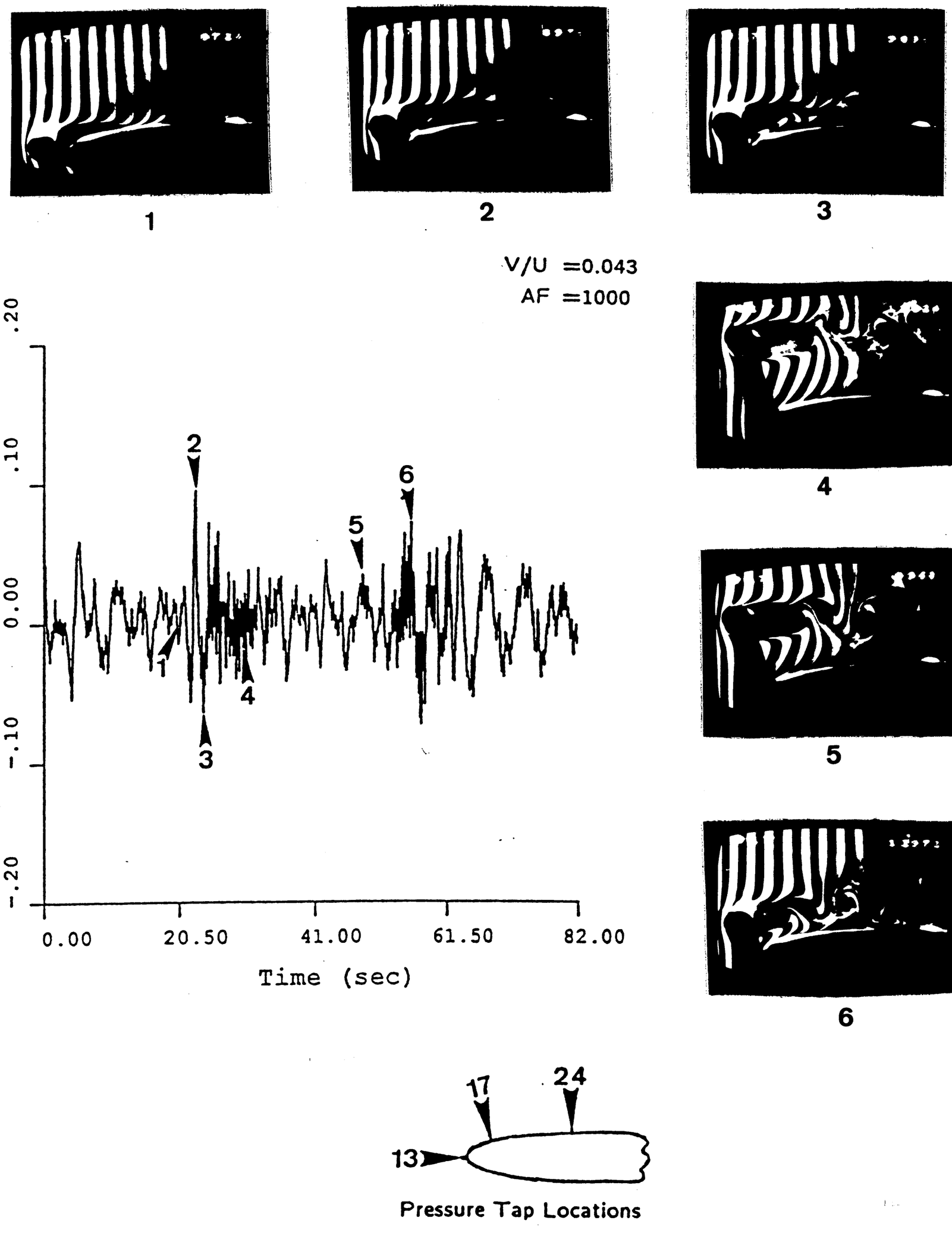

Figure 69 : Correlation between the instantaneous pressure signal and the unsteady flow structure along the edge (Tap No. 24).

1

2

3

4

5

6

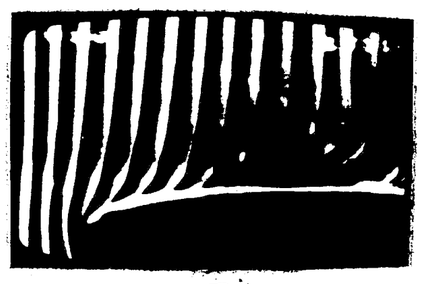

7

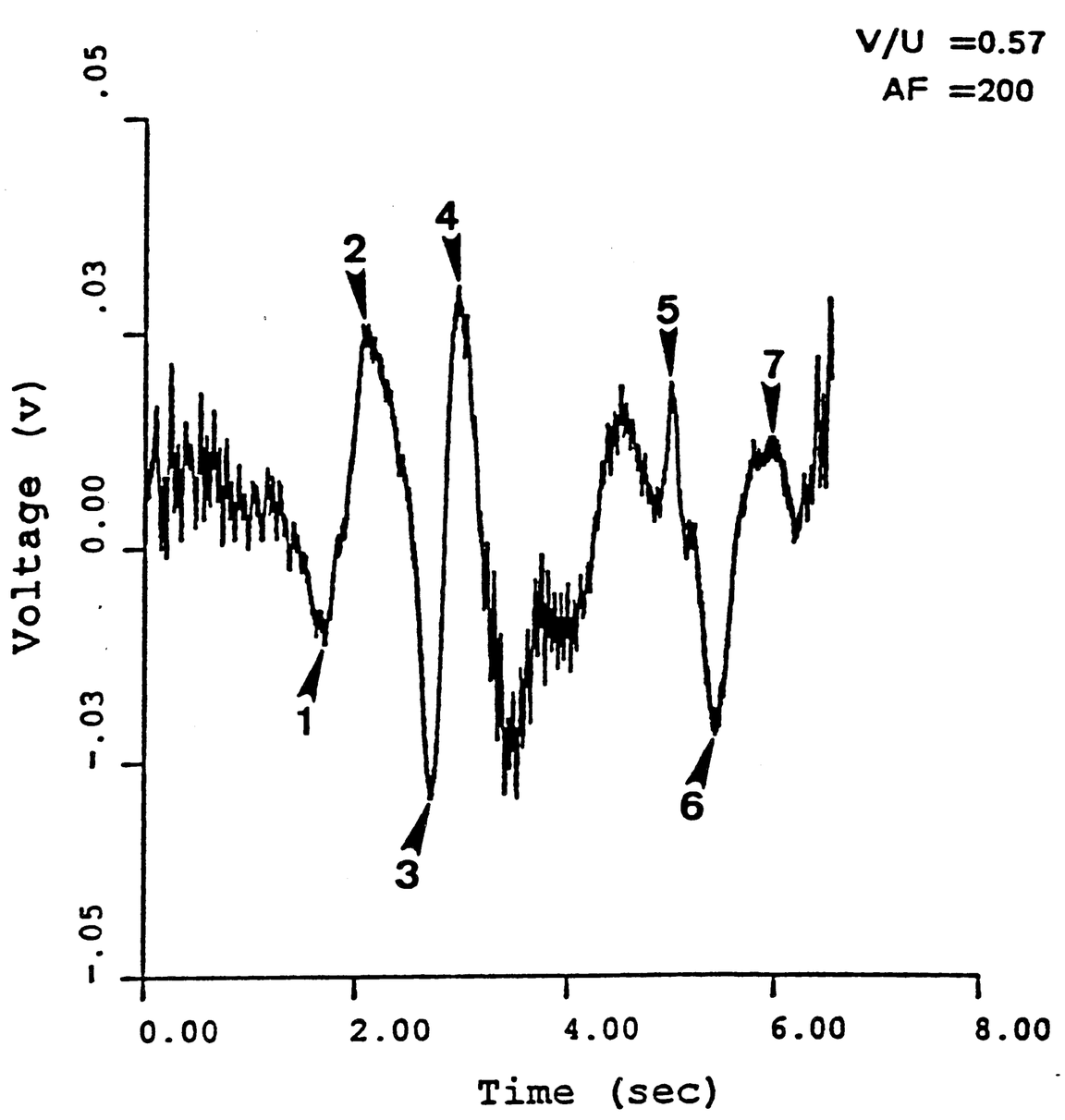

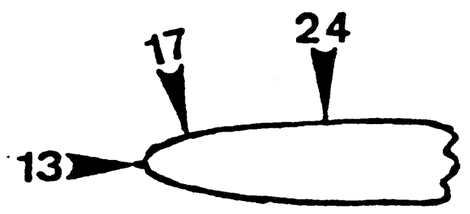

Pressure Tap Locations

Figure 70 : Correlation between the instantaneous pressure signal and the unsteady flow structure along the edge (Tap No. 24).

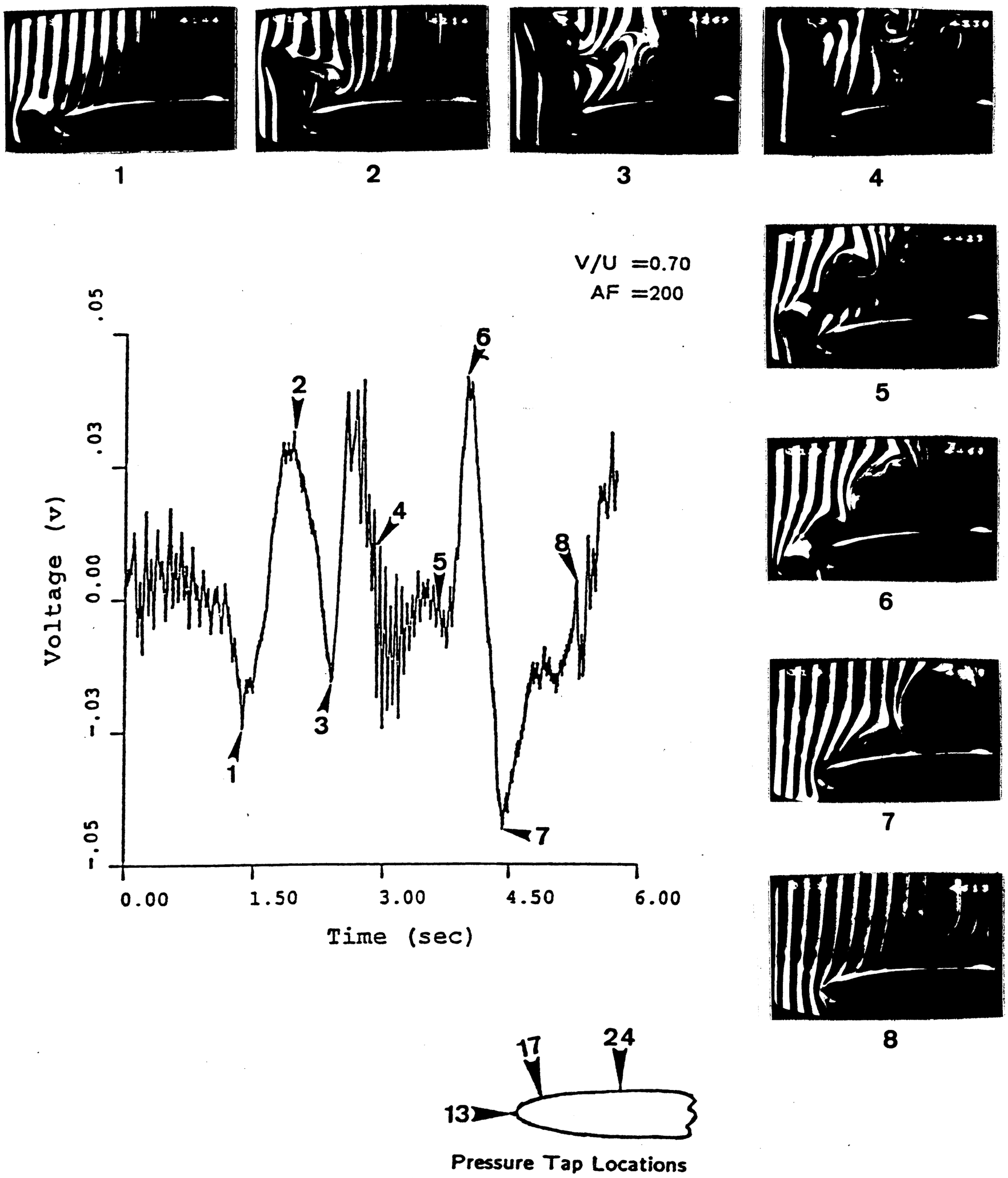

Figure 71 : Correlation between the instantaneous pressure signal and the unsteady flow structure along the edge (Tap No. 24).

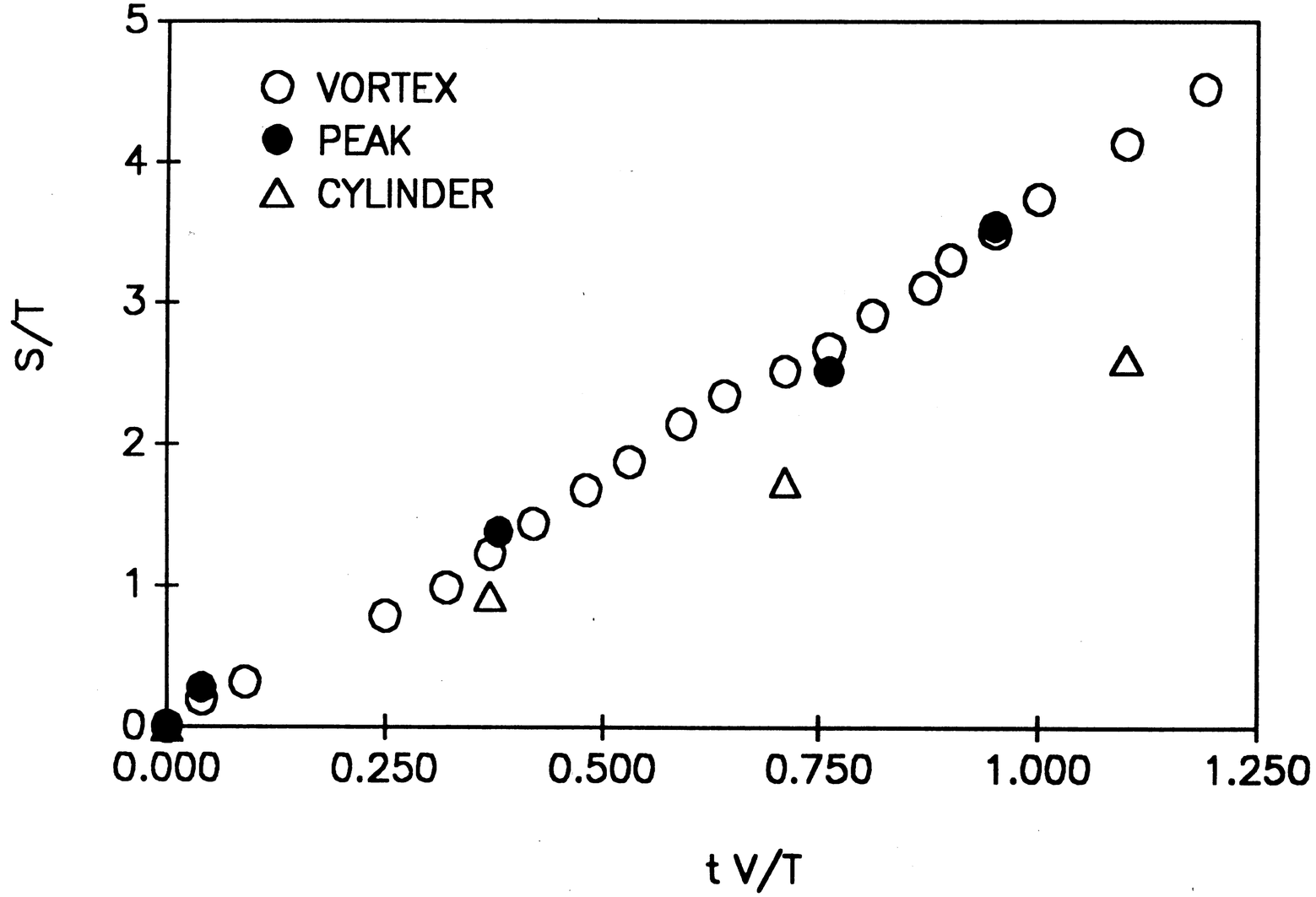

Figure 72 : Plot of displacement of vortex, first negative peak of pressure signal and cylinder vs. time during the upstroke motion along the edge for V/U=0.57 (Tap No.17, 18, 20, 22, 24).

REFERENCES

Erwin, J. R. 1964 "Experimental Techniques", *Section D. of Aerodynamics of Turbines and Compressors*, Princeton University Press.

Fujita, Hajime and Kovasznay, Leslie S. G. 1974 "Unsteady Lift and Radiated Sound from a Wake Cutting Airfoil", *AIAA Journal*, Vol. 12, pp. 1216-1221.

Gursul, I. 1988 "Interaction of Karman Vortex Street with an Elliptical Leading-edge", Ph. D. Thesis, Lehigh University.

Kaykayoglu, R. and Rockwell D. 1985 "Vortices Incident Upon a Leading edge: Instantaneous Pressure Fields", *Journal of Fluid Mechanics*, Vol. 156, pp. 151-172.

Kaykayoglu, R. and Rockwell D. 1986 "Unsteable Jet-edge Interaction. Part 1. Instantaneous Pressure Fields at a Single Frequency", *Journal of Fluid Mechanics*, Vol. 169, pp. 125-149.

Lusseyran, D. & Rockwell, D. 1988 "Estimation of Velocity Eigenfunctions and Vorticity Distributions from the Timeline Visualization Technique", *Experiments in Fluids*, 6, pg. 228-236.

Lefcort, M. D. 1965 "An Investigation Into Unsteady Blade Forces in Turbomachines", *ASME Journal of Engineering for Power*, Vol.87A, 1965, pp. 345-354.

Meyer, R. X. 1958 "The Effect of Wakes on the Transient Pressure and Velocity Distributions in Turbomachines", *Transactions of the ASME*, Vol.80, pp. 1544-1552.

Magness, Charles Lee 1989, Computer Programs for the Pressure Measurement Experiments.

Magness, Charles Lee 1987 "A Visual Study of the Unsteady Flow Structure on A

Pitching Delta Wing", Master Thesis, Lehigh University.

N. H. Kemp and W. R. Sears 1953 "Aerodynamic Interference Between Moving Blade Rows ", *Journal of The Aeronatical Sciences*, Vol. 20, pp. 585-598.

N. H. Kemp and W. R. Sears 1955 "The Unsteady Forces Due to Viscous Wakes in Turbomachines", *Journal of The Aeronatical Sciences*, Vol. 22, pp. 478-483.

Ongoren, A. 1986 "Unsteady Structure and Control of Near-Wakes", Ph.D. Thesis, Lehigh University.

Rockwell, D. O. 1984 "Unsteady Loading of Leading-Edges in Unsteable Flows: An Overview", *AIAA/NASA 9th Aeroacoustics Conference*, October 15-17, Williamsburg, Virginia.

Sohn, D. Y. 1985 "Vortex Interaction with a Leading-edge of Finite Thickness", Master Thesis, Lehigh University.

Schraub, F. A., Kline, S. J., et al. 1965 "Use of Hydrogen Bubbles for Quantitative Determination of Time-Dependent Velocity Fields in Low-Speed Water Flows", Journal of Basic Engineering, *Transactions of ASME*, June, 7, pg. 429-443.

The Positioning Equipment Catalog of Daedal Inc. 1988 "Linear Motion-Positioning Tables".

The Catalog of Compumotor Corporation 1988 "Compumotor Systems".

The PCB Piezotronics Inc. Catalog, 1988 "I.C.P. Transducer Data".

Ziada, S. and Rockwell, D. 1982 "Vortex-Leading Edge Interaction", *Journal of Fluid Mechanics*, Vol. 118, May, pp. 79-107.

VITA

The author was born in Turkey on July 14, 1964. After high school, he enrolled at Istanbul Technical University where he graduated with a B.S. degree in Mechanical Engineering. In August 1987, he began to study at Lehigh University for his Master's degree.